

Université du Québec  
Institut National de la Recherche Scientifique  
Centre Eau Terre Environnement

UTILISATION DE PROFILS VERTICAUX DE CHARGES HYDRAULIQUES  
POUR CONTRAINDRE LA REPRÉSENTATION GÉOSTATISTIQUE DE  
L'HÉTÉROGÉNÉITÉ DANS UN AQUIFÈRE GRANULAIRE

Par  
Patrick Brunet

Mémoire présenté pour l'obtention du grade de  
Maître ès sciences (M.Sc.)  
en sciences de la terre

**Jury d'évaluation**

Président du jury et  
examineur interne

Richard Martel  
INRS - Eau, Terre et Environnement

Examineur externe

Marie Larocque  
Département des sciences de la terre et de  
l'atmosphère  
Université du Québec à Montréal (UQAM)

Directeur de recherche

René Lefebvre  
INRS - Eau, Terre et Environnement

Codirecteur de recherche

Erwan Gloaguen  
INRS - Eau, Terre et Environnement



## REMERCIEMENTS

Je tiens d'abord à exprimer toute ma gratitude à mon directeur de recherche, René Lefebvre, pour la confiance qu'il m'a témoigné tout le long de mon parcours à la maîtrise. Malgré les difficultés qui ont ralenti mon parcours académique, René s'est montré plus que compréhensif et conciliant; l'INRS-ETE dispose maintenant d'un poste de travail "adapté" grâce à lui! Sur le plan académique, sa grande disponibilité a donné lieu à de longues discussions souvent fructueuses, toujours motivantes. Sa grande compétence et sa passion sont une précieuse source d'émulation pour les étudiants.

Merci à mon co-directeur de recherche, Erwan Gloaguen, qui m'a permis de voir l'hydrogéologie sous un autre angle, soit celui de la géostatistique. Sa grande passion et son approche quant au travail de recherche sont une véritable source d'inspiration. Il me faut aussi souligner la contribution et collaboration importante de Daniel Paradis à mes travaux, tant pour l'idée originale du projet que pour les travaux de terrain, le partage des données et les nombreuses discussions. Daniel fera certainement un excellent (co-) directeur de recherche pour les étudiant à venir! Merci aussi à Laurie Tremblay pour sa précieuse collaboration, le partage des données et de ses connaissances sur le site d'étude, ainsi que pour sa passion et sa grande rigueur au travail.

Merci également aux autres membres du jury, Richard Martel et Marie Larocque, pour les commentaires et corrections apportées à ce travail.

Mes collègues du 2402 m'ont véritablement permis de conjuguer travail et plaisir tout au long de ma maîtrise. Merci pour votre enthousiasme, pour votre support, pour toutes les discussions enrichissantes et/ou délirantes.

Enfin, je suis infiniment reconnaissant du support indéfectible de ma conjointe, Émilie, et de mes parents tout au long de mes études.



## RÉSUMÉ

La construction de modèles numériques représentatifs de l'écoulement et du transport de masse est nécessaire afin d'adopter des mesures de mitigation efficaces sur les sites contaminés. La modélisation adéquate d'un site dépend toutefois de notre capacité à représenter l'hétérogénéité de l'aquifère à l'échelle appropriée en fonction du problème étudié. Afin d'évaluer la capacité des modèles numériques à reproduire la dynamique aquifère réelle, contrôlée en partie par l'hétérogénéité des propriétés hydrauliques, il est essentiel de disposer de données de terrain appropriées (e.g. charges, concentrations ou flux) qui reflètent des conditions hydrogéologiques représentatives. Bien que les données de niveaux d'eau puissent être peu sensibles à la distribution des hydrofaciès (HF; matériaux avec des propriétés hydrauliques distinctes) et leurs conductivités hydrauliques (K) respectives, les profils verticaux détaillés de charges hydrauliques peuvent être sensibles à la distribution et la continuité des HF. Ces travaux ont donc pour objectif d'évaluer si de tels profils pourraient ainsi être utilisés afin de contraindre des représentations déterministes ou stochastiques de l'hétérogénéité utilisées dans des modèles numériques.

Une analyse de sensibilité préliminaire des profils de charge hydraulique en fonction de certaines conditions et paramètres hydrauliques a été réalisée à partir de simulations synthétiques d'un modèle simplifié en coupe et en régime permanent. Celles-ci ont permis d'identifier certaines conditions nécessaires à l'utilisation des profils de charge permettant de contraindre les champs de K, soient 1) un contraste de K entre les HF de près de 1.5 ordres de grandeur; 2) un facteur d'anisotropie de près de 1.5 ordres de grandeur; et 3) des gradients hydrauliques suffisants ( $\geq 0.005$ ).

Afin de vérifier le potentiel d'utilisation des profils verticaux de charge hydraulique pour contraindre des représentations de l'hétérogénéité des aquifères à l'échelle du sous-bassin versant, une approche de simulations synthétiques a été utilisée, cette fois basée sur des modèles de référence réalistes produits à partir de données d'un site à Saint-Lambert-de-Lauzon (Québec). Ce site, qui a fait l'objet d'une campagne intensive de caractérisation, correspond à un aquifère hétérogène et anisotrope. Des données de sondages au piézocône (CPT), de teneur en eau et de résistivité (SMR), ainsi que des données de radar géologique et de résistivité de surface

ont été recueillies sur ce site. Ces données ont été compilées et intégrées afin de générer deux modèles numériques d'écoulement de référence sur une coupe 2D le long d'une ligne d'écoulement. Ces modèles de référence présentent des niveaux de continuité du champ de K distincts afin de vérifier l'impact de cette continuité sur les profils de charge. Les données de K de six puits synthétiques (considérées comme les mesures de puits mesurées) ont été extraites de ces modèles afin de générer 100 réalisations de champs de K par statistiques multi-points.

Ensuite, des profils verticaux de charge hydraulique en régime permanent ont été extraits des modèles numériques d'écoulement de référence (charges observées), mais aussi sur les réalisations géostatistiques (charges simulées). Afin d'évaluer la capacité de reproduire la distribution d'HF des modèles de référence à partir des profils de charges extraits, trois approches ont été utilisées sur la base des écarts entre les charge observées et simulées, soient : 1) la sélection des meilleures réalisations géostatistiques multipoints; 2) la méthode de déformation graduelle globale (MDG); et 3) une méthode heuristique basée sur celle des points-pilotes.

Bien que les conditions d'application des profils de charge soient assez restrictives, les résultats des simulations illustrent le potentiel de ce type de données pour contraindre la représentation géostatistique de l'hétérogénéité des aquifères, tant pour le cas de référence continu que discontinu. Par contre, cette capacité pourrait être relativement locale suivant la magnitude des gradients du système d'écoulement et l'orientation de l'écoulement par rapport aux couches. Ainsi, bien que de tels profils puissent aider à préciser la distribution de K là où la variance des réalisations géostatistiques est jugée trop importante, la sensibilité hydraulique des profils de charges aux variations de K devrait être évaluée au préalable. L'applicabilité de l'approche de calibration de modèles numériques par des profils de charge se limite aux aquifères granulaires de surface présentant une certaine continuité dans la distribution des HF relativement à l'échelle du problème. La mise en place de puits par enfoncement (*direct-push*) crépinés sur toute l'épaisseur de l'aquifère facilite l'acquisition de tels profils de charge, tout en réduisant significativement les coûts par rapport aux systèmes d'installation multi-niveaux disponibles.

## ABSTRACT

Representative numerical models of flow and contaminant transport are needed to implement adequate and effective remediation actions at contaminated sites. The development of such models depends however on our capability to represent aquifer heterogeneities at the proper scale for the problem considered. To evaluate the ability of numerical models to reproduce the actual aquifer dynamics, which is in part controlled by aquifer heterogeneities, it is essential to have appropriate monitoring data (e.g., heads, concentrations, flux) that reflect representative hydrogeological conditions. Though water level data may be weakly sensitive to hydrofacies (HF; materials with distinct hydraulic properties) distribution and their respective hydraulic conductivities (K), detailed vertical profiles of hydraulic head may be sensitive to distribution and continuity of HF. Thus, the objective of this project is to assess if such profiles could be used to constrain deterministic or stochastic representations of heterogeneity integrated in numerical models.

A preliminary sensitivity analysis of hydraulic head profiles to certain conditions and hydraulic parameters was carried out using synthetic steady-state flow simulations on a simplified 2D section model. Results show that certain conditions are necessary for effective use of head profile data, namely: 1) K contrasts between HFs near 1.5 orders of magnitude or more; 2) an anisotropy factor of approximately 1.5 orders of magnitude or more; and 3) sufficient hydraulic gradients ( $\geq 0.005$ ).

To assess the potential of vertical hydraulic head profiles to constrain representations of aquifer heterogeneity at a sub-watershed scale, an approach of synthetic simulations based upon realistic reference models was used. The latter were generated with field data from a highly heterogeneous and anisotropic aquifer system of a study site located in Saint-Lambert-de-Lauzon, Quebec. As part of a characterization program of this littoral aquifer system, cone penetration tests (CPT), soil moisture-resistivity (SMR) measurements, ground penetrating radar and surface electrical tomography profiles were acquired throughout the site. To investigate the impact of HF distribution and continuity on vertical head profiles, some of these data were used in order to generate two reference numerical flow models with different levels of continuity on a 2D vertical section along a groundwater flow line. K data were extracted from six synthetic wells in these models in order to generate 100 realizations of K fields with multiple point geostatistics.

The conceptual reference models and geostatistical realizations were integrated in numerical flow models. Following steady-state flow simulations, vertical hydraulic head profiles were then extracted from the reference numerical flow models (observed heads) and from the geostatistical realizations (simulated heads). In order to assess the capacity to reproduce the heterogeneous HF distribution of reference models from extracted head profiles, three approaches were applied based upon observed and simulated head discrepancies, namely: 1) selection of best realizations from multipoint geostatistics; 2) global gradual deformation method (GDM); and 3) a heuristic approach based upon pilot-points method.

Despite the restrictive conditions required for the effective use of vertical head profiles, simulation results illustrate the potential of this type of data to constrain geostatistical representations of aquifer heterogeneity, both for the continuous and discontinuous reference models. However, this diagnostic capacity may be relatively local following the magnitude of flow system gradients and flow directions relative to HF layering. Thus, although such profiles may help define K distribution where variance in geostatistical realizations is considered excessive, hydraulic sensitivity of head profiles to K variations should be assessed beforehand. Applicability of numerical model calibration with head profile data is essentially limited to shallow granular aquifers with a certain continuity of HF distribution relative to the problem scale. Acquisition of vertical head profile data is facilitated by installation of fully screened direct-push wells, which significantly reduce costs compared to common multi-level well systems.



# TABLE DES MATIÈRES

<b>1</b>	<b>INTRODUCTION.....</b>	<b>1</b>
1.1	CONTEXTE GENERAL .....	1
1.2	CONTEXTE SPECIFIQUE.....	3
1.2.1	<i>Niveaux d'eau.....</i>	4
1.2.2	<i>Données sensibles à la distribution de K.....</i>	4
1.3	OBJECTIFS DU PROJET.....	7
1.4	METHODOLOGIE GENERALE .....	8
<b>2</b>	<b>EFFETS DE LA DISTRIBUTION DE K SUR LES PROFILS DE CHARGES HYDRAULIQUES .....</b>	<b>11</b>
2.1	INDICATIONS DU POTENTIEL DES PROFILS VERTICAUX DE CHARGES HYDRAULIQUES : EXEMPLE SYNTHETIQUE .....	11
2.1.1	<i>Modèles numériques synthétiques .....</i>	12
2.1.2	<i>Résultats et analyse .....</i>	14
2.1.3	<i>Implications pour la modélisation du site d'étude .....</i>	23
2.2	SITE D'ETUDE ET DESCRIPTION DES DONNEES DISPONIBLES .....	25
2.3	CONSTRUCTION DES DEUX MODELES DE REFERENCE .....	26
<b>3</b>	<b>USING VERTICAL HEAD PROFILES TO CONSTRAIN THE GEOSTATISTICAL REPRESENTATION OF HETEROGENEITY IN A SHALLOW GRANULAR AQUIFER .....</b>	<b>28</b>
3.1	INTRODUCTION .....	28
3.2	STUDY OBJECTIVES.....	33
3.3	METHODOLOGY .....	34
3.4	STUDY SITE AND AVAILABLE DATA DESCRIPTION.....	36
3.4.1	<i>Study site description.....</i>	36
3.4.2	<i>Slug-tests and geophysical soundings .....</i>	37
3.4.3	<i>Site-specific statistical relations developed between CPT/SMR data and K.....</i>	38
3.4.4	<i>Static and continuous (transient) vertical head profiles.....</i>	39
3.5	CONSTRUCTION OF THE 2 REFERENCE MODELS.....	42
3.5.1	<i>Construction of initial hydrogeological models .....</i>	43

3.5.2	<i>“Selection” and “development” of continuous and discontinuous conceptual models</i> .....	48
3.5.3	<i>Numerical flow model, flow simulations and reference head profiles</i> .....	50
3.5.4	<i>Preliminary assessment of K contrasts</i> .....	53
3.6	UNCONSTRAINED GEOSTATISTICAL SIMULATIONS .....	56
3.6.1	<i>Extraction of HF data from 6 synthetic wells</i> .....	58
3.6.2	<i>Multiple-point simulations</i> .....	58
3.7	MINIMIZATION OF HYDRAULIC HEAD PROFILE MISMATCH .....	59
3.7.1	<i>Mismatch criteria</i> .....	60
3.7.2	<i>Global gradual deformation method</i> .....	61
3.7.3	<i>Local heuristic method with control points</i> .....	65
3.8	RESULTS.....	69
3.8.1	<i>All multiple points realizations: Continuous reference model</i> .....	70
3.8.2	<i>Best realizations relative to the continuous reference model</i> .....	73
3.8.3	<i>Effect of selection and optimization on head differences</i> .....	78
3.8.4	<i>Effect of horizontal spacing between head profiles</i> .....	80
3.8.5	<i>Effect of discontinuity of HF distribution (discontinuous model)</i> .....	84
3.9	DISCUSSION .....	91
3.9.1	<i>Flow pattern of reference models</i> .....	92
3.9.2	<i>Calibration approaches</i> .....	95
3.9.3	<i>Application and limitations</i> .....	98
3.10	CONCLUSION .....	103
<b>4</b>	<b>SYNTHÈSE ET CONCLUSIONS GÉNÉRALES .....</b>	<b>105</b>
4.1	SYNTHESE.....	105
4.2	DISCUSSION .....	107
4.2.1	<i>Sensibilité hydraulique et géostatistique</i> .....	107
4.2.2	<i>Approche d'optimisation et perspectives</i> .....	108
4.2.3	<i>Applicabilité des profils de charge hydraulique pour contraindre l'hétérogénéité des champs de K</i> .....	109
4.2.4	<i>Limitations de cette étude</i> .....	110
4.3	CONCLUSION .....	111
<b>5</b>	<b>REFERENCES .....</b>	<b>113</b>

## LISTE DES TABLEAUX

<i>Tableau 1.1 Étapes générales de l'étude.....</i>	<i>9</i>
<i>Tableau 2.1 Paramètres et configuration du modèle de référence pour les simulations synthétiques. ....</i>	<i>12</i>
<i>Tableau 2.2 Résumé des simulations présentées suite à une analyse paramétrique des impacts sur les profils de charge hydraulique. ....</i>	<i>14</i>
<i>Table 3.1 Statistics of predicted logK (K in m/s) for 4 HF classes with learning machine algorithms.....</i>	<i>45</i>
<i>Table 3.2 Stratigraphic grid statistics (GOCAD®). ....</i>	<i>47</i>
<i>Table 3.3 Some significant attribute specifications for MPG simulation with ISATIS® software for generating an ensemble of reference realizations. ....</i>	<i>48</i>
<i>Table 3.4 Summary of modified homogeneous hydraulic parameters for reference flow models.....</i>	<i>56</i>
<i>Table 3.5 Some significant attribute specifications for MPG simulation with ISATIS® software for generating unconstrained realizations (relative to heads).....</i>	<i>59</i>
<i>Table 3.6 HF proportions for continuous reference model and all MP realizations.....</i>	<i>70</i>
<i>Table 3.7 Summary of the error criteria for the best MP realization, calibration with global gradual deformation and with control points (continuous reference model).....</i>	<i>78</i>
<i>Table 3.8 Statistics of head differences between observed and simulated heads from selected and calibrated realizations. ....</i>	<i>80</i>
<i>Table 3.9 Error criteria of the selected and optimized realizations with increased spacing between the head profiles. ....</i>	<i>84</i>
<i>Table 3.10 HF proportions for discontinuous reference model and all MP realizations.....</i>	<i>85</i>
<i>Table 3.11 Summary of the error criteria for the best MP realization, calibration with global gradual deformation and with control points (discontinuous reference model). ....</i>	<i>91</i>

## LISTE DES FIGURES

Figure 2.1	<i>Représentation des modèles conceptuels utilisés pour l'analyse de la sensibilité des profils de charges hydrauliques à la distribution spatiale et continuité de K.....</i>	12
Figure 2.2	<i>Représentation des conditions aux limites imposées lors des simulations d'écoulement.....</i>	13
Figure 2.3	<i>Illustration d'un puits pour la mesure de profils de charges hydrauliques. Un puits doit mesurer des variations verticales de 5 cm ou plus (<math>\Delta h</math> entre équipotentielles de 0.2 m).....</i>	15
Figure 2.4	<i>Cas homogène et isotrope (<math>q_{top} = 3</math> mm/an et <math>q_{droite} = 30</math> mm/an).....</i>	15
Figure 2.5	<i>Cas hétérogène isotrope avec une couche perméable continue s'insérant dans la matrice silteuse (<math>q_{top} = 15</math> mm/an et <math>q_{droite} = 150</math> mm/an).....</i>	16
Figure 2.6	<i>Cas hétérogènes isotropes avec une couche perméable discontinue s'insérant dans la matrice silteuse. La couche perméable discontinue présente un contraste de K avec le silt (<math>10E-6</math> m/s) de : a) 1 ordre de grandeur (<math>1E-5</math> m/s) ; b) 2 ordres de grandeur (<math>1E-4</math> m/s) ; et c) 3 ordres de grandeur (<math>1E-3</math> m/s). Les flux au sommet et à la frontière droite sont de : 9 et 90 mm/an, 6 et 60 mm/an et 9.5 et 95 mm/an, respectivement.....</i>	17
Figure 2.7	<i>Cas hétérogènes anisotropes avec une couche perméable discontinue s'insérant dans la matrice silteuse. La matrice peu perméable présente un facteur d'anisotropie <math>K_h/K_v</math> de : a) un ordre de grandeur (10) ; b) un ordre de grandeur et demi (50) ; et c) deux ordres de grandeur (100). Les flux au sommet et à la frontière droite sont de : 8.5 et 85 mm/an, 8 et 80 mm/an et 7 et 70 mm/an, respectivement.....</i>	19
Figure 2.8	<i>Cas hétérogènes avec une couche perméable discontinue s'insérant dans la matrice silteuse avec un facteur d'anisotropie de 100. La couche perméable discontinue présente un contraste de K avec le silt (<math>10E-6</math> m/s) de : a) un ordre de grandeur (<math>1E-5</math> m/s) ; b) un ordre de grandeur et demi (<math>5E-5</math> m/s) ; et c) deux ordres de grandeur (<math>1E-4</math> m/s). Les flux au sommet et à la frontière droite sont de : 5.5 et 55 mm/an, 6 et 60 mm/an et 7.0 et 70 mm/an, respectivement.....</i>	21
Figure 2.9	<i>Cas hétérogènes avec une couche perméable discontinue s'insérant dans la matrice silteuse avec un facteur d'anisotropie et un contraste de K entre HF de 100 pour le cas où : a) le flux entrant provient seulement de la frontière droite (pas de recharge au sommet) ; et b) les flux entrant sont augmentés de telle sorte que le gradient global du système soit le double, soit 0.01 (ou une élévation de la nappe de 25 m à droite). Dans ce cas, le même ratio de flux au sommet par rapport au côté droit a été respecté.....</i>	23

Figure 2.10 Site d'étude à Saint-Lambert-de-Lauzon (Québec) avec la représentation de l'ancien site d'enfouissement sanitaire, la localisation des puits et des profils géophysiques effectués (Tremblay et al., 2013).....25

Figure 3.1 Main workflow steps for assessing the potential of hydraulic head profiles to constrain representations of HF distribution, through synthetic simulations based upon realistic reference models. ....35

Figure 3.2 Saint-Lambert-de-Lauzon (Quebec) study area (adapted from Tremblay et al., 2013). .....36

Figure 3.3 K from Multi-level slug-tests: Schematic and field setup (left), with (a) Eslami-Fellenius material type and Tip stress from CPT log, and (b) Collocated detailed log of K values from multi-level slug-tests (Paradis et al., 2013).....38

Figure 3.4 General steps in the learning machine that was used to define hydro-geophysical relationships for hydrofacies and hydraulic properties prediction from unseen geophysical data (Paradis et al. 2011). .....39

Figure 3.5 Vertical head profile data acquired in a fully-screened well (P5): (a) Static head profile at a given time, (b) Eslami-Fellenius material type from CPT data, and (c) Continuous multi-level head data in intervals specified by the gray lines.....41

Figure 3.6 Cross-correlation of continuous head data for upper and lower intervals for well P5. ....42

Figure 3.7 Selected cross-section to build the 2D models: (a) Topography, bedrock, selected cross-section and CPT/SMR locations, (b) Projection of nearby CPT/SMR on the cross-section shown over the aquifer base topography, and (c) Predicted HF from CPT/SMR data along the section (see next section 3.5.1.2 ). .....44

Figure 3.8 Predicted horizontal hydraulic conductivity of four HF classes from the projected CPT/SMR data logs. ....45

Figure 3.9 2D training image from kriging of HF from 12 CPT/SMR soundings. ....47

Figure 3.10 Selected (a) continuous and (b) discontinuous reference models in terms of HF distribution. 49

Figure 3.11 Reference conceptual (a) continuous and (b) discontinuous models with simplified HF definition by merging the three HF with overlapping K values (see figure 3.8).....49

Figure 3.12 Observed and simulated hydraulic head scatter plot at 10 observation wells near the model cross-section for a) continuous reference model, and b) discontinuous reference model. ....50

Figure 3.13	Initial free and moveable top boundary of the reference models (red), simulated water table (blue), water table well data (triangles) and new fixed synthetic top boundary (black) for modeling with head profiles. ....	51
Figure 3.14	Grid of the numerical groundwater flow model with a pseudo-3D mesh (FEFLOW®).....	52
Figure 3.15	Examples of hydraulic head profiles produced by saturated steady-state flow simulation of the continuous reference model with fixed water table.....	53
Figure 3.16	Absolute differences between the hydraulic head field generated with a homogeneous model ( $K(HF1) = K(HF2)$ ) and hydraulic head fields generated from the reference models with an increasing K contrast of HF (arbitrary head difference detection threshold of 5 cm in navy blue).....	55
Figure 3.17	General workflow for assessing the use of head profiles from reference models to constrain geostatistical realizations. ....	57
Figure 3.18	Synthetic observed HF (K) data extracted from 6 profiles with approximately 450 m spacing and statistics.....	58
Figure 3.19	General workflow of the gradual deformation algorithm (adapted from Le Ravalec, 2005).63	
Figure 3.20	Optimization sequence of parameter t with global gradual deformation of conditional realizations, for combination of three realizations (adapted from Le Ravalec & Mouche, 2012).....	64
Figure 3.21	General workflow of model calibration with pilot point method (adapted from Le Ravalec & Hu, 2007).....	66
Figure 3.22	Control-point locations with 100 m spacing in X direction and 0.3 m mean spacing in Z direction. ....	67
Figure 3.23	Subdivision of the modeling area in 5 zones for optimization sequence with control points, based upon topographically estimated flow paths and the approximate location of zero-flux limits (distinct flow zones) .....	69
Figure 3.24	Element-wise standard deviation of HF for all the MPG realizations (100). The standard deviation is minimal near the data logs, whereas it is generally at its maximum between wells. ....	71
Figure 3.25	Continuous reference model (a) and examples of variability in HF distribution and continuity in 3 MP realizations (b, c, d).....	72
Figure 3.26	Error criteria distribution (a, b and c) and statistics (d) from head profile discrepancies with the continuous reference model (at 100m spacing) for all the MP realizations.....	73

Figure 3.27 (a) Selection of best MP realization based upon MAE and RMSE criteria with head profile discrepancies over 0.1 m (points) and corresponding recharge distribution on top of profile, (b) Reference continuous model, and (c) Scatter plot of observed and simulated heads with corresponding mean error criteria..... 74

Figure 3.28 (a) Calibrated realization by gradual deformation based upon MAE and RMSE criteria with head profile discrepancies over 0.1 m (points) and corresponding recharge distribution on top of profile, (b) Reference continuous model, and (c) Scatter plot of observed and simulated heads with corresponding mean error criteria. .... 76

Figure 3.29 (a) Calibrated realization with control points based upon MAE and RMSE criteria with head profile discrepancies over 0.1 m (points) and corresponding recharge distribution on top of profile, (b) Reference continuous model, and (c) Scatter plot of observed and simulated heads with corresponding mean error criteria. .... 77

Figure 3.30 Observed and simulated head differences distribution for the best MP realization and the calibrated realizations with gradual deformation and control points methods..... 79

Figure 3.31 Head difference box plot illustrating the head difference reduction from MP realization selection to global (gradual deformation) and local (control points) calibration methods.... 80

Figure 3.32 Error criteria distribution from head profile discrepancies for all the MP realizations with a) 100 m spacing, b) 200 m spacing and c) 300 m spacing. .... 81

Figure 3.33 Selected (a) and calibrated (b, gradual deformation; c, control points) realizations based upon using head profiles with 100 m, 200 m and 300 m spacing. .... 83

Figure 3.34 Error criteria distribution (a, b and c) and statistics (d) from head profile discrepancies with discontinuous reference model (100m spacing) for all the MP realizations..... 86

Figure 3.35 (a) Selection of best MP realization based upon MAE and RMSE criteria with head profile discrepancies over 0.1 m (points) and corresponding recharge distribution on top of profile, (b) Reference discontinuous model, and (c) Scatter plot of observed and simulated heads with corresponding mean error criteria..... 87

Figure 3.36 (a) Calibrated realization by gradual deformation based upon MAE and RMSE criteria with head profile discrepancies over 0.1 m (points) and corresponding recharge distribution on top of profile, (b) Reference discontinuous model, and (c) Scatter plot of observed and simulated heads with corresponding mean error criteria ..... 88

Figure 3.37 (a) Calibrated realization with control points based upon MAE and RMSE criteria with head profile discrepancies over 0.1 m (points) and corresponding recharge distribution on top of

*profile, (b) Reference discontinuous model, and (c) Scatter plot of observed and simulated heads with corresponding mean error criteria. ....90*

*Figure 3.38 Continuous reference model recharge distribution (top), HF contacts (black thick contours), velocity vectors (arrows) and head differences between homogeneous K model and model with K contrast of 2 orders of magnitude (colored contours, as in figure 3.16). ....93*

*Figure 3.39 Discontinuous reference model recharge distribution (top), HF contacts (black thick contours), velocity vectors (arrows) and head differences between homogeneous K model and model with K contrast of 2 orders of magnitude (colored contours, as in figure 3.16)...93*

*Figure 3.40 Flow lines for the continuous reference model with K contrasts between HF of two orders of magnitude. Note the areas between the thick black contoured volumes and the area delimited in the blue box ( $\Delta\Psi$  corresponds to flow within each stream tube). ....95*

*Figure 3.41 Evolution of the objective functions (MAE and RMSE) against the number of iterations (flow simulations).....97*



# 1 INTRODUCTION

## 1.1 Contexte général

Les modèles hydrogéologiques doivent représenter adéquatement la distribution spatiale de l'hétérogénéité des propriétés hydrauliques des aquifères afin d'étudier l'écoulement des eaux souterraines et le transport de masse à l'échelle du problème investigué. De tels modèles, basés uniquement sur l'intégration déterministe de données mesurées en puits jumelés aux connaissances géologiques du site, mènent à une simplification de la structure spatiale de la réalité géologique. Conséquemment, plusieurs approches géostatistiques ont été développées durant les dernières décennies afin de reproduire l'hétérogénéité spatiale des aquifères, mais aussi afin d'investiguer l'espace des modèles équiprobables qui satisfont les données mesurées et l'*a priori* géologique (de Marsily *et al.*, 2005). L'ensemble de ces modèles permet aussi de quantifier l'incertitude sur les modèles. L'incertitude associée à la représentativité des modèles peut être regroupée en trois catégories selon Refsgaard *et al.* (2012), soit : 1) la structure du modèle géologique (modèle conceptuel); 2) la variabilité à grande échelle des propriétés hydrauliques (ou paramètres effectifs); et 3) la variabilité à petite échelle de ces propriétés (ou paramètres) à l'intérieur de chaque unité géologique. L'incertitude associée à la structure des modèles géologiques (modèle conceptuel) est généralement considérée comme étant la source la plus importante d'incertitude (e.g. Bredehoeft, 2005; Refsgaard *et al.*, 2012), bien qu'elle soit rarement prise en compte dans la modélisation en raison de l'importance des efforts requis. Récemment, des approches ont été suggérées afin de considérer des modèles ou structures alternatives dans le processus de modélisation stochastique (e.g. Refsgaard *et al.*, 2006; Rojas *et al.*, 2008; Ronayne *et al.*, 2008; Seifert *et al.*, 2012; Wellmann *et al.*, 2014).

La variabilité à diverses échelles des propriétés hydrauliques et des paramètres des modèles qui y sont associés et leur incertitude ont fait l'objet de recherches considérables dans les dernières décennies, menant au développement de nombreuses méthodes numériques d'inversion (revues de la modélisation inverse dans Carrera *et al.*, 2005; De Marsily *et al.*, 1999; McLaughlin & Townley, 1996; Zhou *et al.*, 2014). La représentation spatiale de l'hétérogénéité des aquifères passe par la capacité à reproduire la variabilité spatiale de la conductivité hydraulique (K). Cette

hétérogénéité des propriétés hydrauliques dans les aquifères granulaires découle de processus sédimentaires complexes, affectant l'écoulement des eaux souterraines et le transport de masse à plusieurs échelles (Koltermann & Gorelick, 1996). La structure à grande échelle de la conductivité hydraulique contrôle le trajet des eaux souterraines et du transport de masse, alors que la variabilité à petite échelle contrôle la dispersion de la masse (Blouin *et al.*, 2013; Millet *et al.*, 2013; Koltermann & Gorelick, 1996). Les processus chaotiques de déposition peuvent engendrer des variations de la conductivité hydraulique de plusieurs ordres de grandeur sur un même site d'étude (e.g. Freeze & Cherry, 1979; Koltermann & Gorelick, 1996; Sudicky *et al.*, 2010). Les efforts de caractérisation de l'hétérogénéité des paramètres hydrauliques portent généralement sur la conductivité hydraulique, bien que plusieurs autres propriétés soient essentielles pour la modélisation du transport de masse (e.g. porosité, sorption ou dégradation).

La modélisation des aquifères impliquant une problématique locale de transport de masse requière généralement la définition détaillée de l'échelle fine de l'hétérogénéité de K, puisque l'impact de la connectivité y est déterminant (De Marsily *et al.*, 2005). Identifier la connectivité des unités hydrogéologiques, e.g. de barrières ou de voies d'écoulement préférentielles, constitue ainsi une difficulté majeure en hydrogéologie et fait toujours l'objet de recherches soutenues. La modélisation par hydrofaciès (HF) de l'hétérogénéité est particulièrement appropriée dans ce contexte, facilitant ainsi la représentation de la connectivité tout en permettant des changements abrupts des HF et de propriétés plutôt que de générer des champs géostatistiques continus (De Marsily *et al.*, 2005). Frei *et al.* (2009) définissent les hydrofaciès comme des unités formées sous un régime de déposition sédimentaire spécifique et caractérisés par des plages de propriétés hydrauliques distinctes. Ici, nous considérons un hydrofaciès comme une ou des unités géologiques qui présentent un comportement hydraulique statistiquement similaire. Par ailleurs, les problématiques de contamination ponctuelle des eaux souterraines impliquent le transport de masse de zones sources à des récepteurs potentiels sur une échelle de quelques centaines de mètres à quelques kilomètres. Ainsi, la représentation de la connectivité des propriétés hydrauliques à l'échelle locale est généralement facilitée par la définition d'hydrofaciès (e.g. Fleckenstein *et al.*, 2006; Ouelton *et al.*, 2008). La distribution spatiale et l'arrangement des HF du système aquifère (ou connectivité) exercent un contrôle prédominant sur la magnitude du transport de masse dans ce contexte.

Afin de représenter adéquatement la distribution des HF et leurs propriétés hydrauliques respectives, diverses méthodes de simulations géostatistiques ont été utilisées, dont les simulations séquentielles d'indicatrices (Emery, 2004; Journel & Alabert, 1989), les simulations par pluri-gaussiennes ou gaussiennes tronquées (Galli et al., 1994; Mariethoz *et al.*, 2009), les simulations par probabilités de transitions (Carle & Fogg, 1996; Carle, 1999) ou les simulations par points-multiples (Hu & Chuginova, 2008; Straubhaar *et al.*, 2011; Strebelle, 2002). Ces approches permettent d'intégrer les données existantes sur les propriétés hydrauliques (les données) et l'information sur leur arrangement spatial (les connaissances géologiques) pour produire des réalisations équiprobables des distributions des HF et subséquentement des champs de paramètres hydrauliques. La représentation des propriétés hydrauliques et des structures internes propres à chaque HF doit alors s'appuyer sur des mesures à petite échelle, en nombre suffisant à l'intérieur de chaque HF identifié.

Que ce soit dans un cadre déterministe ou stochastique, la validité de la paramétrisation du (des) modèle(s) est considérée sur la base de la concordance entre les variables d'état simulées (e.g. charges hydrauliques, concentrations) et les données observées. Dans le cadre géostatistique, les méthodes d'inversion stochastique sont couramment utilisées, permettant ainsi d'automatiser la calibration des paramètres des modèles. Elles visent essentiellement à déterminer les paramètres inconnus du modèle en intégrant divers types de données de terrain et les connaissances géologiques du site tout en préservant la distribution des variables. En somme, la plausibilité hydraulique des modèles est basée sur la reproduction de variables d'état indirectes pour lesquelles des données sont disponibles.

## 1.2 Contexte spécifique

La modélisation stochastique en hydrogéologie doit être supportée par des mesures de variables d'état (données) qui sont sensibles à l'hétérogénéité des paramètres à l'échelle de l'étude. Les données les plus couramment utilisées en hydrogéologie pour la calibration des paramètres hydrauliques des modèles ne présentent pas toutes la même sensibilité en fonction des paramètres étudiés et du problème donné. Dépendamment du problème, les variables d'état peuvent présenter une faible sensibilité aux paramètres du modèle, i.e. que le niveau d'information contenue à leur sujet est faible (Carrera *et al.*, 2005).

### 1.2.1 Niveaux d'eau

L'ajustement manuel ou automatique (inversion) des paramètres des modèles hydrogéologiques a toujours été effectué presque exclusivement sur les mesures de niveaux d'eau (charges hydrauliques moyennes). Les données les plus fréquemment rencontrées (et parfois le seul type de données) sont ces charges hydrauliques, alors qu'elles contiennent parfois peu d'information quant à la conductivité hydraulique (Carrera *et al.*, 2005). Avec le développement des méthodes d'inversion stochastiques en hydrogéologie, on constate que les problèmes inverses sont généralement mal posés et qu'ils ne peuvent être résolus sans l'usage de certaines suppositions et contraintes additionnelles (Zhou *et al.*, 2014). Les problèmes mal posés peuvent générer des solutions non-unicues ou instables. Ceci est essentiellement issu du déséquilibre entre le nombre de paramètres à estimer par rapport au nombre de données disponibles, ainsi que de la faible sensibilité des observations par rapport aux paramètres à estimer. De nombreux exemples dans la littérature illustrent le fait que les niveaux d'eau en régime permanent puissent être reproduits par diverses représentations de l'hétérogénéité (e.g. Capilla *et al.*, 1998; Doherty, 2003).

Ainsi, puisque les charges hydrauliques statiques aux puits sont relativement peu sensibles aux variations spatiales de conductivité hydraulique, l'ajout de plus de mesures de charge hydraulique peut ne pas améliorer de façon significative la qualité de l'estimation. Inclure un plus petit nombre de mesures d'autres types de variables, telles de concentrations dissoutes, pourrait être d'un apport plus considérable (McLaughlin & Townley, 1996).

### 1.2.2 Données sensibles à la distribution de K

Selon le problème étudié, certains types de données peuvent se révéler plus sensibles aux valeurs et distributions des champs de K le long d'une voie d'écoulement. L'ajout de données de flux aux données de charges hydrauliques dans la calibration permet d'accroître la sensibilité aux transmissivités (Carrera *et al.*, 2005). De plus, l'inclusion des flux permet de s'affranchir en partie de la forte corrélation entre la conductivité hydraulique (K) et la recharge (R), facilitant ainsi la calibration d'un modèle unique (Poeter & Hill, 1997). Par contre, la magnitude exacte et la distribution spatiale de la recharge n'est pratiquement jamais connue, ce qui laisse cette indétermination entière ( $q = Ki$ , où q et K sont inconnus). Les données de flux aux exutoires sont

intégratrices : elles permettent de stabiliser le problème inverse mais pas de résoudre sa non-unicité.

- Depuis trente ans, les charges hydrauliques transitoires ont été intégrées dans les approches d'inversion numérique (e.g. Carrera & Neuman, 1986; Sun & Yeh, 1992) et leur apport quant à la réduction des erreurs des variables d'état prédites a été démontré. Plus spécifiquement, les données de charges transitoires peuvent aider à estimer la distribution spatiale de K. Par exemple, Wiese and Nützmann (2011) ont utilisé des données de charge hydraulique transitoires lors d'essais de pompage dans un algorithme d'inversion avec des points pilotes et régularisation (PEST) afin de déterminer la distribution et la continuité spatiale d'un aquitard situé entre deux aquifères. Ronayne *et al.* (2008) ont utilisé des charges transitoires lors d'essais de pompage pour restreindre les réalisations représentant des chenaux de haute conductivité hydraulique (générés par statistiques multi-points). Zhou *et al.* (2011) et Xu *et al.* (2013) ont également démontré la capacité, à partir de telles données, de restreindre le champ de réalisations de K plausibles par l'utilisation des filtres de Kalman d'Ensemble (EnKF). Bien que cette dernière approche pose toujours certains défis quant au caractère non Gaussien des champs de K ou la réduction de la covariance avec le temps, les EnKF permettent d'assimiler efficacement le nombre important de données que pourraient impliquer des charges transitoires.

- Le transport de masse est une variable sensible à la distribution des diverses propriétés hydrauliques du milieu, en particulier aux conductivités hydrauliques. Par exemple, Wen *et al.* (2002) ont utilisé des courbes d'arrivée de traceurs avec la technique d'inversion d'auto-calibration séquentielle (*Sequential Self-Calibration*). Selon ces auteurs, les données de charges transitoires portent de l'information sur la distribution spatiale de K près des puits, alors que les données de traceurs fournissent de l'information sur la connectivité spatiale entre les puits. Plus récemment, les résultats de l'étude de Llopis-Albert and Capilla (2009b) à partir des données d'un essai de traceurs corroborent les conclusions de Wen *et al.* (2002), alors qu'ils intègrent des données transitoires de charges hydrauliques et de concentrations de traceurs avec l'approche inverse de Conditionnement Graduel (CG). L'intégration de ces données dans un cas fortement hétérogène en 3D permet de reproduire les courbes d'arrivée tout en identifiant l'importance de voies de cheminement préférentiel. Toutefois, dans bien des cas le temps requis pour réaliser des essais de traceurs pour produire des réponses représentatives est jugé excessif (De Marsily *et al.*, 2005).

- Les données de traceurs isotopiques (e.g. tritium) peuvent fournir de l'information sur l'âge ou temps de résidence de l'eau souterraine. Un simple modèle advectif de l'âge des eaux souterraines peut permettre de comparer les données simulées et observées. Par contre, les effets de dispersion ainsi que de mélange des eaux compliquent considérablement l'interprétation de telles données. Afin d'être en mesure de comparer les données d'âge observées à des âges simulés représentatifs, Goode (1996) a développé une approche de simulation directe produisant la distribution spatiale de l'âge moyen et qui inclus les processus advectifs et dispersifs. Une telle distribution permet alors d'évaluer les paramètres d'écoulement et de transport du (des) modèle(s) à partir des âges simulés et observés. Varni and Carrera (1998) ont développé des équations permettant de simuler les effets de la dispersion dans le système d'écoulement en amont des points d'échantillonnage, produisant l'âge moyen et la variance de l'âge en ces points. Comme l'âge des particules est fonction de la trajectoire et des vitesses, cette donnée est fonction des flux divisés par la porosité effective ( $n_{eff}$ ). Les flux étant essentiellement contrôlés par la recharge (R) et la distribution de K dans le système, au moins un ces trois paramètres ( $n_{eff}$ , K ou R) doit être connu sur l'ensemble du domaine. De plus, la complexité des effets combinés de la diffusion de matrice, de la possible variation des sources, de la prise de mesures et le mélange près des zones d'émergence (puits et champs d'écoulement convergents) compliquent l'utilisation de l'âge comme un paramètre de calibration (Sanford, 2011; Varni & Carrera, 1998). Ainsi, lorsque l'âge est utilisé dans la calibration de modèles, la reproduction des âges est quasi-systématiquement de moindre qualité que celle des charges observées (Sanford, 2011). Par contre, ces auteurs soulignent l'impact significatif de la variabilité spatiale de la conductivité hydraulique sur la distribution des âges, et en particulier de la présence de couches de faible conductivité. En raison de cette grande sensibilité des âges à l'hétérogénéité des systèmes d'écoulement, Sanford (2011) recommande malgré tout leur utilisation pour la calibration de modèles à une ou deux dimensions. Millet *et al.* (2013) ont ainsi pu discriminer qualitativement la représentativité de diverses représentations de champs de K en 2D d'un site contaminé à partir de données d'âge ( $^3\text{H}$ - $^3\text{He}$ ).

- Par ailleurs, des recherches récentes suggèrent l'inclusion de résultats de méthodes géophysiques continues latéralement dans le processus inversion pour représenter le champ K des modèles. Par exemple, Straface *et al.* (2011) intègrent des données de charges hydrauliques et de potentiel ou polarisation spontané (SP) dans un processus d'inversion conjointe afin de

définir l'hétérogénéité de  $K$  dans un aquifère en 3D. Ruggeri *et al.* (*accepté*) démontrent l'apport de l'intégration de données électriques multi-échelles dans le cadre de simulations séquentielles bayésiennes de la conductivité hydraulique d'un aquifère en 2D.

En somme, les types de données présentés précédemment possèdent des avantages et inconvénients, en fonction du problème spécifique étudié. Elles peuvent aider à valider la plausibilité hydraulique de réalisations générées à partir de données de  $K$  et de charges hydrauliques. Par contre, elles sont soit des approximations indirectes de l'hétérogénéité de  $K$ , relativement longues et coûteuses à réaliser ou difficiles à intégrer quantitativement dans un cadre d'inversion automatique. Ainsi, l'évaluation de la plausibilité hydraulique de réalisations géostatistiques contraintes à partir de données simples et directes demeure un besoin bien réel en caractérisation des aquifères hétérogènes. Les niveaux d'eau, couramment utilisés pour la calibration des modèles, sont généralement des valeurs de charge moyenne sur toute la longueur crépinée du puits, alors que l'on voudrait en tirer de l'information sur la variabilité spatiale des paramètres de modèles hétérogènes. Pourtant, la distribution locale des charges hydrauliques est sensible aux variations du champ de conductivité hydraulique, *a fortiori* le long de puits d'observation. Ainsi, des profils verticaux détaillés des charges hydrauliques locales réalisés dans des puits pourraient améliorer l'estimation de la distribution spatiale de la conductivité hydraulique, mais le potentiel de l'utilisation de telles données doit être évalué.

### 1.3 Objectifs du projet

Plusieurs méthodes de simulation géostatistique permettent de générer de multiples réalisations de champs de conductivité hydraulique équiprobables, conditionnées aux diverses données de terrain ainsi qu'à de l'information géologique a priori. Malgré le conditionnement de ces réalisations, les réponses attendues en termes de variables d'état prédites (e.g. concentrations) peuvent varier considérablement. Bien que cette approche permette de quantifier l'incertitude rattachée aux prédictions des modèles (Refsgaard *et al.*, 2012), la difficulté de contraindre directement la distribution de la  $K$  peut produire des résultats qui exagèrent cette incertitude ou rendent cette incertitude trop importante quant aux décisions à prendre suite aux réponses apportées par la modélisation.

L'objectif principal de ce travail de recherche est d'étudier le potentiel d'utilisation de profils verticaux détaillés de charges hydrauliques pour contraindre les réalisations produites par simulation géostatistique. Pour ce faire, l'étude de la distribution et continuité de K est facilitée par une approche de modélisation par hydrofaciès dont les avantages ont été présentés précédemment. De cet objectif principal découlent les objectifs secondaires suivants :

- i. Étudier la distribution verticale des charges hydrauliques comme indicateur potentiel de la distribution et de la continuité des HF;
- ii. Évaluer l'utilisation des différences de charges hydrauliques provenant des profils pour la sélection et la calibration de réalisations stochastiques de champs de K;
- iii. Analyser les effets de la continuité des HF, des contrastes de K des HF et de l'espacement horizontal des profils de charges sur les modèles calibrés résultants.

L'utilisation de données de charges hydrauliques détaillées verticalement pour contraindre des réalisations de champs de K n'est pas documentée dans la littérature. Elle présente un intérêt manifeste dans le contexte de modélisation stochastique du transport de masse afin de réduire le niveau d'incertitude des prédictions et éventuellement faciliter la prise de décision de gestionnaires.

#### 1.4 Méthodologie générale

Ces travaux visent essentiellement à valider le concept et les conditions d'utilisation de profils de charges hydrauliques détaillés dans le cadre de la modélisation géostatistique stochastique, à partir de modélisation numérique d'écoulement en 2D utilisant des champs de K hétérogènes. Bien que les objectifs présentés correspondent à un exercice de modélisation entièrement synthétique, il y a également lieu de vérifier l'applicabilité de cette approche sur un site d'étude, situé à St-Lambert-de-Lauzon près de Québec. Ainsi, l'approche retenue représente une forme intermédiaire entre un cas d'étude réel et un cas synthétique ; des modèles de référence ont été produits en 2D de façon réaliste à partir des données de terrain recueillies au site de St-Lambert-de-Lauzon, suivi d'un exercice synthétique à partir de ces modèles afin d'étudier l'utilisation de



profils de charge. Les travaux se sont donc déroulés en deux temps : 1) produire des réalisations de champ de K en 2D réalistes et représentatives du site d'étude et en sélectionner deux comme modèles de référence; et 2) procéder à un exercice synthétique à partir de ces deux modèles de référence, en générant des réalisations géostatistiques de champs de K en 2D à partir de données partielles extraites de ces modèles et y intégrant des données de profils de charge détaillés. Les principales étapes de la méthode proposée sont résumées au tableau 1.1.

**Tableau 1.1** Étapes générales de l'étude.

<p>Construction de modèles de référence (2) représentatifs du site d'étude</p>	<ol style="list-style-type: none"> <li>1) Sélectionner une coupe le long d'une ligne d'écoulement et y projeter les sondages au piézocône limitrophes</li> <li>2) Calculer K à partir des données de sondage au piézocône et classifier en HF (2)</li> <li>3) Générer des réalisations d'HF par la méthode des points-multiples (MP)</li> <li>4) Sélectionner et développer deux modèles numériques d'écoulement de référence (un continu et un discontinu)</li> </ol>
<p>Simulations géostatistiques de champs de K et intégration des données de profils de charge détaillés</p>	<ol style="list-style-type: none"> <li>5) Extraire de six puits synthétiques des données (HF/K) à partir du modèle de référence continu</li> <li>6) Générer 100 réalisations d'HF à partir des données extraites du modèle de référence continu</li> <li>7) Simuler l'écoulement en régime permanent et extraire des données de profils de charge à partir des modèles de référence et des 100 réalisations</li> <li>8) Sélectionner et calibrer les réalisations d'HF sur la base des données de profils de charge hydraulique</li> </ol>

Afin de construire des modèles de référence représentatifs et conditionnés aux données du site d'étude, la modélisation géostatistique initiale a été faite sur la base de données de sondages au piézocône converties en valeurs de K. Les données des sondages situés sur ou à proximité d'une

coupe le long d'une ligne d'écoulement y ont été projetées. Des relations statistiques développées précédemment entre des données colocalisées de sondages au piézocône et K (Paradis *et al.*, soumis) ont supporté la prédiction d'HF et de K aux sondages le long de la coupe. Des 100 réalisations d'HF simulées en 2D par statistiques multi-points à partir de ces données, deux réalisations présentant des niveaux de continuité distincts ont été sélectionnées afin de servir de modèles de référence. Les deux réalisations sélectionnées constituent des extrema en termes de continuité des HF, soit une réalisation continue et une discontinue. Ensuite, des simulations d'écoulement en régime permanent utilisant les propriétés de ces modèles de référence ont permis de calculer des profils détaillés de charge hydraulique, pour des niveaux d'hétérogénéité de K connus le long de six puits synthétiques.

Une fois les deux modèles de référence produits, des réalisations géostatistiques d'HF ont été générées à partir de profils de K extraits des six puits synthétiques provenant de ces modèles. Les réalisations géostatistiques générées sont contraintes aux données de K, ainsi qu'à l'élévation de la nappe des modèles de référence. Les profils de charges hydrauliques extraits des simulations d'écoulement sur chacune de ces réalisations ont ainsi pu être comparés aux profils de charge des modèles de référence. La vérification de la représentativité du champ de K des réalisations sélectionnées a donc été faite sur la base de la concordance entre les profils de charge "observés" (modèles de référence) et simulés (réalisations). De plus, la capacité de reconstituer le champ de K des modèles de référence à partir de données de profils de charge a été étudié en utilisant deux approches de calibration, toujours sur la base de minimisation des écarts de charge hydraulique. L'impact des contrastes de K entre les HF et de l'espacement entre les profils de charge sur la capacité de reproduire les champs de référence a également été considéré.

## **2 EFFETS DE LA DISTRIBUTION DE K SUR LES PROFILS DE CHARGES HYDRAULIQUES**

Puisque les variations des charges hydrauliques dues à l'hétérogénéité du champ de conductivité hydraulique sont relativement faibles (De Marsily *et al.*, 2005), les conditions et paramètres favorables à l'utilisation de telles données doivent être explorés. Pour ce faire, des simulations d'écoulement à partir d'un modèle synthétique sont présentées dans la section suivante. Ensuite, le site d'étude et les données recueillies sont présentées (section 2.2) puis deux modèles de référence sont développés (section 2.3) à la lumière des résultats des essais synthétiques et des données disponibles.

### **2.1 Indications du potentiel des profils verticaux de charges hydrauliques : exemple synthétique**

L'objectif de cette section est de présenter une brève étude de la sensibilité des charges hydrauliques par rapport aux variations de K à partir de simulations d'écoulement en régime permanent sur un modèle synthétique simplifié en 2D. Puisque la distribution des charges hydrauliques est affectée par divers paramètres et conditions des modèles, l'analyse de la sensibilité des charges a été réalisée en fonction de l'impact de ces paramètres sur les variations verticales dans les profils de charge hydraulique. En effet, afin d'indiquer une capacité potentielle de diagnostic sur la distribution de K, les profils verticaux de charges hydrauliques doivent présenter des gradients ou variations verticales associées aux valeurs voisines de K. Sinon, des profils uniformes de charges n'apportent pas plus d'information que la simple valeur d'élévation de la nappe. Dans le contexte de problématiques de transport de masse, la caractérisation de la continuité (ou connectivité) des couches de matériaux plus perméables est de première importance. Ainsi, les simulations synthétiques portent sur la modélisation d'une couche perméable de continuité variable dans une matrice moins perméable.

La modélisation numérique a été réalisée avec le logiciel FLONET/TR2 (Molson & Frind, 2013), qui utilise une approche par éléments finis pour résoudre les équations d'écoulement en milieu saturé et en régime permanent en 2D.

### 2.1.1 Modèles numériques synthétiques

Pour les simulations numériques synthétiques suivantes, la distribution de K est simplifiée par une approche avec des HF de K homogène. Afin d'évaluer la sensibilité des charges hydrauliques à la distribution et connectivité des HF (K), les deux modèles conceptuels évalués consistent en une couche perméable continue ou discontinue enchâssée dans une matrice moins perméable (figure 2.1). Les dimensions du système sont de 1000 m de longueur pour une épaisseur de 20 m de sédiments. Les valeurs de K assignées aux deux HF représentés doivent être représentatives des types de sédiments pour lesquels l'approche proposée pourrait être applicable, soit essentiellement des sables et silts. Les valeurs des paramètres pour le modèle de référence des simulations synthétiques sont présentées au tableau 2.1. Les valeurs de K des HF sont toujours considérées comme étant homogènes, ainsi qu'isotropes dans le cas des modèles de référence.

Tableau 2.1 Paramètres et configuration du modèle de référence pour les simulations synthétiques.

HF	Kh (m/s)	Kv (m/s)	Épaisseur (m)
<b>Matrice silteuse</b>	1.0E-6	1.0E-6	20
<b>Lentille de sable</b>	1.0E-4	1.0E-4	3

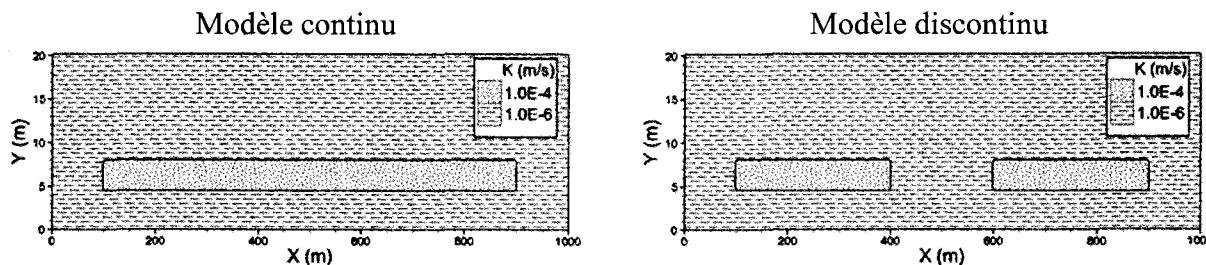
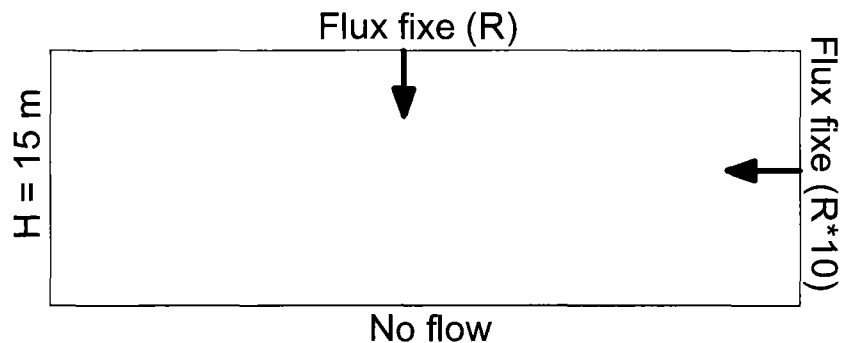


Figure 2.1 Représentation des modèles conceptuels utilisés pour l'analyse de la sensibilité des profils de charges hydrauliques à la distribution spatiale et continuité de K.

Le modèle est discrétisé de telle sorte que la dimension des mailles triangulaires soit de 2 m en X par 0.5 m en Z. Compte tenu des dimensions du modèle (1000 m par 20 m), le modèle compte

501 nœuds en X et 41 nœuds en Z, pour un total de 40 000 éléments triangulaires (20541 nœuds).

Les conditions aux limites pour la modélisation en écoulement sont illustrées à la figure 2.2. La base du modèle est considérée imperméable avec un flux nul (condition de type 2 ou Neumann), le côté gauche correspond à une charge imposée (type 1 ou Dirichlet), le flux imposé au dessus du modèle correspond à un taux de recharge fixe (type 2) alors que le flux entrant à droite est toujours imposé à une valeur correspondant à un dixième de celui de la recharge (au-dessus). Pour chacune des simulations, les flux entrants sont ajustés afin que l'élévation de la nappe à la frontière droite soit de 20 m. Ceci permet d'assurer un gradient global qui soit le même pour chaque simulation (0.005 m/m) afin de vérifier l'effet isolé de chaque modification des paramètres ou conditions du modèle. Le fait de maintenir un ratio fixe pour le flux à la frontière droite par rapport à la recharge facilite l'ajustement de ces valeurs afin de maintenir un gradient global à peu près constant.



**Figure 2.2** Représentation des conditions aux limites imposées lors des simulations d'écoulement.

Les principaux paramètres ou conditions du modèle pouvant affecter les profils de charges hydrauliques sont étudiés, soit : 1) le niveau de continuité du HF perméable; 2) les contrastes de K entre les 2 HF; 3) l'anisotropie du HF peu perméable; 4) le gradient global du système; et 5) l'orientation des flux par rapport à la couche perméable. Les conditions de 13 simulations sont résumées au tableau 2.2 et les résultats sont présentés à la section suivante (2.1.2).

**Tableau 2.2** Résumé des simulations présentées suite à une analyse paramétrique des impacts sur les profils de charge hydraulique.

1. Homogène et isotrope (1)
2. Hétérogène continu : contraste de K de 2 ordres de grandeur (o.g.), isotrope (1)
3. Hétérogène discontinu : contraste de K de 1-2-3 o.g., isotrope (3)
4. Hétérogène discontinu : contraste de K de 2 o.g., anisotropie du silt de 1-1.5-2 o.g. (3)
5. Hétérogène discontinu : anisotropie de 2 o.g., contraste de K de 1-1.5-2\* o.g. (3)
6. Hétérogène discontinu : contraste de K et anisotropie de 2 o.g., gradients x 2 (1)
7. Hétérogène discontinu : contraste de K et anisotropie de 2 o.g., flux latéral seulement; pas de recharge au dessus du modèle (1)

\* Répétition du cas 4 avec anisotropie et contraste de K de 2 ordres de grandeur pour fins de comparaison

### 2.1.2 Résultats et analyse

Les résultats présentés et leur interprétation ont été faits essentiellement sur la base de la visualisation des lignes de courant et équipotentiellles. Afin de faciliter l'interprétation, les équipotentiellles dans toutes les figures représentent des incréments de 0.2 m, couvrant ainsi la plage de 15 m (condition fixe à la limite gauche) à 20 m (par l'ajustement des flux entrants). Les profils de charge hydraulique doivent démontrer des variations d'environ 5 cm ou plus verticalement pour être supérieures aux erreurs potentiellles de mesure (environ 3 cm, selon Fisher & Twining, 2011). Ainsi, pour que des variations verticales de charges hydrauliques soient mesurables, un puits fictif (vertical) sur la figure 2.3 devrait être près d'intercepter deux lignes équipotentiellles (ou davantage).

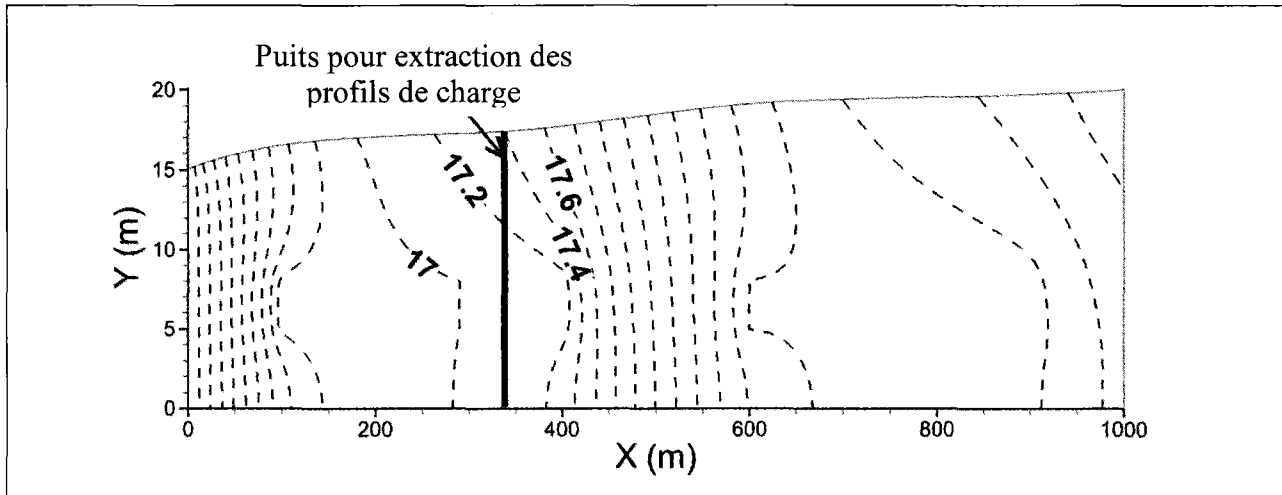


Figure 2.3 Illustration d'un puits pour la mesure de profils de charges hydrauliques. Un puits doit mesurer des variations verticales de 5 cm ou plus ( $\Delta h$  entre équipotentiels de 0.2 m).

Les résultats sont présentés suivant la séquence d'analyse paramétrique décrite au tableau 2.2. D'abord, le cas homogène et isotrope (figure 2.4) permet de visualiser des lignes d'écoulement aux trajectoires régulières et continues; les équipotentiels verticales ne montrent aucune variation des charges puisque l'écoulement est essentiellement horizontal. Dans un tel cas, la distribution des charges hydrauliques ne dépend que de la configuration des conditions aux frontières.

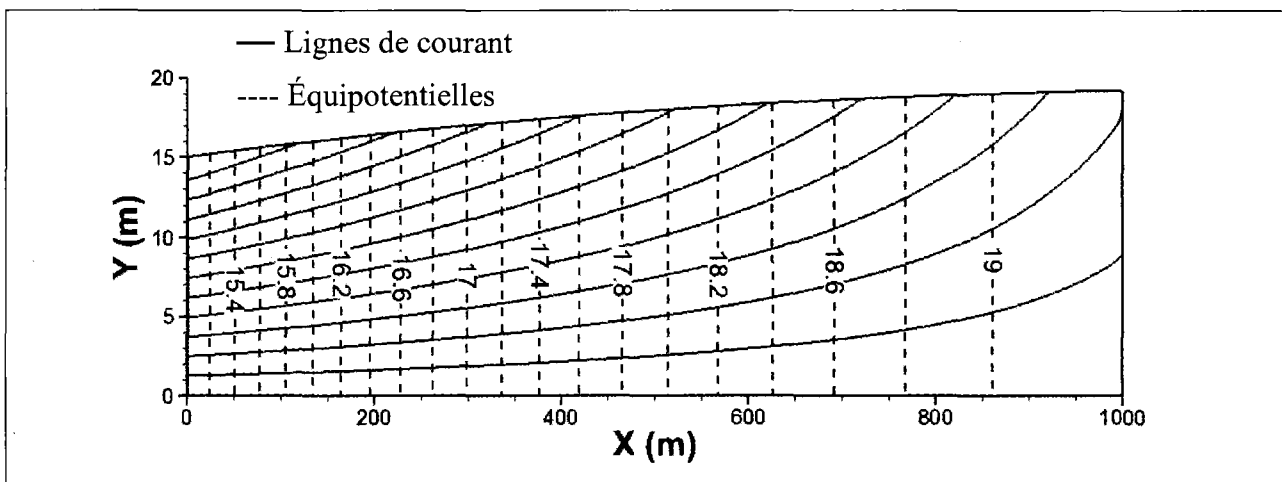


Figure 2.4 Cas homogène et isotrope ( $q_{\text{top}} = 3 \text{ mm/an}$  et  $q_{\text{droite}} = 30 \text{ mm/an}$ ).

Avec l'ajout d'une couche perméable continue de sable dans la matrice silteuse, les lignes d'écoulement sont considérablement déviées (figure 2.5). La perte de charge jusqu'à l'exutoire se concentre là où la couche perméable n'est plus présente, soit aux premiers et derniers 100 mètres, comme la réduction locale de K cause une augmentation des gradients ( $i$  ou  $\Delta h/\Delta L$ ) pour un flux à peu près constant ( $q = Ki$ ). Par contre, les équipotentielles sont essentiellement verticales, puisque l'écoulement converge/diverge rapidement aux limites de la couche perméable suivant la loi tangentielle de réfraction des lignes d'écoulement à une limite géologique dans un milieu hétérogène (Freeze & Cherry, 1979):

$$\frac{K_1}{K_2} = \frac{\tan(\theta_1)}{\tan(\theta_2)} \quad [1]$$

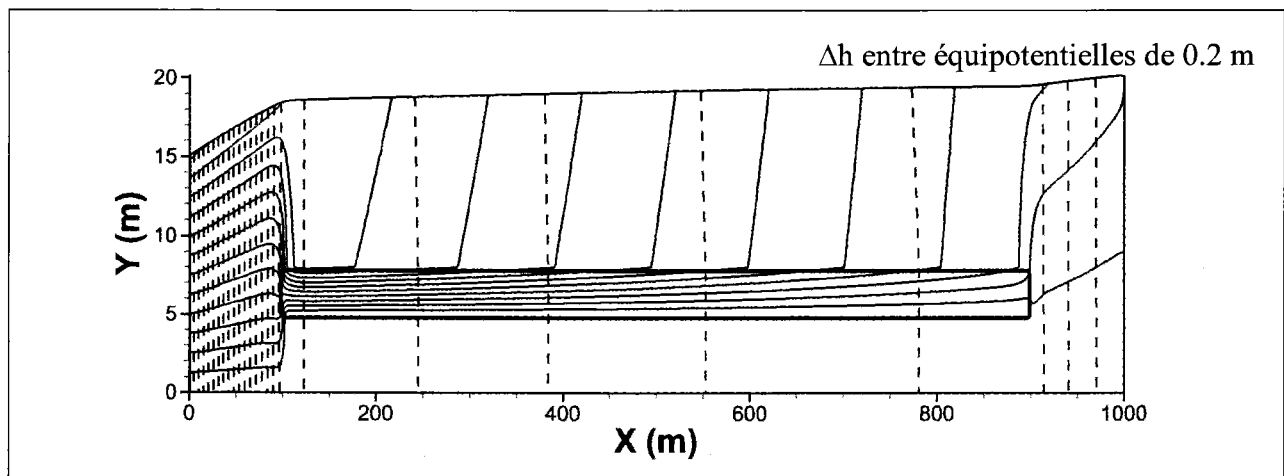


Figure 2.5 Cas hétérogène isotrope avec une couche perméable continue s'insérant dans la matrice silteuse ( $q_{\text{top}} = 15 \text{ mm/an}$  et  $q_{\text{droite}} = 150 \text{ mm/an}$ ).

L'effet d'une discontinuité dans la couche perméable a été considéré (figure 2.6) tout en variant le contraste de K entre les deux HF de un, deux et trois ordres de grandeur. L'écoulement converge vers la couche plus perméable mais se redistribue sur toute l'épaisseur de la matrice silteuse au niveau de la section discontinue. Les lignes d'écoulement traversent l'épaisseur de silt par une trajectoire d'autant plus courte que le contraste de K est grand; elles sont pratiquement verticales avec des contrastes de K de 2 et 3 ordres de grandeur. Dans ce contexte, les équipotentielles restent donc linéaires puisque les composantes de l'écoulement sont essentiellement horizontales ou verticales. Ainsi, peu importe le contraste de K entre les HF



anisotropes en présence, les profils de charge hydraulique ne fournissent aucune information de plus que des mesures d'élévation de la nappe.

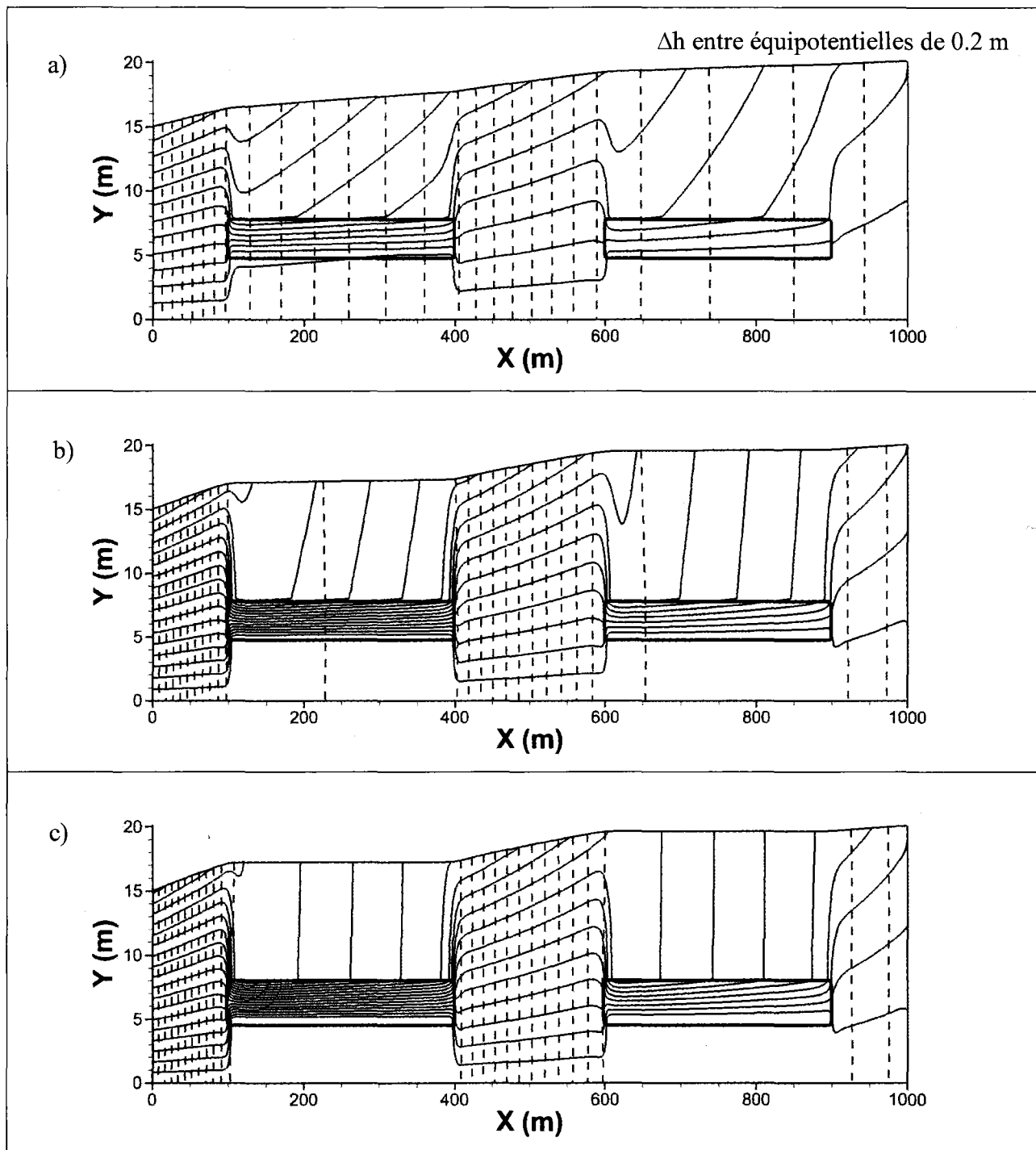
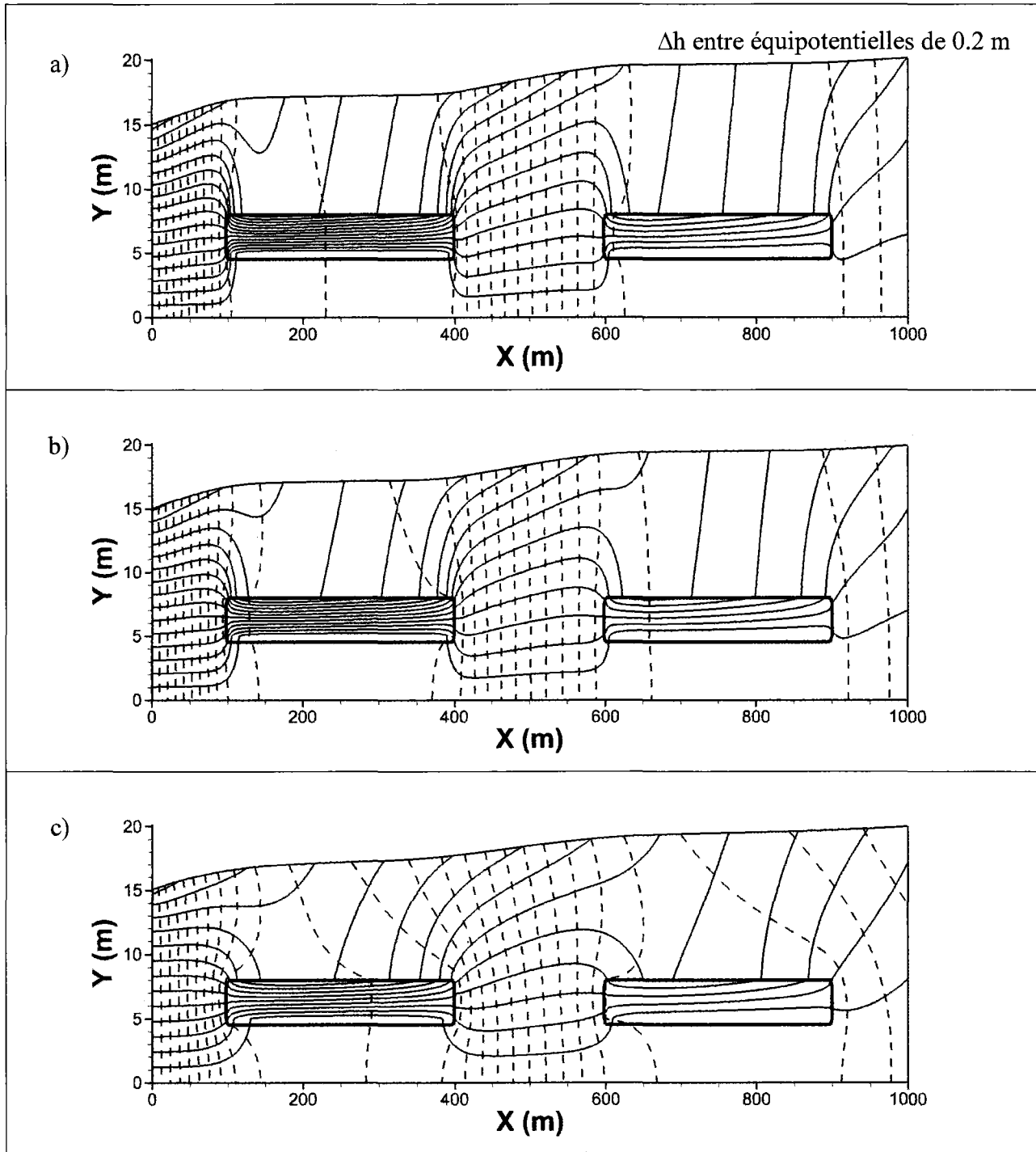


Figure 2.6 Cas hétérogènes isotropes avec une couche perméable discontinue s'insérant dans la matrice silteuse. La couche perméable discontinue présente un contraste de  $K$  avec le silt ( $10E-6$  m/s) de : a) 1 ordre de grandeur ( $1E-5$  m/s) ; b) 2 ordres de grandeur ( $1E-4$  m/s) ; et c) 3 ordres de grandeur ( $1E-3$  m/s). Les flux au sommet et à la frontière droite sont de : 9 et 90 mm/an, 6 et 60 mm/an et 9.5 et 95 mm/an, respectivement.

Puisque le contraste de  $K$  n'est pas suffisant pour déceler des variations dans les profils verticaux de charges, des facteurs d'anisotropie croissants ont été imposés à l'HF peu perméable en maintenant le contraste de  $K$  entre HF à deux ordres de grandeur (figure 2.7). Avec un petit facteur d'anisotropie (10), les équipotentielles ne sont que très légèrement déviées de la verticale : les composantes de l'écoulement sont essentiellement verticales ou horizontales. Les équipotentielles commencent à présenter des inflexions déviant de la verticale avec un facteur d'anisotropie de 50, mais celles-ci restent très limitées au niveau des extrémités des couches perméables. Ce n'est qu'avec un facteur d'anisotropie d'environ 100 (ou plus) que des variations significatives dans les profils verticaux de charge hydraulique sont observables, là où se trouvent les couches perméables. Les variations dans les profils verticaux de charge semblent donc être d'abord tributaires de l'anisotropie du faciès peu perméable. Lorsque le facteur d'anisotropie augmente, la faible conductivité verticale ralentit la progression verticale de l'écoulement, d'où la composante bidirectionnelle de celui-ci. Par contre, les profils demeurent relativement droits entre les couches perméables (i.e. au niveau des discontinuités).



**Figure 2.7** Cas hétérogènes anisotropes avec une couche perméable discontinue s'insérant dans la matrice silteuse. La matrice peu perméable présente un facteur d'anisotropie  $K_h/K_v$  de : a) un ordre de grandeur (10) ; b) un ordre de grandeur et demi (50) ; et c) deux ordres de grandeur (100). Les flux au sommet et à la frontière droite sont de : 8.5 et 85 mm/an, 8 et 80 mm/an et 7 et 70 mm/an, respectivement.

Puisque le facteur d'anisotropie joue un rôle clé dans la distribution des charges, le contraste de  $K$  nécessaires entre les 2 HF dans un contexte anisotrope a été évalué. En maintenant un facteur d'anisotropie de 100 pour l'HF peu perméable, les résultats d'un contraste de  $K$  de 1, 1.5 et 2 ordres de grandeur entre les HF sont illustrés à la figure 2.8. Bien que certaines inflexions soient maintenant perceptibles avec un contraste de  $K$  d'un seul ordre de grandeur (par rapport aux cas isotropes), elles ne semblent généralement pas suffisantes pour être clairement identifiables par des mesures de terrain. Par contre, un contraste de  $K$  de 1.5 ordres de grandeur révèle maintenant des inflexions significatives des équipotentielles. Suivant la configuration particulière du modèle simplifié, les contrastes minimaux de  $K$  entre HF doivent être d'environ de 1.5 ordres de grandeur avec un facteur d'anisotropie de près de deux ordres de grandeur du HF moins perméable.

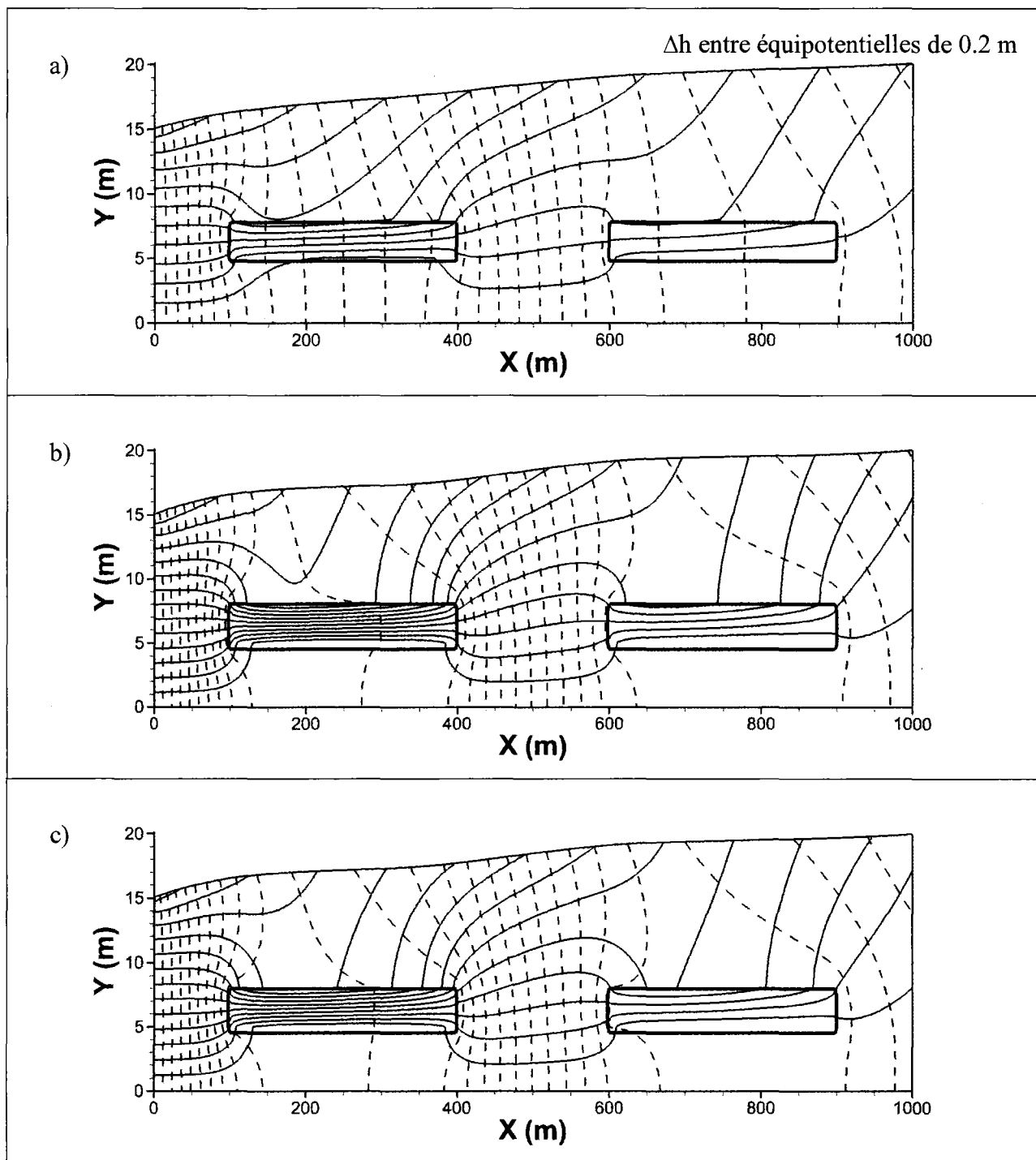


**Figure 2.8** Cas hétérogènes avec une couche perméable discontinue s'insérant dans la matrice silteuse avec un facteur d'anisotropie de 100. La couche perméable discontinue présente un contraste de  $K$  avec le silt ( $10E-6$  m/s) de : a) un ordre de grandeur ( $1E-5$  m/s) ; b) un ordre de grandeur et demi ( $5E-5$  m/s) ; et c) deux ordres de grandeur ( $1E-4$  m/s). Les flux au sommet et à la frontière droite sont de : 5.5 et 55 mm/an, 6 et 60 mm/an et 7.0 et 70 mm/an, respectivement.

Enfin, les impacts de deux autres facteurs ont été évalués, soit l'orientation générale des flux et les gradients globaux du système d'écoulement (figure 2.9). Dans le premier cas, la déviation des équipotentiels est nettement moindre que pour le cas avec recharge au sommet du modèle; les déviations se limitent aux extrémités des couches (sur environ 100 m). Ainsi, l'orientation de l'écoulement par rapport aux couches a un impact significatif sur les profils de charges résultants. Ces résultats suggèrent que dans le cadre d'une problématique où l'on voudrait préciser la distribution de  $K$  pour un système d'écoulement et des couches perméables essentiellement horizontales, les profils de charge ne seraient pas des mesures d'un apport particulièrement significatif puisque l'étendue des secteurs présentant une déviation des charges verticales serait très limitée.

Dans le second cas (figure 2.9 b), le ratio de flux entrant au sommet (recharge) par rapport à la frontière droite est le même, mais cette fois ces flux sont augmentés afin de doubler le gradient global du système (0.01 m/m ou  $\Delta h$  total de la nappe de 10 m). Comme les mêmes contrastes de  $K$  et facteurs d'anisotropie sont appliqués (100), les changements aux équipotentiels sont dus à l'augmentation des gradients hydrauliques. La distribution des charges hydrauliques présente des variations verticales sur pratiquement tout le modèle, mis à part à proximité de l'exutoire où une condition limite de charge fixe est imposée. Ainsi, l'utilisation des profils de charge hydraulique est plus favorable dans un contexte où les gradients hydrauliques sont suffisamment élevés.

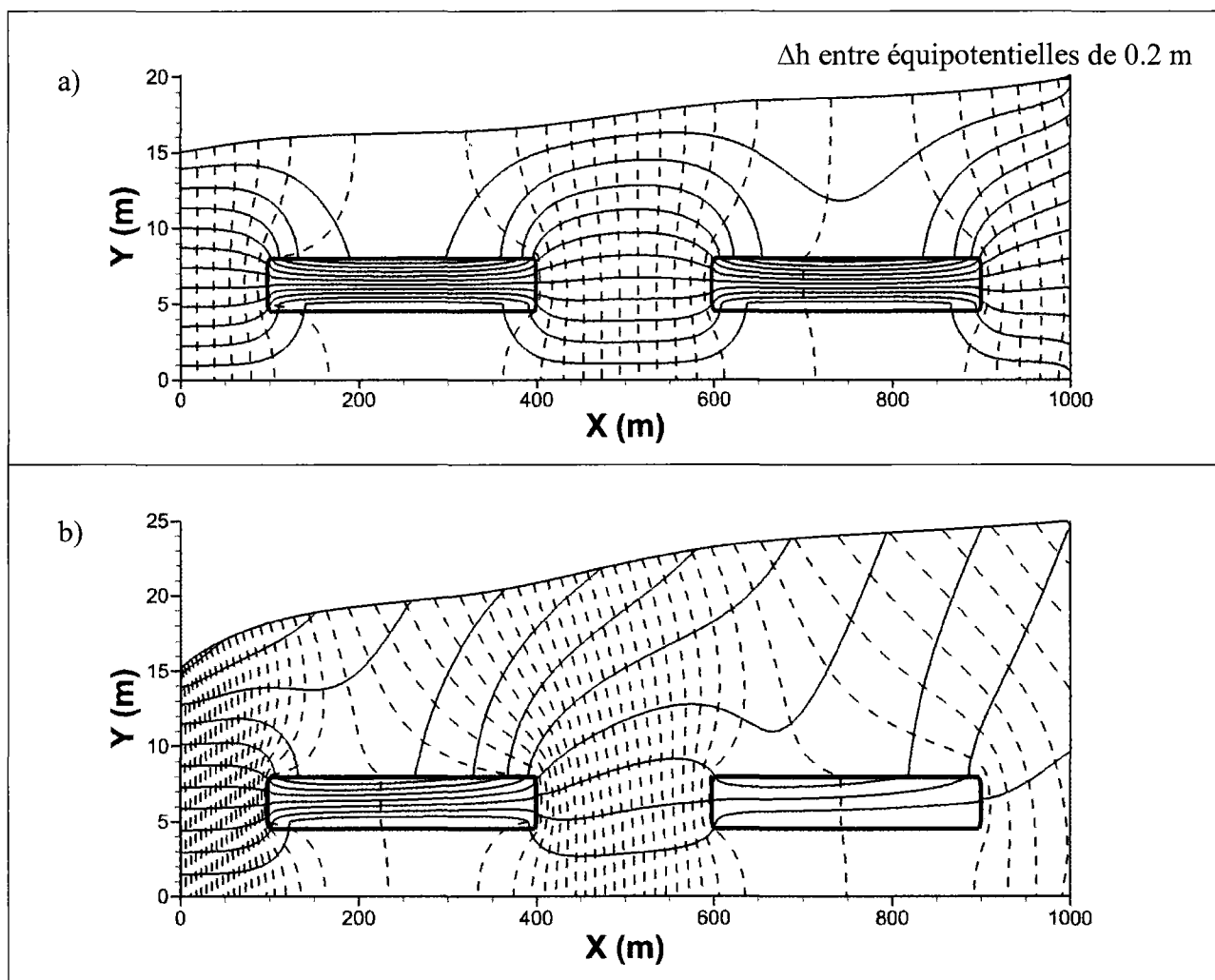


**Figure 2.9** Cas hétérogènes avec une couche perméable discontinue s'insérant dans la matrice silteuse avec un facteur d'anisotropie et un contraste de K entre HF de 100 pour le cas où : a) le flux entrant provient seulement de la frontière droite (pas de recharge au sommet) ; et b) les flux entrant sont augmentés de telle sorte que le gradient global du système soit le double, soit 0.01 (ou une élévation de la nappe de 25 m à droite). Dans ce cas, le même ratio de flux au sommet par rapport au côté droit a été respecté.

### 2.1.3 Implications pour la modélisation du site d'étude

Les simulations précédentes mettent en lumière certaines propriétés et conditions nécessaires afin que l'utilisation de profils de charges hydraulique puisse être utile à la définition de la distribution de la conductivité hydraulique d'un aquifère. D'abord, un ordre et demi de grandeur de contraste des valeurs de K des HF est requis, alors que le facteur d'anisotropie des HF moins perméables doit être approximativement de deux ordres de grandeur (ou davantage). Ces

conditions sont assez restrictives en termes de potentiel d'application des profils de charges hydrauliques. Par contre, plusieurs conditions du système aquifère peuvent favoriser ou atténuer les variations verticales dans les profils de charge. D'une part, des systèmes où les gradients sont généralement modérés ou forts sont plus favorables à des variations mesurables des charges dans les profils. Même lorsque les gradients régionaux sur une échelle kilométrique sont relativement faibles, il est possible que les gradients des écoulements locaux soient suffisamment élevés pour produire des modifications de charges attribuables à l'hétérogénéité de plus proche surface.

Par ailleurs, la présence de couches continues ou discontinues peut passer inaperçue dans un contexte où l'orientation de l'écoulement est parallèle par rapport à celui des couches. Pour des systèmes aquifères dans un climat humide, la recharge est moins sensible aux conditions de la proche surface (de Vries & Simmers, 2002); la distribution de la recharge est généralement diffuse par opposition à une recharge plutôt localisée dans les régions (semi-) arides (Scanlon *et al.*, 2002). Ainsi, une recharge distribuée en milieux humides sera généralement favorable aux variations verticales des charges hydrauliques en ajoutant une composante verticale à l'écoulement. Finalement, le niveau de complexité du système d'écoulement associé au degré d'hétérogénéité du champ de  $K$  affectera la variabilité verticale des profils de charge. La faible variabilité dans l'orientation et la distribution des couches perméables dans ces exemples synthétiques sont possiblement des conditions défavorables à l'utilisation diagnostique de la distribution des charges hydrauliques. Encore une fois, ces exemples illustrent la sensibilité relativement faible des charges relativement aux changements importants de  $K$ , alors que celles des vitesses et du temps de résidence est élevée. De Marsily *et al.* (2005) rappellent qu'en considérant un aquifère stratifié avec un écoulement parallèle aux couches, l'hétérogénéité verticale ne produit aucune variation verticale dans la distribution des charges alors que les vitesses peuvent varier significativement d'une couche à l'autre. Ces auteurs soulignent ainsi la quasi-impossibilité d'inférer l'hétérogénéité de  $K$  à partir des seules données de charge hydraulique.

Certaines limitations de ces simulations synthétiques peuvent en affecter les résultats, telle la modélisation en deux dimensions qui néglige la possibilité que l'écoulement puisse contourner latéralement un secteur moins perméable localement. Au-delà des contrastes de  $K$  nécessaires entre les HF, les résultats démontrent que la distribution des charges hydrauliques est d'abord tributaire de l'anisotropie des HF moins perméables. C'est celle-ci qui déforme le champ de



charges hydrauliques et permet conséquemment de déduire la présence et distribution de couches plus perméables. Bien que ces résultats préliminaires soulignent l'applicabilité limitée des profils de charge, ils permettent malgré tout de préciser les conditions pour lesquelles l'utilisation des profils de charge pourrait être profitable. Les paramètres utilisés dans la modélisation devront tenir compte de ces résultats.

## 2.2 Site d'étude et description des données disponibles

Les travaux documentés dans cette section font partie d'un programme de caractérisation multidisciplinaire portant sur l'étude du transport de lixiviat dans les environs d'un ancien site d'enfouissement sanitaire, dont les principaux travaux sont résumés par Tremblay *et al.* (2013).

Le site d'étude est localisé à Saint-Lambert-de-Lauzon au Québec, à près de 35 km au sud de la ville de Québec. La zone d'étude comprend un ancien site d'enfouissement sanitaire municipal sur une étendue de près de 12 km<sup>2</sup> (figure 2.10).

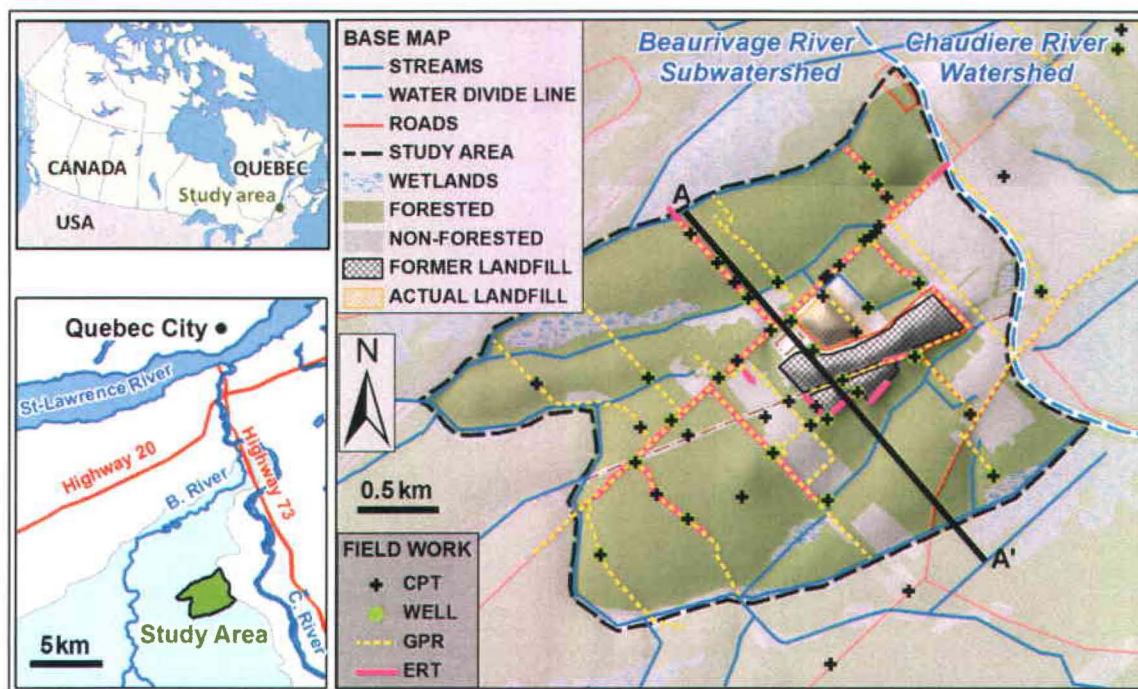


Figure 2.10 Site d'étude à Saint-Lambert-de-Lauzon (Québec) avec la représentation de l'ancien site d'enfouissement sanitaire, la localisation des puits et des profils géophysiques effectués (Tremblay *et al.*, 2013).

L'aquifère étudié est composé de sédiments quaternaires sur une épaisseur moyenne d'une dizaine de mètres, constituant un aquifère essentiellement non confiné. Cet aquifère doit l'hétérogénéité de ses dépôts sédimentaires aux processus sédimentaires complexes ayant mené à la présence d'une grande variété de types de sédiments (Parent *et al.*, 1999), qui vont des silts argileux jusqu'à des sables grossiers. Parmi les travaux de caractérisation réalisés, des essais de perméabilité *in-situ* à charge variable (*slug test*) ont été réalisés de façon détaillée à plusieurs niveaux pour quelques puits, où des sondages géophysiques au piézocône (*CPT-SMR*) colocalisés ont produit des données de résistance en pointe, de frottement, de résistivité et de teneur en eau. Des relations statistiques spécifiques au site ont été développées entre ces données géophysiques et les données de K colocalisées afin de pouvoir inférer K des seules données de sondages au piézocône (Paradis *et al.*, soumis). Ainsi, des données de K avec une résolution verticale de 15 cm sont disponibles aux 53 sondages au piézocône distribués sur l'ensemble du site. Par ailleurs, des données d'élévation de nappe aux puits ainsi que des profils verticaux de charge hydraulique ont été recueillis. Les données de K et d'élévation de la nappe ont supporté la production de modèles de référence présentés à la section suivante.

### 2.3 Construction des deux modèles de référence

L'étude du potentiel des données de profils verticaux de charge hydraulique afin de contraindre des réalisations géostatistiques de K est basée sur la calibration de profils de charge à partir de modèles de référence dont l'hétérogénéité est connue. Ainsi, la production de modèles de référence plus complexes et potentiellement représentatifs du système d'écoulement d'un vrai site d'étude permet d'analyser ce potentiel dans un contexte plus réaliste. Les principales étapes pour la production des modèles de référence sont développées en détail dans la section 3.5 et résumées ici :

- 1) Construction des modèles hydrogéologiques initiaux :
  - i. Sélection d'une ligne d'écoulement pour la localisation de la modélisation en 2D (coupe A-A' sur figure 2.10);
  - ii. Projection des profils de K tirées des données de sondages au piézocône (CPT/SMR) sur la coupe et de la distribution d'hydrofaciès (HF);

- iii. Production de réalisations de champs d'HF par statistiques multi-points avec ISATIS (Geovariances, 2012);
- 2) Sélection et développement de deux modèles de référence, dits *continu* et *discontinu* : regroupement de trois HF peu perméables en un seul et attribution de valeurs homogènes intra-HF de  $K_h$  et  $K_v$ ;
- 3) Calcul de l'écoulement sur les deux modèles numériques (*continu* et *discontinu*):
  - i. Simulations d'écoulement avec une nappe libre (incluant la zone non-saturée) pour chaque modèle;
  - ii. Calibration de la recharge en fonction des données d'élévation de la nappe recueillies sur le site d'étude;
  - iii. Extraction de l'élévation de la nappe simulée des deux modèles de référence calibrés;
  - iv. Nouvelles simulations d'écoulement (2) avec une condition de charges fixes (type 1) à la surface du modèle, correspondant à la nappe simulée (milieu saturé seulement);
  - v. Extraction des profils verticaux de charge hydraulique des 2 modèles de référence calibrés et à nappe fixe;
- 4) Évaluation préliminaire des contrastes de  $K$  nécessaires avec un niveau d'anisotropie fixe.

Une fois les modèles de référence construits et la distribution des charges hydrauliques générée par les simulations d'écoulement, les données de  $K$  et de charge hydraulique qui en découlent ont été considérés comme des observations. La suite de ces travaux porte sur la modélisation synthétique réalisée à partir des modèles de référence pour vérifier le potentiel d'application des profils de charge (sections 3.6 à 3.10).

## NOTICE

The following chapter is not intended for article submission in such a long format; it should be divided in two separate articles on: **1) Generating geostatistical HF models representative of the study site (3.1 to 3.5), and 2) Selection and calibration of K realizations based upon detailed vertical hydraulic head profiles (3.6 to 3.10)**

### **3 USING VERTICAL HEAD PROFILES TO CONSTRAIN THE GEOSTATISTICAL REPRESENTATION OF HETEROGENEITY IN A SHALLOW GRANULAR AQUIFER**

Patrick Brunet<sup>1</sup>, René Lefebvre<sup>1</sup>, Daniel Paradis<sup>1&2</sup>, Erwan Gloaguen<sup>1</sup>, Laurie Tremblay<sup>1</sup>

<sup>1</sup> *Institut national de la recherche scientifique, Centre Eau Terre Environnement (INRS-ETE), 490 rue de la Couronne, Québec, QC, Canada G1K 9A9*

<sup>2</sup> *Geological Survey of Canada, 490 rue de la Couronne, Québec, QC, Canada G1K 9A9*

#### **3.1 Introduction**

Numerical models must represent the spatial distribution of relevant hydraulic aquifer properties at the scale of the problem at hand to provide a realistic description of groundwater flow and mass transport. To obtain such an accurate spatial distribution of hydraulic properties, geostatistical simulations are commonly used as they provide multiple equiprobable estimates of property values and their uncertainty. Geostatistical realizations satisfy field data regarding property values and reproduce the expected spatial structure of these properties, through the use of two-point spatial covariance (Matheron, 1963) or multiple-point statistics (Strebelle, 2002). Representation of the spatial distribution of hydraulic parameters, such as hydraulic conductivity (K) and porosity (n), is a critical aspect of hydrogeological numerical modeling. Geostatistical simulation goes one step further than parameter estimation, providing a range of possible parameter distributions and related uncertainties.

The heterogeneity of hydraulic properties in granular aquifers is the result of complex sedimentary processes. This heterogeneity affects groundwater flow and mass transport at different scales. Koltermann and Gorelick (1996) suggest that the large scale structure of hydraulic conductivity controls the path of groundwater flow and advective mass transport, whereas small scale variability controls mass dispersion. Moreover, hydraulic conductivity may span several orders of magnitude on a same study site (e.g. Freeze & Cherry, 1979; Koltermann & Gorelick, 1996; Sudicky *et al.*, 2010), whereas porosity varies on a much smaller scale. Thus, characterization of hydraulic parameter heterogeneity generally focuses more on K. Modeling issues relating to mass transport generally require a more detailed definition of heterogeneity than when only flow is considered, as the impact of connected features is determinant on mass transport fate (De Marsily *et al.*, 2005). Identification of connected features such as flow barriers or preferential flow paths remains an important challenge in hydrogeology.

Hydrofacies (HF) are geological units of distinct hydraulic properties (Frei *et al.*, 2009; Ouillon *et al.*, 2008). Defining the spatial distribution of HF enables to reproduce their connectivity while allowing abrupt geometry and property changes, rather than generating continuous geostatistical parameter fields (De Marsily *et al.*, 2005). Such representation is especially important when dealing with groundwater contamination involving mass transport from source zones to receptors on an intermediate scale of a few hundreds to a few kilometers square. At such a scale, the definition of the spatial distribution of HF also facilitates the representation of hydraulic property heterogeneity (e.g. Fleckenstein *et al.*, 2006; Ouillon *et al.*, 2008). Many common geostatistical simulation methods enable the simulation of the spatial pattern of HF with many equiprobable realizations. These include indicator sequential simulation (Emery, 2004; Journel & Alabert, 1989), pluri- and truncated gaussian simulation (Galli *et al.*, 1994; Mariethoz *et al.*, 2009), transition probability simulation (Carle & Fogg, 1996; Carle, 1999) and multiple-point simulation (Hu & Chuginova, 2008; Straubhaar *et al.*, 2011; Strebelle, 2002). These approaches allow the conditioning of geostatistical simulations to hydraulic property data and the integration of prior geological knowledge. Afterward, representation of hydraulic properties and small scale structure within each HF can be defined according to the required spatial resolution level of the problem.

Although the computed realizations of HF or hydraulic parameters are all theoretically equiprobable in terms of property data and prior structure representation, they are not hydraulically equiprobable. The spread of uncertainty of the geostatistical realizations is not linked to the hydraulic uncertainty but represents the maximum entropy. Whether in a deterministic or stochastic setting, the validity or representative nature of generated spatial distributions of parameters has to be properly assessed in numerical flow and transport models relative to modeling objectives. This assessment is based upon the capacity of numerical models to reproduce observed state variables, i.e. the agreement between simulation results and field observations (e.g. heads or concentrations). Thus, in order to produce one or many optimal parameter distributions from previously generated geostatistical realizations, flow and transport simulation results are used for parameter calibration. The latter is consequently an inverse modeling approach. However, as the number of parameters to calibrate generally greatly outnumbers the observed state variables, direct solving of the inverse equations is almost impossible (Zhou *et al.*, 2014). This issue has led to the development of many iterative inverse numerical methods over the past decades (Carrera *et al.*, 2005; De Marsily *et al.*, 1999; McLaughlin & Townley, 1996; Zhou *et al.*, 2014), which enable automatic calibration of model parameters.

The hydraulic plausibility of model parameter distributions thus relies on the sensitivity of the state variables to model parameters. Consequently, it is imperative that inverse modeling in hydrogeology be done with state variable measurements that are sampled to be sensitive to parameter heterogeneity at the study scale. However, state variable observations are generally scarce and may provide integrative information on parameter heterogeneity. Data commonly used in hydrogeology for hydraulic parameter calibration of models show uneven sensitivity according to the given parameter and problem setting; state variables may enclose low information content on parameter values (Carrera *et al.*, 2005).

### **Data needed for numerical model calibration**

From manual iterative calibration of homogeneous model parameters in the early ages of numerical hydrogeological modeling to today's automatic inverse procedures, **hydraulic heads** measured in wells have long been the sole data used for model calibration (Anderson &

Woessner, 1992). With the development of stochastic inverse methods, ill-posedness of most numerical problems in hydrogeology has entailed specification of certain suppositions and additional constraints (Zhou *et al.*, 2014). Using only mean hydraulic heads in the inverse procedure for definition of heterogeneous model parameters yields non-unique or instable solutions, as the result of discrepancy between the number of data and parameters to estimate and the low sensitivity of head observations to parameters (K). As adding more head observations in steady-state modeling may not significantly improve the estimated heterogeneity representations, including a small number of other data types such as dissolved concentrations could prove more valuable (McLaughlin & Townley, 1996).

In order to better reproduce the actual distribution and connectivity of hydraulic parameters, data included in the calibration procedure must be sensitive to parameter values along the entire flow path. For instance, adding **flux data** to hydraulic heads in the calibration procedure generally increases the sensitivity to transmissivities (Carrera *et al.*, 2005). Moreover, including flux data helps alleviating the strong correlation between hydraulic conductivity (K) and recharge (R), which facilitates calibration of a unique model (Poeter & Hill, 1997). Nevertheless, flux data at boundaries (recharge or discharge) are integrative; they may stabilize the inverse problem but not resolve its non-unicity.

Benefits of integrating **transient head** data in numerical inverse approaches have been demonstrated, as the reduction of errors in state variable predictions may be significant (e.g. Carrera & Neuman, 1986; Sun & Yeh, 1992). Initially used for calibration of parameter values, transient head data were more recently exploited to estimate the spatial distribution of K. For example, Wiese and Nützmann (2011) use transient heads during pumping tests to define the distribution and continuity of an aquitard between two aquifers, while Ronayne *et al.* (2008) used the same type of data to constrain realizations of high-permeability channels. As integrating a large volume of time-varying data may prove computationally inefficient for large heterogeneous models, use of an Ensemble Kalman Filter (EnKF) approach can considerably alleviate this burden (Xu *et al.*, 2013; Zhou *et al.*, 2011).

Mass transport is sensible to hydraulic parameter values and their spatial distribution, particularly to hydraulic conductivity. Thus, use of dissolved mass or geochemical **tracers** can provide information on spatial connectivity between wells, while transient heads carry

information on K distribution in well vicinity (Llopis-Albert & Capilla, 2009a; Wen *et al.*, 2002). However, in many cases the time required for such tracer experiments in order to provide representative answers is considered excessive (De Marsily *et al.*, 2005).

Isotopic tracer data can provide information on groundwater **age** or residence time, e.g. tritium-helium or  $^{14}\text{C}$  methods (Murphy *et al.*, 2011; Sanford *et al.*, 2004). In order to compare age data with representative simulated ages, Goode (1996) developed a direct numerical simulation approach to obtain the spatial distribution of mean age (as age "mass"), which considers both advective and dispersive processes. Evaluation of model performance relative to age data is somewhat more complex, as dispersion and mixing processes in combination with measurement error and potential source variations proscribes use of age data in automatic quantitative calibration procedures (Sanford, 2011; Varni & Carrera, 1998). Thus, age reproduction in model calibration procedures is quasi-systematically poorer than that of head data (Sanford, 2011). Nevertheless, since age data is very sensible to heterogeneity of flow systems as in the presence of low permeability layers, Sanford (2011) still suggests their use in one or two dimensional models. For example, Millet *et al.* (2013) have identified the more representative heterogeneous 2D hydraulic conductivity field of a contaminated aquifer using age data ( $^3\text{H}$ - $^3\text{He}$ ).

**Geophysical methods** have long been used to help define or constrain aquifer large-scale structure. However, recent research demonstrates that geophysical data can be used as direct constraints within the inverse procedure for representing heterogeneity of K fields. For example, Straface *et al.* (2011) include hydraulic head data and spontaneous polarization (SP) in a joint inversion scheme to characterize the heterogeneity of K of a 3D aquifer model.

The aforementioned data types all exhibit advantages and limitations relative to the specific problem at hand. Using such data can help validate the hydraulic plausibility of stochastic realizations generated from K data. However, these data either remain integrative information on K heterogeneity, relatively long and costly to acquire or cannot be integrated automatically in inverse calibration procedures. Thus, there is still a need for evaluating the hydraulic plausibility of geostatistical realizations of heterogeneous aquifers from simple and direct data.

Water levels commonly used for parameter calibration are mean values over the entire well, which possibly intercepts various materials with distinct hydraulic properties. Trying to extract detailed information on the spatial variability of hydraulic properties in heterogeneous settings



from such water level data is mathematically implausible in the context of ill-posed problems (De Marsily *et al.*, 2005). Nonetheless, local vertical distributions of hydraulic heads may be sensitive to variations in K fields under certain circumstances, as suggested in the nonlinear relationship between K and heads in flow equations. However, the local distribution of heads do not solely depend on K distribution but also on boundary conditions, K contrasts and anisotropy (Freeze & Cherry, 1979). Thus, the potential of detailed vertical profiles of hydraulic heads to improve the representation of the spatial distribution of K needs to be assessed.

### 3.2 Study objectives

The main objective of this study is to assess the potential use of detailed vertical head profiles to constrain geostatistical representations of K heterogeneity, using for that purpose an example of geostatistical K simulations of a shallow granular aquifer. Thereby, this work aims at developing and verifying the potential of an approach that could be used to assess the hydraulic plausibility of heterogeneous HF and K fields that are integrated in a numerical groundwater flow model. The latter can predict the spatial distribution of hydraulic heads, which can be compared to detailed vertical profiles of head observations. As connectivity of high permeability features exerts a strong control on flow and particularly mass transport, the capacity of such an approach to reproduce HF (dis)continuity is of utmost importance. Secondary objectives arising from the main objectives are summarized as follows:

1. Assess the use of the vertical distribution of hydraulic heads as a potential indicator of HF distribution and continuity;
2. Assess the application of observed versus simulated head differences from vertical profiles for the selection and calibration of stochastic geostatistical realizations of heterogeneous K fields;
3. Analyze the effects of HF continuity, K contrasts between HF and horizontal spacing of head profiles on resulting calibrated numerical model.

### 3.3 Methodology

To verify the utility of vertical head profiles as potential indicators of aquifer heterogeneity, two synthetic reference numerical flow models were developed with geostatistical and numerical modeling approaches, on the basis of actual data collected from a real field site. These two reference models, which have been further considered as representing the “true” field conditions, were taken as end-member set of conditions from geostatistical realizations of the system displaying distinct levels of hydrofacies continuity. The reference model conditions were thus obtained using an intermediate approach between a real and a synthetic case.

The approach used in this work includes two distinct parts: 1) construction of two realistic reference aquifer models with distinct spatial distributions and continuity of hydrofacies; and 2) generation of multiple geostatistical HF realizations from these reference models and exploitation of discrepancies in observed and simulated vertical head profiles produced from steady-state flow simulations. Realization selection or calibration techniques have been used in order to obtain HF realizations that allow a better reproduction of the head profiles when integrated in a numerical groundwater flow model. For numerical model calibration, the global gradual deformation method and a heuristic approach inspired from the pilot-point method have been assessed. These main steps are detailed in figure 3.1.

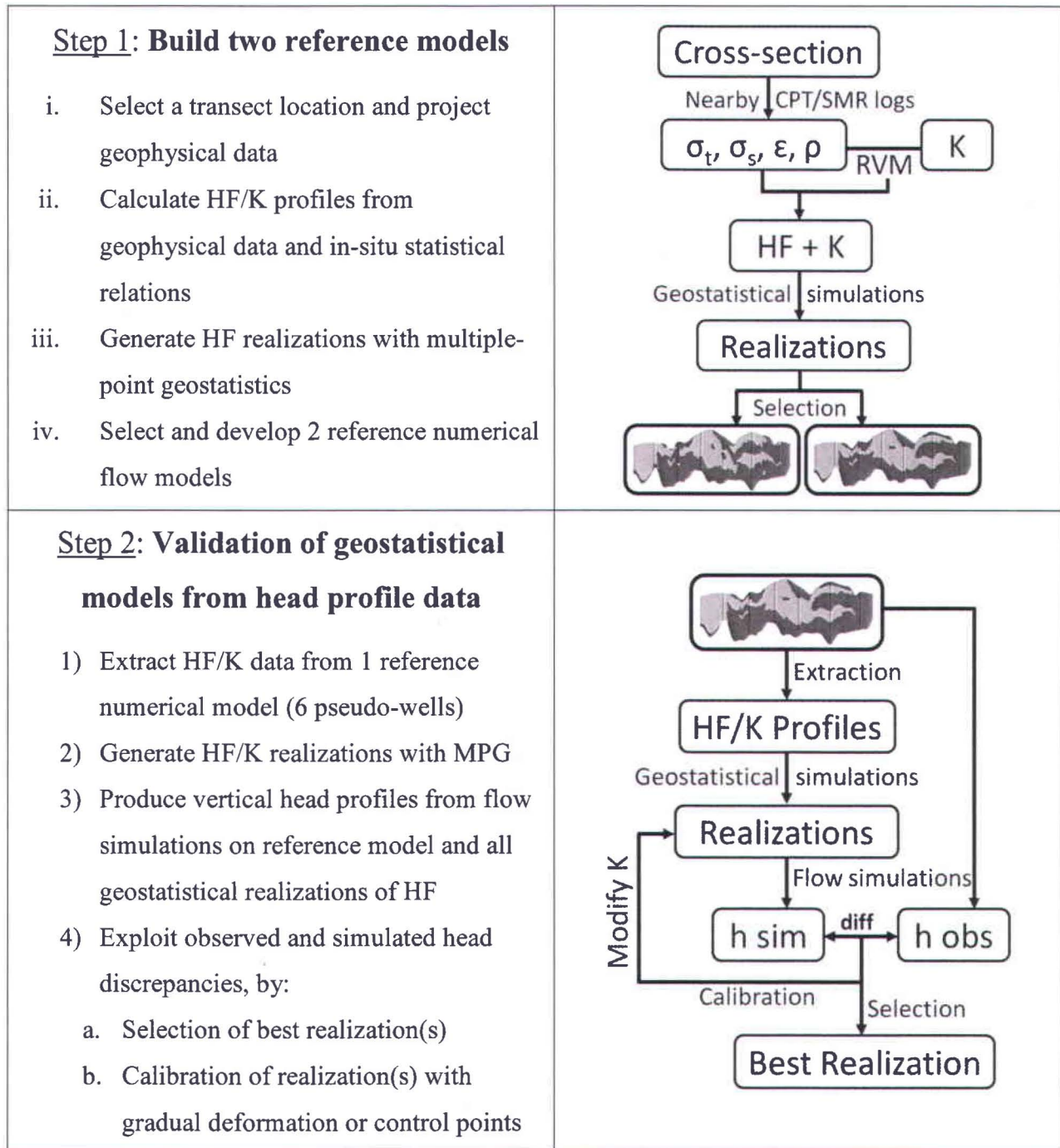


**Figure 3.1** Main workflow steps for assessing the potential of hydraulic head profiles to constrain representations of HF distribution, through synthetic simulations based upon realistic reference models.

### 3.4 Study site and available data

The work documented in this paper is part of a multidisciplinary characterization program aiming to study the transport and fate of leachate in the surroundings of a former landfill (Tremblay *et al.*, 2013; Paradis *et al.*, 2014).

#### 3.4.1 Study site description

The study site is located in Saint-Lambert-de-Lauzon, Quebec (Canada), 35 km south of Quebec City. It covers a 12 km<sup>2</sup> sub-watershed of the Beaurivage River surrounding a decommissioned municipal landfill (figure 3.2).

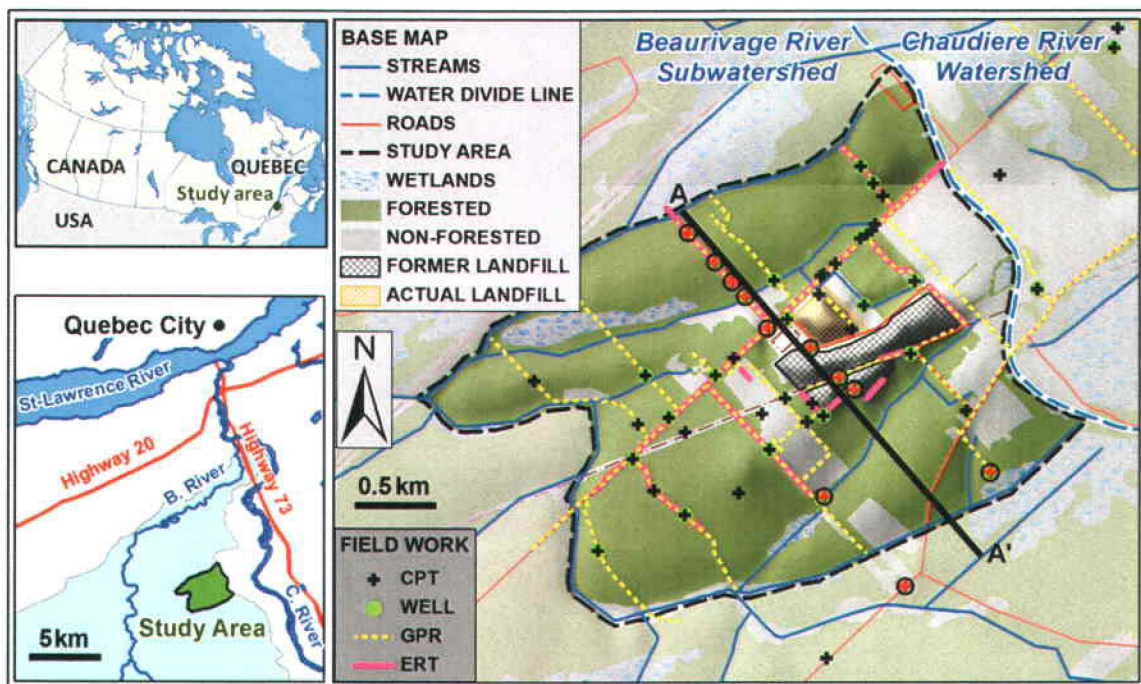


Figure 3.2 Saint-Lambert-de-Lauzon (Quebec) study area (adapted from Tremblay *et al.*, 2013).

The decommissioned Saint-Lambert-de-Lauzon landfill was operated during 24 years, from 1974 to 1997. During this period, the wastes were placed directly on a 10 m thick unconfined aquifer, which has led to the generation of a leachate plume. An extensive characterization program was

initiated in 2006 to delineate the plume and assess the efficacy of the natural attenuation of the plume. The aquifer is composed primarily of surficial quaternary sediments 5 to 20 m thick that were deposited and reworked by the Champlain Sea (Bolduc, 2003). These sediments consist mostly of fine to medium sand, but sediments can range from coarse sand to clayey silt (Paradis, 2010). During deposition, the system was controlled by sea tides and currents, as well as by the Chaudière River current and sediment supplies. This complex depositional environment is responsible for the heterogeneity of the aquifer material (Parent et al. 1999) and the presence of a wide range of sediment types.

Site characterization was carried out while focusing on the integration of multiple data sources (Tremblay *et al.*, 2013). Data from ground penetrating radar (GPR) profiles, electrical resistivity tomography (ERT) and CPT soundings have been integrated in 3D for supporting numerical model building (Bélanger *et al.*, 2010), whereas GPR velocity fields have been inferred from collocated-cokriging of direct-push permittivity and resistivity logs and GPR profiles (Gloaguen *et al.*, 2012). Detailed characterization of the heterogeneous distribution of hydraulic properties (Paradis *et al.*, accepted) at the study scale (12 km<sup>2</sup>) required the development of new characterization approaches (Paradis *et al.*, in correction; Paradis & Lefebvre, 2013; Paradis *et al.*, 2011). Assessment of recharge distribution (Tremblay *et al.*, submitted) and groundwater geochemistry (Tremblay, 2013) has entailed further understanding of the aquifer system.

### **3.4.2 Slug-tests and geophysical soundings**

During the characterization program, multi-level slug tests were conducted to collect K data along wells on 280 intervals (figure 3.3). The left figure (13a) shows the field set up, consisting of two packers on each side of a screened 15-cm section, which is the same as up-scaled data collected from collocated cone penetration tests (CPT), soil moisture and resistivity (SMR) soundings. The central figure (13b) shows an example of tip stress from a CPT sounding and the corresponding Eslami-Fellenius material types (Eslami & Fellenius, 1997). The corresponding K measurements for a well on the right figure (13c) illustrate the relatively weak relation between the material types and the K values. This has triggered the development of a data integration approach based on learning machines to predict HF and Kh from CPT/SMR data (Paradis *et al.*, submitted). Besides K measurements, multi-level slug tests also provided detailed profiles of

hydraulic head; noticing the effect of  $K$  on these head profiles triggered the idea of exploiting this type of data to constrain the geostatistical simulation of HF or  $K$  heterogeneity.

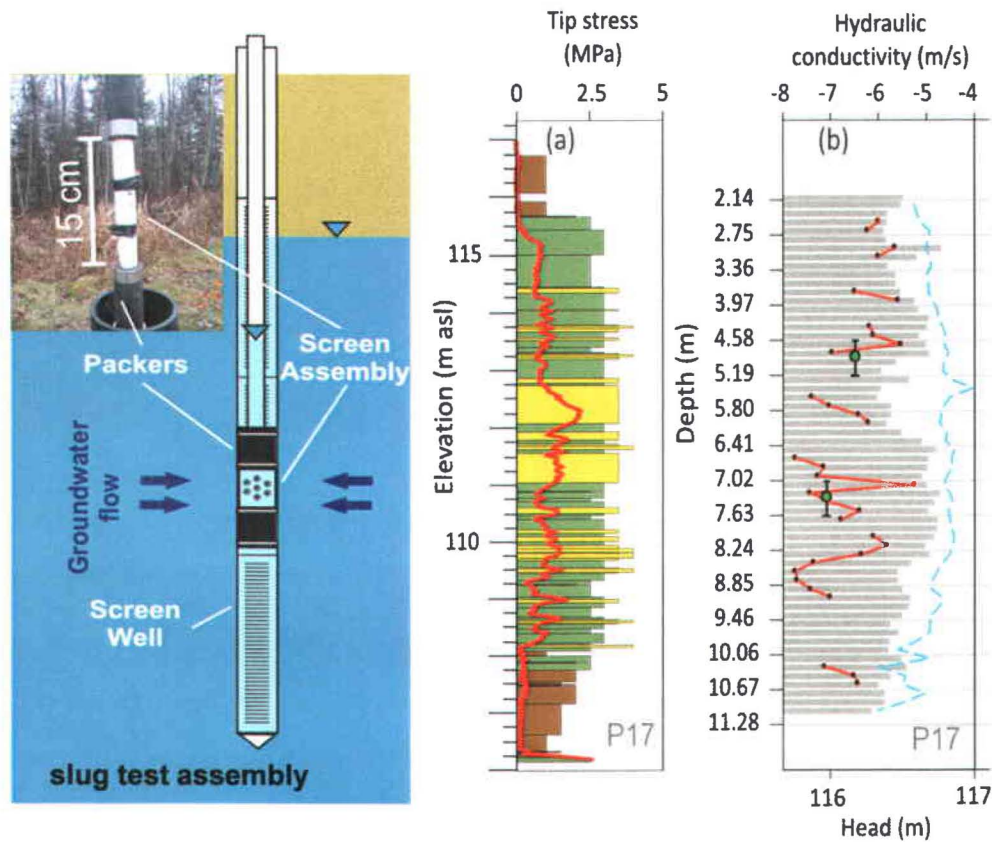


**Figure 3.3**  $K$  from Multi-level slug-tests: Schematic and field setup (left), with (a) Eslami-Fellenius material type and Tip stress from CPT log, and (b) Collocated detailed log of  $K$  values from multi-level slug-tests (Paradis et al., 2013).

### 3.4.3 Site-specific statistical relations developed between CPT/SMR data and $K$

Estimation of hydraulic data from CPT/SMR data considerably alleviates the load of the aquifer characterization, as this approach efficiently increases the spatial coverage of data acquisition. To estimate the hydraulic conductivity, a data integration approach proposed by Paradis et al. (2011; submitted) based on a learning machine (relevance vector machine) has been exploited to predict HF and  $K_h$  from CPT/SMR data. As the adopted learning machine approach is based on empirical site-specific relations, this circumvents simplifying suppositions of grain-size relations

with K. The main steps of this method to define hydro-geophysical relationships are illustrated in figure 3.4. The learning machine is composed of two main algorithms: unsupervised clustering (HF definition) and supervised classification (HF prediction) and regression (K prediction). Detailed explanations and rationale on this procedure can be found in Paradis et al. (2013 and submitted).

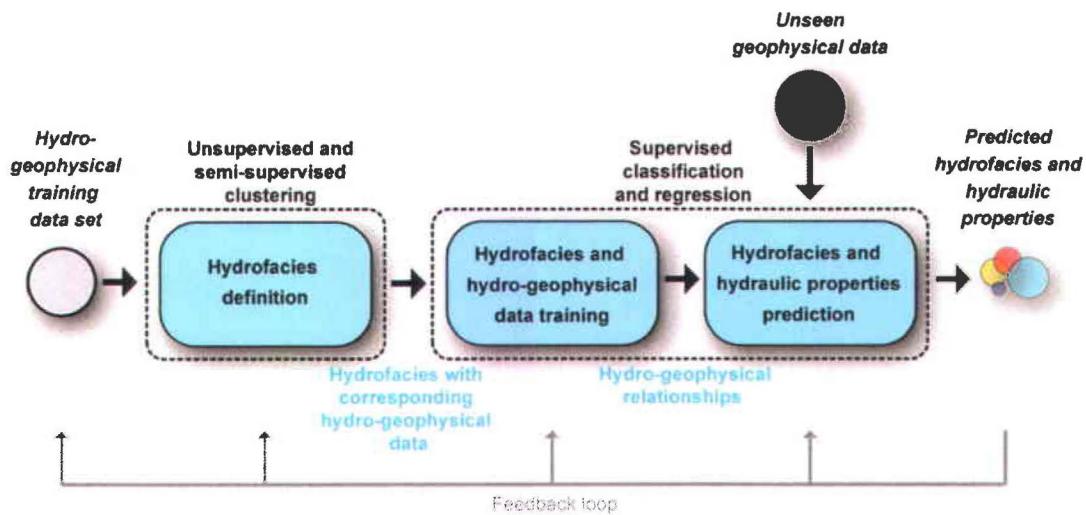


Figure 3.4 General steps in the learning machine that was used to define hydro-geophysical relationships for hydrofacies and hydraulic properties prediction from unseen geophysical data (Paradis et al. 2011).

### 3.4.4 Static and continuous (transient) vertical head profiles

In addition to this extensive dataset, detailed vertical head profiles were measured at eight selected wells. The field setup is quite similar to the packer slug tests (figure 3.3) but with multiple screens and packers to cover a larger section of the well. With pressure transducers and data loggers in each PVC well screen between packers, static measurements of hydraulic head are taken by sweeping across the entire length of a fully screened well. Based on field observations, a recording time of approximately 30 minutes between each measurement is sufficient for stabilization of heads in the lesser permeable intervals. Where significant deviations in the head profiles have been noticed, multi-level continuous monitoring of heads was recorded in seven wells over 16 intervals, for a period of over eight months.

A typical example of static and continuous vertical head profiles acquired in a well is presented in figure 3.5 with the corresponding lithology log of the well. On the left of this figure, the static head profile at a given time presents a significant head difference between the upper permeable layer (around 2 m depth) and the lower permeable layer (around 6 m depth) when referring to the log (figure 3.5, middle) showing the material type. These fluctuations in head profiles have been noticed in many monitoring wells. Moreover, the continuous monitoring of heads for these intervals (figure 3.5, right) reveals patterns of head fluctuations with time that are quite similar, although in this case a slight attenuation of the fluctuations is noticeable in the lower section due to the semi-confined condition of this layer. The cross-correlation of the monitored intervals for each of the eight wells is generally near to one, except under such semi-confined conditions (wells P5, P7 and P23) where cross-correlation drops down as low as 0.86 with time lags up to 34 hours (8 hour lag for deeper interval of well P5; figure 3.5 and figure 3.6). This type of information in continuous head profiles (attenuation and time lag) at certain well intervals could potentially be used as an indicator of the level of confinement and lateral continuity of confining layers, but this is not further discussed in this paper. Furthermore, despite the information contained in the acquired static and transient head profiles, lack of spatial and vertical coverage of these data over the study site has prevented their exploitation in this article.



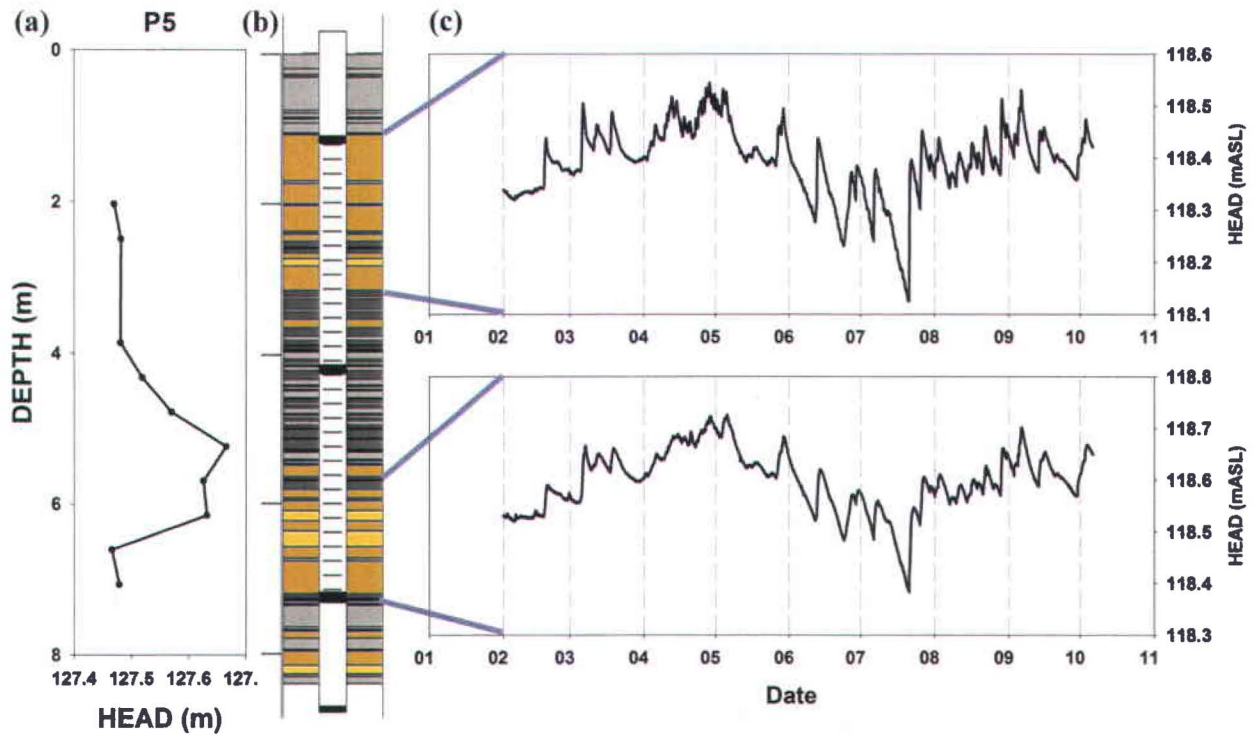


**Figure 3.5** Vertical head profile data acquired in a fully-screened well (P5): (a) Static head profile at a given time, (b) Eslami-Fellenius material type from CPT data, and (c) Continuous multi-level head data in intervals specified by the gray lines.

Nevertheless, the ratio of the heads between well intervals remains quite similar with time for all the monitored wells, suggesting the head profile shape or gradients are generally constant in time. These findings are in agreement with Meyer et al. (2008) and Fischer & Twining (2011) who have done multilevel groundwater monitoring of hydraulic head in rock and sediment aquifers, respectively. Overall, these preliminary field data on eight wells suggest that there might be a measurable effect of HF (or K) distribution on vertical head profiles and that static profiles should be generally have a similar shape over time.

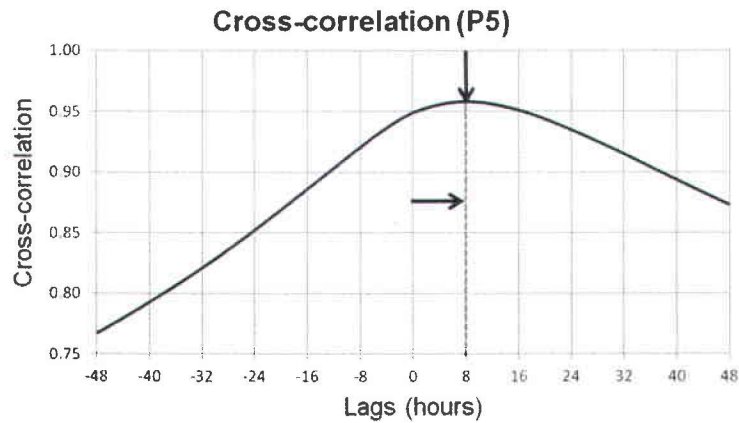


**Figure 3.6** Cross-correlation of continuous head data for upper and lower intervals for well P5.

### 3.5 Construction of the two reference models

To assess the potential of vertical head profiles to constrain geostatistical simulations of HF or K, synthetic head profiles were derived from two numerical flow models which have distinct HF distribution and continuity. Even though synthetic models are to be used, we aimed to follow as much as possible an approach similar to that of an actual field assessment of HF or K heterogeneity. The production of the two 2D reference models has thus been based on the available CPT/SMR logs and K data at the study site. First, stochastic realizations of HF distribution were generated with Multiple Points Geostatistics (MPG) honoring the site data. Then one “continuous” reference conceptual model and another “discontinuous” reference conceptual model, in terms of permeable HF connectivity, were developed based upon selected geostatistical realizations. The HF and K distributions of these reference conceptual models were then integrated in a numerical flow model. Flow simulations on these two reference models were then used to generate “observed” head distributions for later comparison with the ones that would be obtained using geostatistical simulations of HF (and K) based on the CPT/SMR logs. In fact, a comparison was made between head profiles at selected locations from the reference models and the corresponding ones based on geostatistical simulations, considering unconstrained and constrained geostatistical simulations by hydraulic head profiles. This approach has thus allowed an assessment of the potential for hydraulic head profiles to be used:

1) as a geostatistical model validation tool to identify realizations that are hydraulically plausible or not; or 2) as a constraint of the geostatistical models using two alternative approaches, global gradual deformation and a heuristic control point method.

### **3.5.1 Construction of initial hydrogeological models**

#### *3.5.1.1 Select transect location*

In order to produce results that are relevant in terms of hydrogeological setting of the study site, the location of a transect to be used for the development of the 2D conceptual models along a flow line was based on a piezometric map. The CPT/SMR data, site topography (DEM), rivers and impermeable till surface were mapped in GOCAD® (figure 3.7) to support the production of realistic and plausible reference conceptual models. The selected transect (A-A' figure 3.2 and figure 3.7) crosses the study domain NW-SE and is located near nine CPT/SMR soundings that are less than 150 m in the central and north-western part of the transect. For the south-eastern part, no CPT/SMRs are found in vicinity of the cross-section as this area has a very poor coverage of soundings due to access limitations. Nevertheless, three CPT/SMRs soundings up to 400 m distance have been projected on the cross-section to build the reference models. Since the study area is mostly flat, little rescaling of the projected geophysical logs was done to fit them into the cross-section bounding surfaces (topography and bedrock). The predicted HF distribution from CPT/SMR data (see next section) on these logs is illustrated in figure 3.7c.

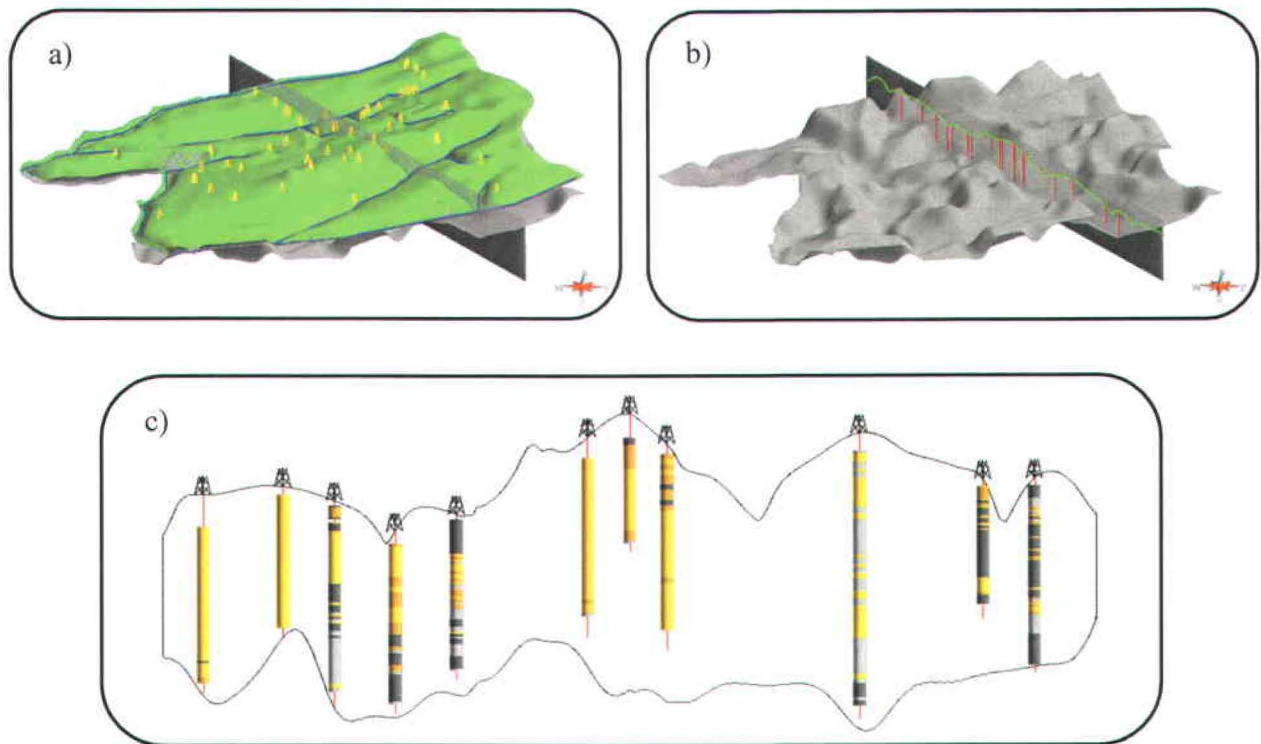


**Figure 3.7** Selected cross-section to build the 2D models: (a) Topography, bedrock, selected cross-section and CPT/SMR locations, (b) Projection of nearby CPT/SMR on the cross-section shown over the aquifer base topography, and (c) Predicted HF from CPT/SMR data along the section (see next section 3.5.1.2 ).

### 3.5.1.2 HF and K profiles from CPT/SMR logs

As mentioned above, empirical site-specific relations developed by Paradis et al. (2011; submitted) between CPT/SMR and hydraulic conductivity (K) data supported the estimation of HF class and hydraulic conductivity from the geophysical logs. Considering all the CPT/SMR and collocated Kh data acquired in the study area, HF and Kh prediction with training on a validation subset provided best parameters and number of HF classes (4) for subsequent prediction from CPT/SMR data alone (Paradis et al., 2013 and submitted). Running the learning machine algorithms (HF clustering, HF classification and K regression) with the projected CPT/SMR data yielded a significant overlap of predicted hydraulic conductivity for HF1, HF2 and HF3 (figure 3.8).

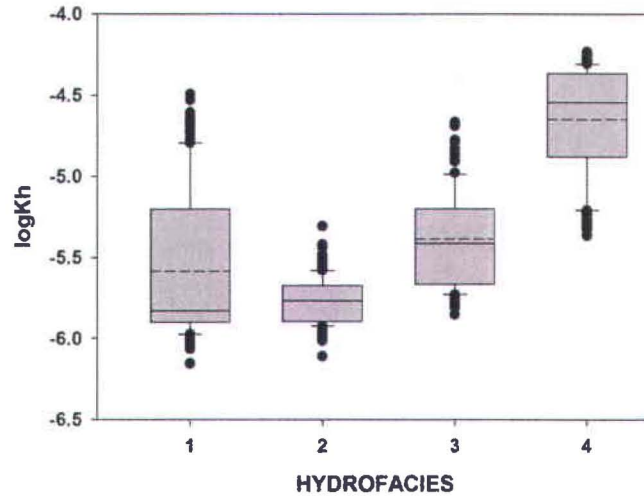


**Figure 3.8** Predicted horizontal hydraulic conductivity of four HF classes from the projected CPT/SMR data logs.

Classification and regression schemes with the study site data proved optimal with four HF classes, for best predictive capacity in preliminary testing of the algorithm. These preliminary results have hampered meaningful modeling of HF and K distribution, as the first HF has a predicted mean logK that differs by only 0.2 logK(m/s) with the second HF. Moreover, the standard deviation of HF1 is considerably large (0.463 log (m/s)) and encompasses entirely the logK distribution of HF2 and HF3 (table 3.1). Since these data have been produced, considerable improvement has been achieved for the site’s HF classification and K regression from CPT/SMR data (Paradis et al., submitted).

**Table 3.1** Statistics of predicted logK (K in m/s) for 4 HF classes with learning machine algorithms.

HF	Median logK (m/s)	Mean logK (m/s)	Std Dev logK (m/s)
1	-5.83	-5.58	0.46
2	-5.76	-5.77	0.14
3	-5.41	-5.38	0.29
4	-4.34	-4.65	0.33

### 3.5.1.3 Generate HF realizations with Multiple-Points Geostatistics

As the physical processes responsible for sediment deposition may be different at various scales and sedimentation events, generating numerical models with a single heterogeneity pattern throughout the study site at one scale may prove unsatisfactory. To tackle this difficulty, an increasingly common procedure in geostatistical modeling of heterogeneous fields is adopting a hierarchical approach: 1) modeling of the geological structure or large-scale heterogeneity and 2) generation of heterogeneous parameter distribution or local-scale heterogeneity (Blouin *et al.*, 2013; De Marsily *et al.*, 2005; Mariethoz *et al.*, 2009; Wellmann *et al.*, 2014). The first step of modeling geological structure or large-scale heterogeneity is an attempt to adequately capture and reproduce sedimentation events. The large scale heterogeneity can be assimilated to hydrofacies (HF) distribution, whenever the material deposited during a sedimentation event share common hydraulic properties. Rather than modeling complex physical processes responsible for the small scale heterogeneity within each HF, the local scale heterogeneity is commonly addressed with a random function model. Several methods have been developed in the last decades to simulate small-scale heterogeneity, such as the sequential gaussian simulation (Deutsch *et al.*, 1992), LU decomposition (Alabert, 1987; Davis, 1987) or simulated annealing (Deutsch & Cockerham, 1994).

In this study, the geostatistical modeling focused on generating larger scale structure (sedimentation events) conditioned to the study site data. Many simulation methods are related in the scientific list (e.g. dell'Arciprete *et al.*, 2012; Lee *et al.*, 2007). Here, the modeling focus was not as much on the length of structures nor on specific HF transitions, but rather on shape and connectivity of the permeable HF. Using multiple-points statistics has proven satisfactory and efficient in that matter, particularly as the initial data (HF logs) shows evident non-stationary HF distribution. A major difficulty with using multiple-points algorithms, namely producing a representative 3D training image, was circumvented since the modeling has been done in 2D. To provide a training image, the HF data from the 12 logs were kriged on a 2.8 km long stratigraphic grid in GOCAD® (figure 3.9). The choice of kriging to interpolate HF between the logs was based upon: 1) GPR profiles along this cross-section indicating flat layering; 2) an interpreted geological cross-section showing relatively continuous layering; and 3) the relatively dense data coverage of the cross-section (12 logs on 2.8 km). The stratigraphic grid of 19618 elements (table 3.2) is relatively fine in Z direction (mean cell thickness of 0.31 m) to ensure

proper representation of layering and eventually capture head profile variations at the same scale as the collected field data (0.3 m).

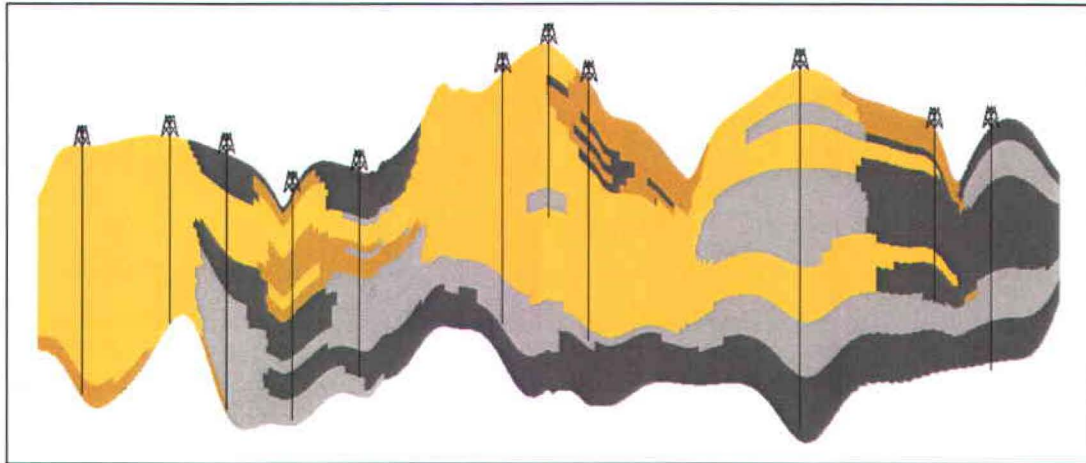


**Figure 3.9** 2D training image from kriging of HF from 12 CPT/SRM soundings.

**Table 3.2** Stratigraphic grid statistics (GOCAD®).

<b>Grid width (m)</b>	<b>Mean grid thickness (m)</b>	<b># cells</b>	<b>Mean cell thickness (m)</b>	<b>Cell width (m)</b>
<b>2857</b>	<b>10.56</b>	<b>19618</b>	<b>0.31</b>	<b>4.95</b>

The training image, well data and stratigraphic grid were transferred directly in ISATIS® with a plug-in extension fully integrated in GOCAD®, with XYZ to UVW coordinate transformation to perform multiple-point statistics and simulations along the stratigraphy. Then, various attributes and parameters can be used as spatial constraints in the multiple-point simulation implemented in ISATIS® (IMPALA) to guide the simulation process (table 3.3). Amongst the most significant attributes are the interpolated HF proportion map and the integration of auxiliary data (X or Z coordinates), which constrains the simulation process according weight factors. Other attributes such as the search neighborhood (Liu, 2006) or scan path type have significant effects on the HF continuity and distribution.

**Table 3.3** Some significant attribute specifications for MPG simulation with ISATIS® software for generating an ensemble of reference realizations.

<b>MP attributes</b>	<b>Value</b>	<b>Description</b>
HF proportions weight	0.4	Rather than correcting the simulations based on target proportions (servosystem correction; Liu, 2006), a weight factor is attributed to an interpolated map of well HF proportions. Overweighting this attribute produces very continuous HF realizations.
Auxiliary data	X coordinates	Adding auxiliary data such as X or Z coordinates can help reproducing trends in the training image. The HF distribution in the training image (and well data) is clearly non stationary in the X-direction.
Multiple grids	3	The use of multiple grids allows reconciling the small template size and the reproduction of long-range patterns (Hu & Chugunova, 2008; Strebelle, 2002). To do so, the simulation is done sequentially on coarse to fine grids.

Once the optimal set of attributes and parameters were found, 100 MPG realizations were imported back in the GOCAD® stratigraphic grid.

### **3.5.2 “Selection” and “development” of continuous and discontinuous conceptual models**

In order to assess the application of head profiles to validate geostatistical HF models with different levels of HF continuity, 2 reference models were selected with different HF distributions. The selected realizations are "end-members" in terms of HF continuity, named hereafter "continuous" and "discontinuous" reference models (figure 3.10). Although there was a relatively dense coverage of the cross-section with converted HF logs, 2 areas have significant differences of continuity, namely around 850 m and 1900 m where the layering of HF1 is interrupted by presence of other HF. In consequence, these HF distributions are expected to generate different flow patterns and head profiles near these areas.



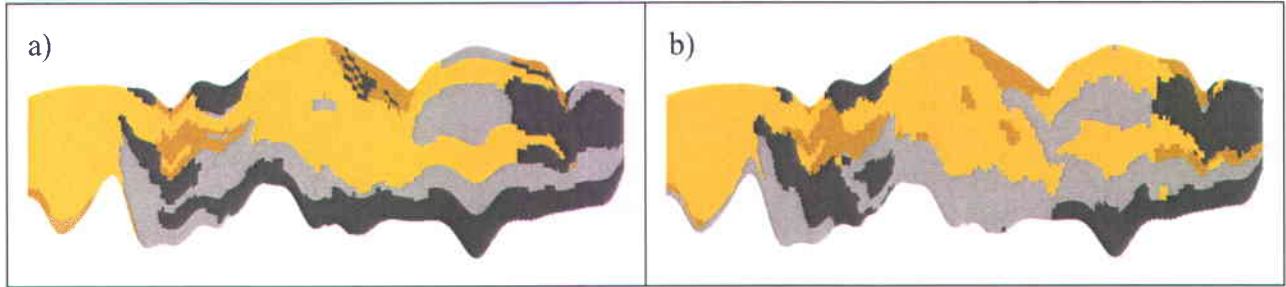


**Figure 3.10** Selected (a) continuous and (b) discontinuous reference models in terms of HF distribution.

As stated earlier (section 3.5.1.2), the HF and K profiles generated with the learning machine algorithms (Paradis et al., submitted) initially produced significant K overlap between HF, which may obscure the effect of layer continuity in assessment of head profile potential use. First, as the first three HF have a significantly lower mean and median K value, they have been merged into one unique HF. As the recognition of small-scale heterogeneity is beyond the scope of this study, homogeneous values of K have been attributed rather than simulating K fields within each HF. This simplification avoids blurring the simulation results by isolating the effects of layer continuity. However, simulation of small-scale heterogeneity would have been crucial if subsequent transport simulation had been considered. The K values attributed to HF1 and HF2 are  $-4.34$  and  $-5.66 \log K$  (m/s), respectively.

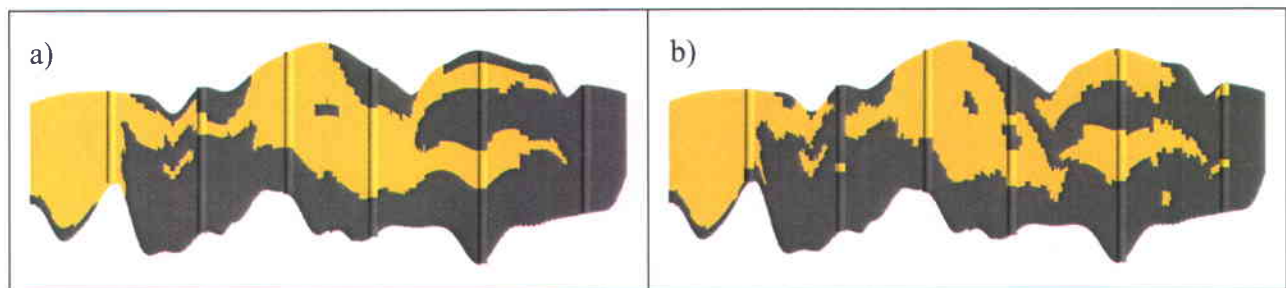


**Figure 3.11** Reference conceptual (a) continuous and (b) discontinuous models with simplified HF definition by merging the three HF with overlapping K values (see figure 3.8).

### 3.5.3 Numerical flow model, flow simulations and reference head profiles

The geostatistical models of HF (and K) were integrated in a numerical groundwater flow model. The problem settings for flow simulations in FEFLOW® (DHI-WASY, 2012) were defined for steady-state and saturated simulations, initially with a free moveable surface at the top and nine following deformable surfaces to allow the mesh to adapt to water table fluctuations. A fixed distributed recharge rate on the top of the model was found iteratively by fitting the simulated heads with real head data from 10 nearby wells (figure 3.12). Although matching of observed heads is generally good, lower heads were more difficult to reproduce in both reference models. This might be due to presence of drains that have not been taken in account in the modeling process.

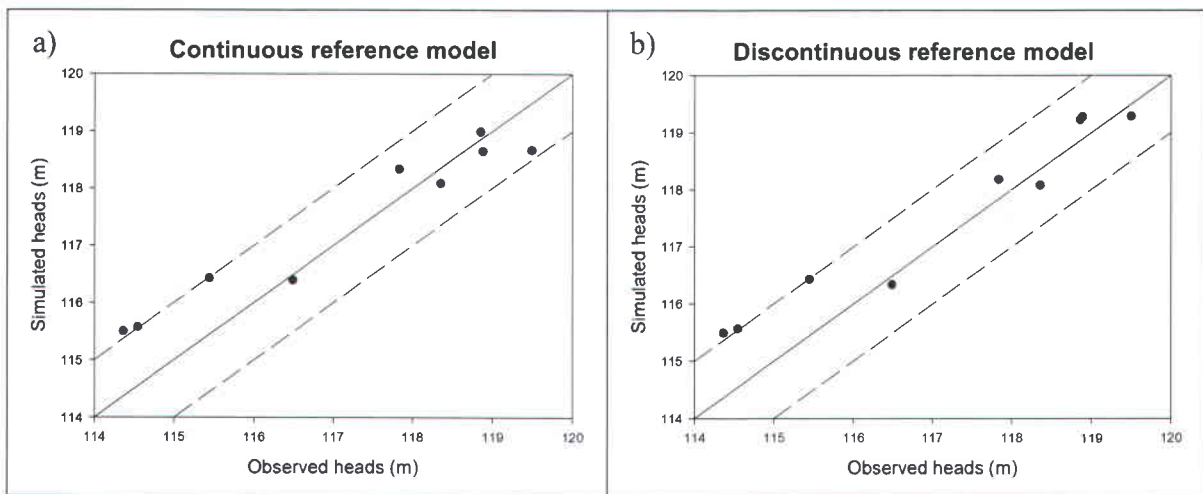


**Figure 3.12** Observed and simulated hydraulic head scatter plot at 10 observation wells near the model cross-section for a) continuous reference model, and b) discontinuous reference model.

At first, the numerical model encompassed the entire 2D area from the topography (top) to the bedrock (bottom) but two main difficulties occurred with a free water table, namely: 1) instabilities in solving flow near the surface and 2) the huge sensibility of the model to HF distribution on top of the model with a fixed recharge distribution. The latter could have been solved by optimizing recharge distribution and HF distribution simultaneously, but studying the isolated effect of HF distribution would have proven somewhat more complex. As our main objective remains assessing the potential of head profiles to constrain geostatistical simulations,

the modeling domain was modified by imposing a fixed top boundary to the models (fixed heads) corresponding to the simulated water table from the calibrated continuous and discontinuous reference model flow simulations (figure 3.13). The topography being the initial free and moveable top boundary (long dash) is lowered, after flow simulation, to the water table (short dash), and the upper slices of the model are lowered accordingly. A new synthetic top boundary (line) was then generated, based on the simulated water table and real water table elevation data from the study site (triangles). The latter had been used for calibration of the simulated water table from the initial models, but note that calibration was suboptimal in the central section of the model where the water table drops significantly lower than well data; this has been "corrected" when generating the synthetic top boundary.

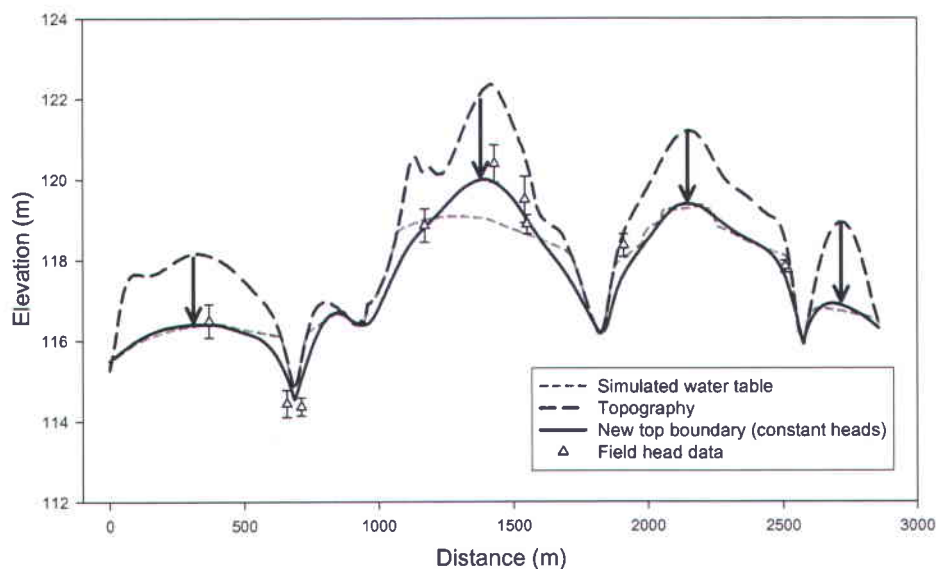
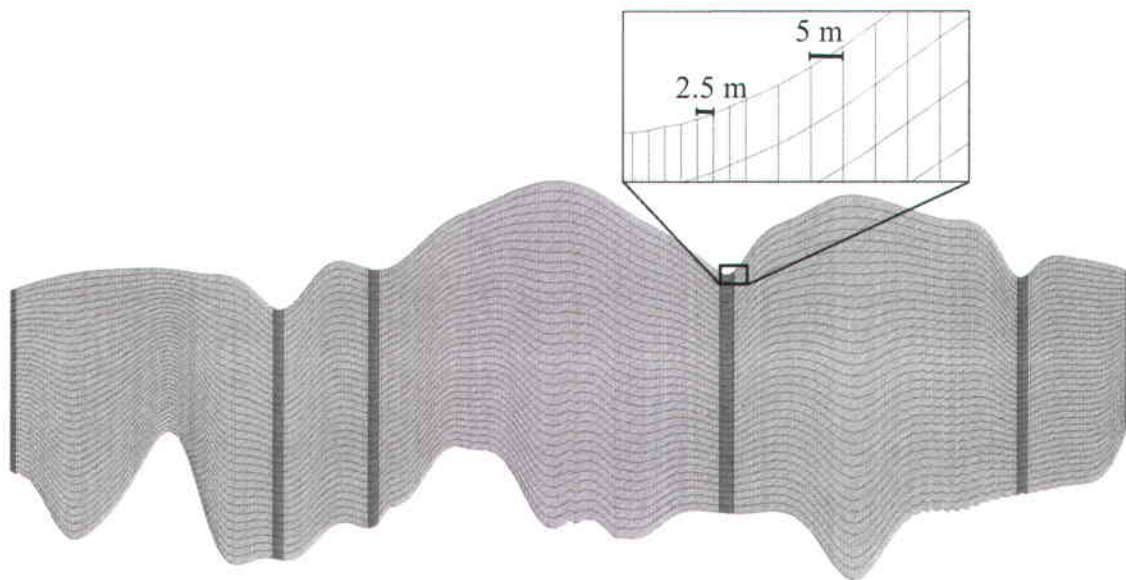


**Figure 3.13** Initial free and moveable top boundary of the reference models (topography), simulated water table, water table well data and new fixed synthetic top boundary for modeling with head profiles.

The new model grid was generated proportionally between this new top boundary and the base of the aquifer and the K field was imported back from the initial reference models in GOCAD®. The problem settings of the new reference flow models now introduce a fixed top slice with a boundary condition of fixed heads representing the water table. Although it assumes knowledge of the water table elevation along the entire cross-section, this approach ensures that further

simulated head profile fluctuations are solely related to HF distribution. Furthermore, fixing the water table following the land topography and many water level observations is appropriate for representing recharge in the context of steady-state modeling in conditions of humid climate, where low topographic relief and low water table depths prevail (Sanford, 2002).

The grid of the flow model (figure 3.14) in FEFLOW® is in pseudo-3D, as the model was attributed a horizontal width of 5 m (figure 3.14). The decision of modeling in pseudo-3D rather than 2D was supported by the capacity to control the generation of a mesh identical to the geological model, thus avoiding difficulties related to grid scale or smoothness. Since the stratigraphic grid in GOCAD® is made of rectangular elements, the flow grid elements were simply divided in triangular prisms and then refined near the rivers as they represent potential high-gradient outflow locations. The number of layers of the refined model stays at 34, but now has a total number of elements of 45696 with a mean element size of 5m x 5.3m x 0.3m (aspect ratio 1.06) and refined element size of 2.5 m x 2.65 m x 0.3 m (aspect ratio of 1.06).



FEFLOW (R)

**Figure 3.14** Grid of the numerical groundwater flow model with a pseudo-3D mesh (FEFLOW®).

The steady-state flow simulations on the reference continuous and discontinuous models provided hydraulic head fields from which head profiles were extracted every 100 m along the models. Typical head profiles simulated with the continuous reference model are illustrated in figure 3.15. The effect of layering on heads can be seen on the right and left profiles, as generally the head loss occurs in the less permeable HF. Near the rather homogeneous middle section, the profile is flat. The head profiles extracted from the reference models have been considered as observed data for later evaluation of head data mismatch.

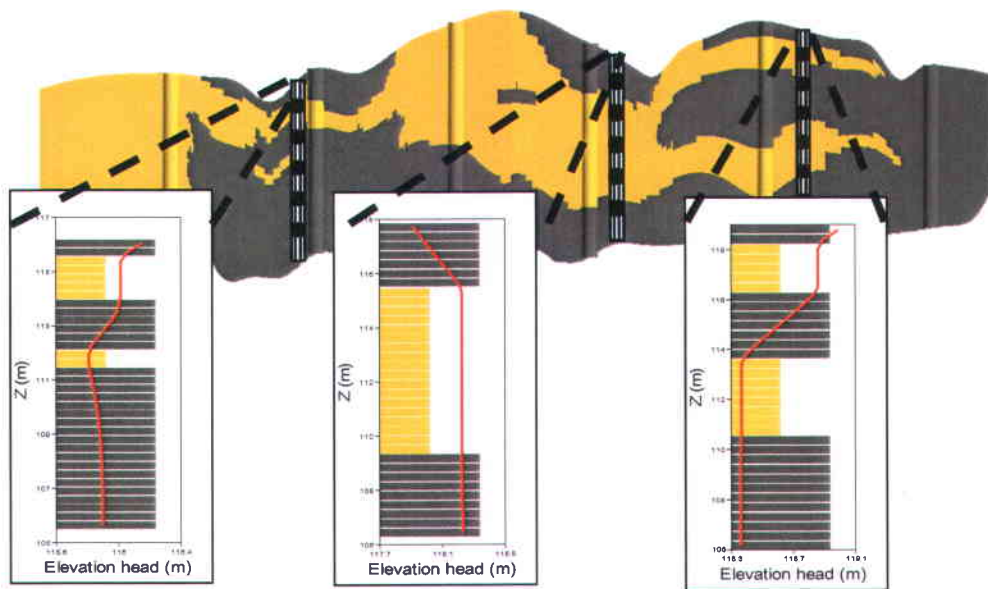


**Figure 3.15** Examples of hydraulic head profiles produced by saturated steady-state flow simulation of the continuous reference model with fixed water table.

### 3.5.4 Preliminary assessment of K contrasts

Distribution and continuity of HF may affect the flow (and transport) field according to the respective HF hydraulic properties and contrasts. For example, higher contrast of hydraulic conductivity ( $K(HF1)/K(HF2)$ ) should produce significantly different hydraulic head distribution fields than the homogeneous case, and conversely weaker K contrasts should produce less differences. In order to get a preliminary idea of required K contrasts between HF to get measurable effects on the resulting flow field, the effect of increasing K contrasts of the two HF

was assessed with a fixed vertical-horizontal anisotropy factor of 10. The K contrast of HF for both reference models was iteratively increased from one to three orders of magnitude and the resulting hydraulic head fields recorded. Difference of simulated hydraulic head fields with the field from the initial homogeneous case ( $K(HF1)/K(HF2) = 1$ ) provides an insight on the localization and magnitude of head differences with increasing K contrasts. For example, head field differences for K contrasts between HF of 10, 50 and 100 are illustrated in figure 3.16, from which the main observations are:

- i. There is initially an increase of the area of significant head differences (e.g. sensitive to K contrasts) up to a K contrast of approximately 1.5 orders of magnitude (O.M.), and then this area where heads are sensitive to K modifications stabilizes;
- ii. At K contrasts of two orders of magnitude and more, only the magnitude of the head difference increases;
- iii. Areas which are homogeneous are not affected by the increasing contrasts of K; the heads remain essentially the same;
- iv. With a threshold of 5 cm head difference for this particular study, a K contrast between HF of approximately 1.5 orders of magnitude or more is required.

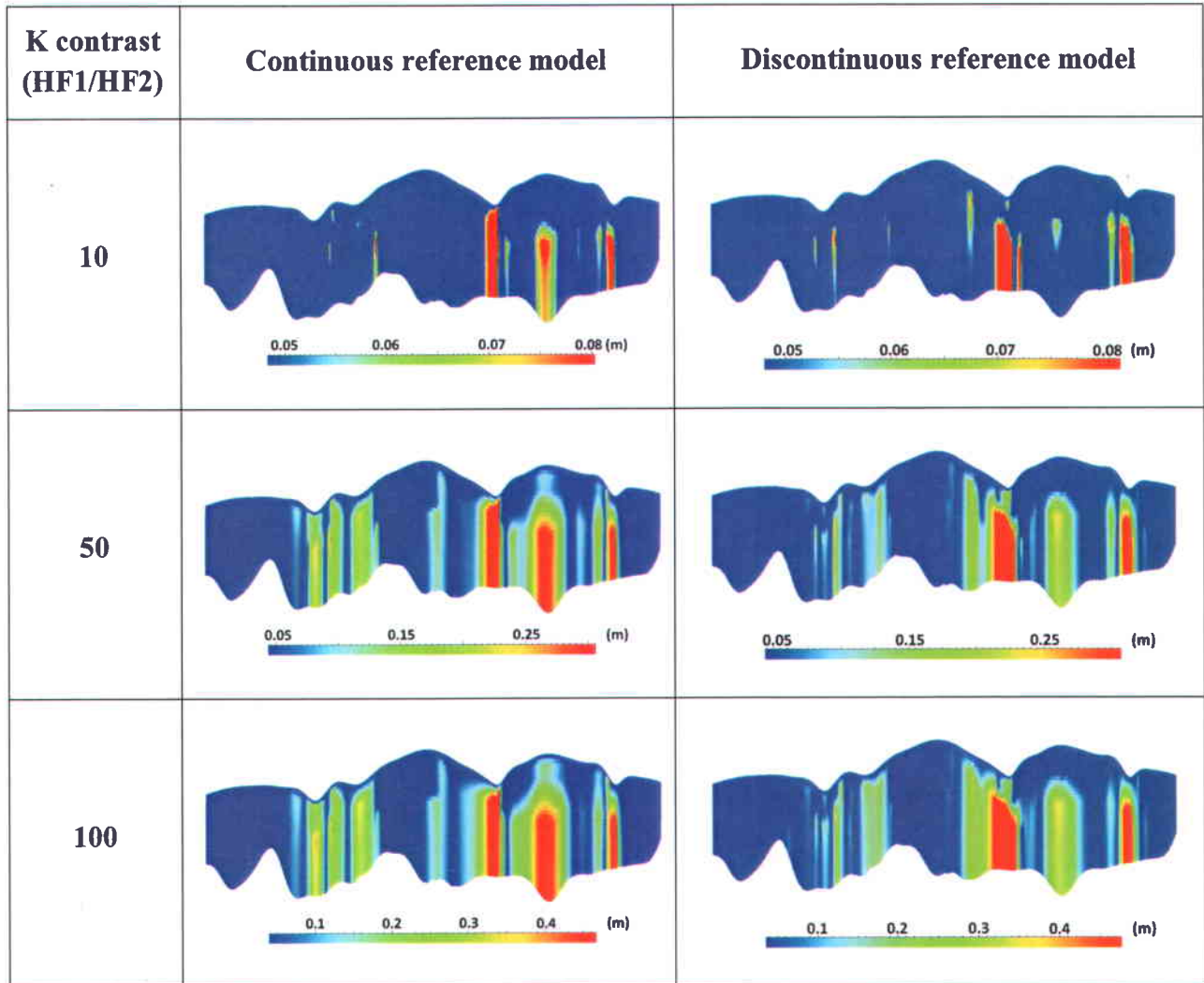


**Figure 3.16** Absolute differences between the hydraulic head field generated with a homogeneous model ( $K(HF1) = K(HF2)$ ) and hydraulic head fields generated from the reference models with an increasing K contrast of HF (arbitrary head difference detection threshold of 5 cm in navy blue).

In light of these preliminary results, the mean K difference between the two HF predicted from the learning machine algorithms ( $K(HF1) / K(HF2) = 20$ ) might not be sufficient to produce significant head differences over the heterogeneous (layered) areas of the models. To ensure measurable differences in the simulated head profiles, the K of HF2 was lowered by one order of magnitude yielding a K contrast of nearly 133 (~two O.M.) between the two HF. As for  $K_h/K_v$  anisotropy, available  $K_v$  field data has been attributed to corresponding HF classification. The mean anisotropy ratios are of eight for HF1 and 30 for HF2; the same ratio was applied after  $K_h$  modification of HF2. According to previous synthetic simulations presented in section 2.1,

higher anisotropy ratio should have been imposed to the less permeable HF (HF2) in order to ensure measurable effects of K heterogeneity on head distribution. These final hydraulic parameters of reference models are summarized in table 3.4.

**Table 3.4 Summary of modified homogeneous hydraulic parameters for reference flow models.**

HF	Kh		Kv		Kh / Kv
	m/s	log10(m/s)	m/s	log10(m/s)	
HF1	4.61E-05	-4.34	6.02E-06	-5.22	8 (~1 O.M.)
HF2	3.47E-07	-6.46	1.16E-08	-7.94	30 (1.3 O.M)
Kh1 / Kh2	133 (2 O.M.)				

### 3.6 Unconstrained geostatistical simulations

The main idea of assessing the potential of head profiles to constrain K realizations involves exploiting the misfit between head profiles generated from geostatistical realizations and those of the reference models. The general workflow for testing use of head profiles from realistic but synthetic reference models for constraining geostatistical realizations is as follows (figure 3.17):

- 1) Extract from reference models synthetic K data (or HF) from six boreholes with approximately 450 m spacing, which are further considered as "field or observed" K data;
- 2) Generate with multiple-point geostatistics (MPG) 100 realizations that fit both the K data and the water table or mean well heads (modeling with fixed water table as top boundary, section 3.5.3);
- 3) Execute steady-state flow simulations on all the realizations to provide simulated head profile data to be compared with the "observed" head profiles from the reference models;
- 4) Determine which are the most plausible realizations in terms of head profile differences (model selection);



- 5) Adjust HF distribution of the best realization to achieve the best fit of vertical head data as possible (model calibration) with the global Gradual Deformation (GD) method or by using local control points (CP);
- 6) Compare the selected and optimized models with the reference models to verify the effectiveness head profiles for determining HF distribution and continuity.

The initial realizations generated from CPT/SMR logs to produce the reference models could not be used again for head profile concept proofing. They showed relatively limited HF distribution variability, as they were fairly well constrained by the 12 geophysical soundings. New geostatistical realizations with lesser constraints were needed to fully assess the diagnostic value of head profiles.

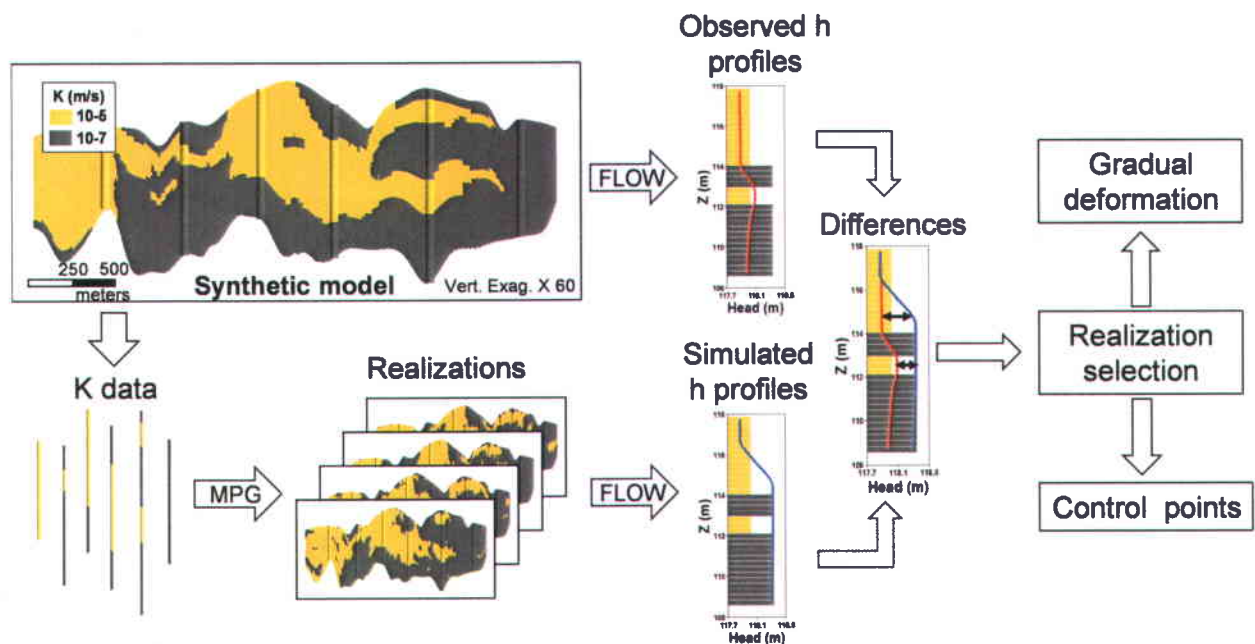


Figure 3.17 General workflow for assessing the use of head profiles from reference models to constrain geostatistical realizations.

### 3.6.1 Extraction of HF data from six synthetic wells

The production of geostatistical realizations generally requires densely sampled hydraulic parameters, namely continuous (or indirect) K values from wells or geophysical soundings. The reference models being considered as “field truth”, six HF (K) profiles were sampled from these models as "observed" data at approximately 450 m spacing. The sampling density was defined so as to properly guide the geostatistical simulation process without constraining the continuity definition of the layering. Water table elevation information or constraint is implicitly applied in modeling, as the reference models and simulation grid top boundary corresponds to the water table.

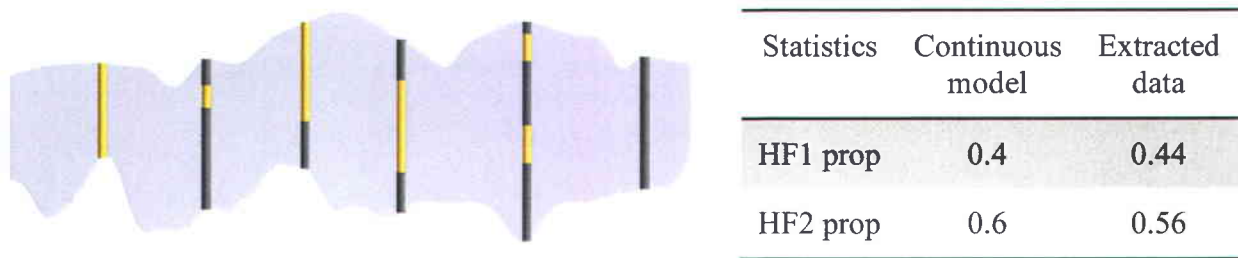


Figure 3.18 Synthetic observed HF (K) data extracted from 6 profiles with approximately 450 m spacing and statistics.

### 3.6.2 Multiple-point simulations

The multiple-points simulations aim at producing realizations respecting the observed synthetic well data, but with significant variability between the wells in order to avoid constraining a priori the solution space. This implies that there is limited geological knowledge between the wells, which has implications on the use of a training image (TI) and the choice of simulation parameters. For simplicity reasons, the initial TI used for generating the reference models was used here. Realizations with significant variability have been produced because of the selected data and the importance of simulation parameters (table 3.4):

- 1) Half the number of wells (6) have been exploited as conditioning data;

- 2) No auxiliary data (X or Z location) were added to guide the simulation process as to which area the multiple-point statistics should refer;
- 3) The weight of the kriged proportion variable was lowered to avoid forcing continuity (a weight of 0 would lead to practically no layering of the realizations).

The realizations generated are presented in the results section (3.8.1).

**Table 3.5** Some significant attribute specifications for MPG simulation with ISATIS® software for generating unconstrained realizations (relative to heads).

MP attributes	Value	Explanation
<b>HF proportions weight</b>	0.2	The weight attributed to HF proportion interpolation affects the continuity of realizations. Assuming no other information on HF distribution and continuity is available, this weight must be relatively low
<b>Auxiliary data</b>	none	In this case we deliberately exclude such information, assuming again we have no other information on HF distribution in order to explore a larger solution space.
<b>Multiple grids</b>	3	Same as previously (table 3.4)

### 3.7 Minimization of hydraulic head profile mismatch

As stated previously, the basis for selecting or optimizing realizations is the exploitation of discrepancies in observed and simulated hydraulic heads from vertical profiles. We thus need criteria to characterize such deviations. Also, besides the use of hydraulic head profiles for model selection, i.e. judging if an unconstrained geostatistical realization is hydraulically plausible, head profiles were used to constrain the realizations. Following the sections on the deviation criteria, we thus present two methods that were used to constrain geostatistical realizations, namely: 1) the global gradual deformation method; and 2) a local heuristic approach based on the pilot point method.

### 3.7.1 Mismatch criteria

In statistics, the mean squared error (MSE) is a common error criteria used to quantify the difference between values produced from an estimator and the true values. It is a measure of the average of the squared errors between the observed and simulated hydraulic heads, in this particular case. The MSE is the second moment of the error, corresponding to the sum of the estimator variance and the squared bias (Hines *et al.*, 2011):

$$MSE(\hat{\theta}) = E(\hat{\theta} - \theta)^2 \quad [1]$$

$$\begin{aligned} MSE(\hat{\theta}) &= E[\hat{\theta} - E(\hat{\theta})]^2 + [\theta - E(\hat{\theta})]^2 \\ &= V(\hat{\theta}) + (bias)^2 \end{aligned} \quad [2]$$

Thus, for an unbiased estimator, the MSE is the variance of the estimator. To have the same units as the quantity being estimated (meters), the square root of MSE yields the root-mean-square error (RMSE). Correspondingly, for an unbiased estimator the RMSE is the square root of the variance, or standard deviation. Notice that the errors are squared before they are averaged; RMSE is a quadratic error criteria, which gives a relatively higher weight to large errors. This means the RMSE is most useful when large errors are particularly unwanted.

Preliminary results have showed that the magnitude of the errors related to the continuity of HF distribution is generally outbalanced by larger systematic errors that can occur all along one or many wells. Larger weight bestowed to these errors can impede selection or optimization of elsewhere satisfactory realizations. Thus, selecting a linear error criterion, such as the mean absolute error (MAE), has proven more effective at approaching the structure of the reference fields.

$$MAE(\hat{\theta}) = E |\hat{\theta} - \theta| \quad [3]$$

The MAE measures the average magnitude of the errors, where all the individual differences are weighted equally in the average. For assessing average model performance, the RMSE should not be used without other information for it would be « impossible to discern to what extent

RMSE reflects central tendency (average error) and to what extent it represents the variability within the distribution of squared errors » (Willmott & Matsuura, 2005). The MAE and the RMSE can be used together to characterize the variation in the errors in a set of estimates; the greater difference between them, the greater the variance in the individual errors in the sample. The RMSE should always be larger or equal to the MAE; if they are equal, then all the errors are of the same magnitude.

### 3.7.2 Global gradual deformation method

The calibration of hydrogeological model parameters to direct and indirect data is an inverse problem (Carrera *et al.*, 2005). In this context, the calibration of a model realization is calculated by minimizing an objective function (optimization problem) quantifying the level of fit between the observed and the simulated data. However, for relatively large models with one or many parameter values (e.g. K or porosity) per grid cell, the inverse problem is said ill-posed as the number of parameters greatly exceeds available independent data and large variations in the data space are produced by small perturbation in the parameter space (Sun, 1995). Hence, the problems is numerically unstable, meaning that small errors in heads can result in strong errors in the estimated transmissivities (Doherty, 2003). Regularization can be used to reduce these instabilities. Inverse problem theory (Tarantola, 1987) provides a general framework for integrating prior hydrogeological knowledge and measured data into the following objective function :

$$J(\mathbf{y}) = \frac{1}{2} (\mathbf{g}(\mathbf{y}) - \mathbf{d}_{obs})^t \mathbf{C}_D^{-1} (\mathbf{g}(\mathbf{y}) - \mathbf{d}_{obs}) + \frac{1}{2} (\mathbf{y} - \mathbf{y}_0)^t \mathbf{C}_Y^{-1} (\mathbf{y} - \mathbf{y}_0) \quad [4]$$

The first term on the right hand side represents the *likelihood constraint*, which is a measure of the observed and simulated data mismatch.  $\mathbf{C}_D$  is the covariance matrix quantifying the experimental uncertainties (and implicitly theoretical uncertainties) and is assumed diagonal. The second term represents the *prior constraint*, which evaluates the departure of the aquifer model  $\mathbf{y}$  from the prior aquifer model  $\mathbf{y}_0$ .  $\mathbf{C}_Y^{-1}$  is the inverse of the covariance matrix of the model parameters, which represents the main challenge as the number of parameters is generally very large. The minimization of the objective function, either by gradient-based or randomized

optimization techniques, yields an optimal solution  $y$  close to both the observed data and the prior model.

In order to make this inverse problem tractable, various parameterization techniques have been developed to reduce significantly the number of parameters, such as partitioning the domain in subdomains or "zonation" (Clifton & Neuman, 1982), the pilot-point method (De Marsily *et al.*, 1984; RamaRao *et al.*, 1995), the sequential self-calibration method (Gómez-Hernández *et al.*, 1997), the gradual deformation method (GDM; Hu, 2000; Le Ravalec-Dupin & Nøtinger, 2002) or the gradual conditioning method (GCM; Capilla & Llopis-Albert, 2009). These techniques allow a reduction of the data mismatch by modifying the parameter values of the model while preserving the spatial variability pattern of the prior model.

The gradual deformation method developed by Hu (2000) is an efficient simulation algorithm which involves non-linear combination of independent Gaussian random fields, producing a chain of Gaussian realizations respecting the first two statistical moments of the parent Gaussian fields. The random fields are combined with weights, which are adjusted to minimize the data mismatch:

$$y(t) = y_1 \cos(t) + y_2 \sin(t) \quad [5]$$

$y(t)$  is produced by calibrating the weight parameter  $t$  applied on the independent realizations  $y_1$  and  $y_2$  to nonlinear data (e.g. hydraulic heads). Once the optimal parameter  $t$  is found, the optimized realization  $y(t)$  is combined with a new independent realization to further decrease the objective function ; this optimization sequence is pursued until satisfactory minimization of the objective function is obtained. This property can be used to easily generate multiple Gaussian fields all respecting the second order moment to compute global optimization in a one parameter space (figure 3.19).

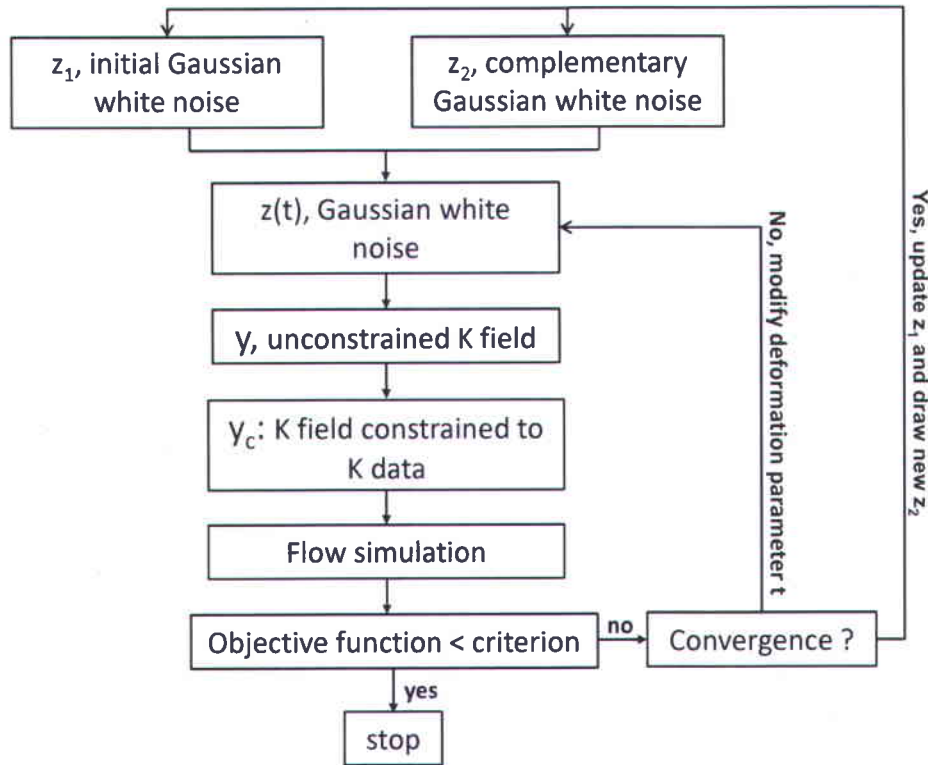


Figure 3.19 General workflow of the gradual deformation algorithm (adapted from Le Ravalec, 2005).

Figure 3.19 shows the workflow of the original optimization framework using gradual deformation. This algorithm works particularly well in second order stationary fields. Here, it was decided to allow the optimized fields to depart from the generating high order statistics coming from the training image. This only preserves the unbiased nature while permitting to depart from the training image statistics if the convergence improves.

The gradual deformation method has been further extended to non-Gaussian realizations generated with indicator (Hu *et al.*, 2001) algorithms and to conditional realizations (Hu, 2002). The latter shows that under a covariance and a conditioning constraint, the linear combination of conditional random functions provides a framework for parameterizing directly conditional stochastic models (Hu, 2002). In this study, the realizations generated from the synthetic well HF data are already conditioned within the MP algorithm, therefore the framework developed by Hu (2002) has been used. To speed up the search for an optimum, a series of conditional realizations of a random function  $Y(x)$  can be linearly combined and still produce a conditional realization of  $Y(x)$  under the previous constraints:

$$y(x) = \sum_i \alpha_i y_i(x) \quad [6]$$

For a combination of 3 realizations ( $i=3$ ), parameters  $\alpha_i$  are parameterized by (Hu, 2002):

$$\begin{cases} \alpha_1 = \frac{1}{3} + \frac{2}{3} \cos t \\ \alpha_2 = \frac{1}{3} + \frac{2}{3} \sin(-\frac{\pi}{6} + t) \\ \alpha_3 = \frac{1}{3} + \frac{2}{3} \sin(-\frac{\pi}{6} - t) \end{cases} \quad [7]$$

The parameter  $t$  ranges from  $-\pi$  to  $\pi$ ; the realizations  $y_1(x)$ ,  $y_2(x)$  and  $y_3(x)$  are exactly reproduced at  $t = 0, \frac{2}{3}\pi$  and  $-\frac{2}{3}\pi$ , respectively. The optimization sequence of parameter  $t$  is illustrated in figure 3.20.

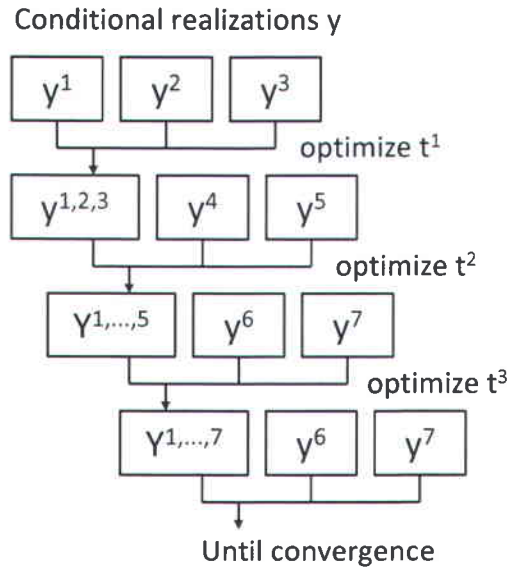


**Figure 3.20** Optimization sequence of parameter  $t$  with global gradual deformation of conditional realizations, for combination of three realizations (adapted from Le Ravalec & Mouche, 2012).

A linear combination of independent Gaussian random functions will give a Gaussian random function with the same mean and variance (Hines *et al.*, 2011). In this study, the realizations simulated with multiple-point statistics do not have a stationary spatial structure defined by a variogram. Nevertheless, the combined model realizations need not be necessarily stationary and gradual deformation of a realization should preserve the spatial variability of the stochastic



model according to Hu *et al.* (2001). Even if the initial realizations share the same multiple point statistics, the successive combinations might result in statistics that partially deviate from them and spatial structure preservation cannot be as readily assessed as variogram reproduction. Nevertheless, one might question the objective of strictly respecting prior information on the aquifer structure rather than starting off with this prior and allowing the realizations to diverge from it, if high-quality data (e.g. transient heads or head profiles) induce such deviation. The necessity of preserving prior structure or not is a question to some debate (Zhou *et al.*, 2014). In Here, the framework proposed by Hu (2002) was implemented successfully to deform MP realizations with respect to head profile data.

### 3.7.3 Local heuristic method with control points

The approach applied in this work is mostly inspired from the pilot point method, which is a wide-spread geostatistical technique for conditioning groundwater models. It was first developed by De Marsily *et al.* (1984); RamaRao *et al.* (1995) later extended the pilot point methodology to the calibration of random fields, and many further developments have been proposed (e.g. Doherty, 2003; Lavenue & de Marsily, 2001). Pilot points serve as surrogate parameters at which locations the values are estimated in the inverse-modeling process. The basic principle of the method is to introduce control points to make local modifications to parameter values (e.g. K) in the model. The parameter value at each pilot point is drawn from a uniform distribution bounded within plausible parameter values. Then, the estimated values are interpolated onto the modeling domain to preserve the statistical properties of the model. Rather than estimating parameters in every cell of the model, this approach greatly decreases the number of parameters to estimate. Integration of the pilot point values in a conditional random function model ( $Y_c$ ) is relatively straightforward:

$$Y_c(x) = Y_{dK}(x) + [Y(x) - Y_{udK}(x)] \quad [8]$$

$$\begin{cases} Y_{dK} : \text{kriged data and PP} \\ Y : \text{unconditional realisation} \\ Y_{udK} : \text{kriged unconditional data} \end{cases}$$

The general workflow for model calibration with pilot points is summarized in figure 3.21. First, an unconditional realization is simulated from a stochastic generator integrating solely the spatial statistics (mean, variance and covariance). Next, pilot point locations are selected and their values initialized. The unconditional realization is then constrained by the data (e.g. K) and the pilot points values. Flow simulation of this constrained realization produces simulated state-variables (e.g. heads) which are compared to observed state-variables through the following objective function:

$$J(y) = \frac{1}{2} (g(y) - d_{obs})^t C_D^{-1} (g(y) - d_{obs}) \quad [9]$$

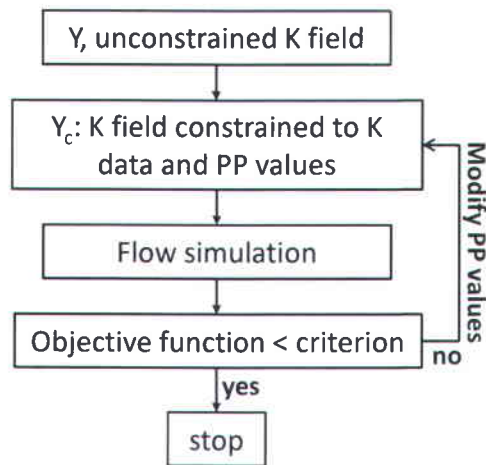


**Figure 3.21** General workflow of model calibration with pilot point method (adapted from Le Ravalec & Hu, 2007).

If the objective function  $J(y)$  reaches the convergence criterion, the minimization process stops. Otherwise, pilot point values are modified and steps 2 to 4 are repeated until convergence. Notice that the objective function  $J(y)$  is reduced to the likelihood term of equation 4, as the prior term relating to the parameter covariance is implicitly integrated in the minimization process through kriging of the pilot point values. Thus, the modified realizations all respect the initial variogram at each iteration. Consequently, kriging of pilot point values implies an impact on the surrounding area within one correlation length. To ensure the fitting of prior spatial statistics, their location must thus be restricted at one correlation length spacing or more. If the

geostatistical prior term is included in the objective function (eq. 4), the number and location of pilot points is not limited anymore. Selecting optimal pilot point numbers and locations has been the subject of many studies, and different strategies may be applied. They may be either added sequentially one by one (e.g. LaVenue *et al.*, 1995), predefined in a regular grid (e.g. Capilla *et al.*, 1997) or selected according to gradient-based sensitivity analysis (Doherty *et al.*, 2011).

The main characteristics of the heuristic control point approach applied in this work are stated here, relative to the pilot point method. First, the objective function used to calibrate realizations to reference head profiles was restricted to the likelihood term (eq. 9). As mentioned earlier, modeling was performed assuming no prior information on HF (K) spatial distribution is available. In this study, modeling flow in a simple 2D setting alleviates the computational burden and thus the necessity of using sensitivity analysis for control point location. The control points have been regularly spaced as to cover the entire model domain. Using regular grids generally implies distances of at least one correlation length between pilot points to preserve structure. Since the reference models and realizations are non-stationary and characterized by their multiple point statistics rather than by a variogram, the correlation length is not relevant for selecting control point spacing. The control points were arbitrarily set at the head profile locations, i.e. at 100 m spacing in X direction and at a mean 0.3 m in Z direction (figure 3.22).

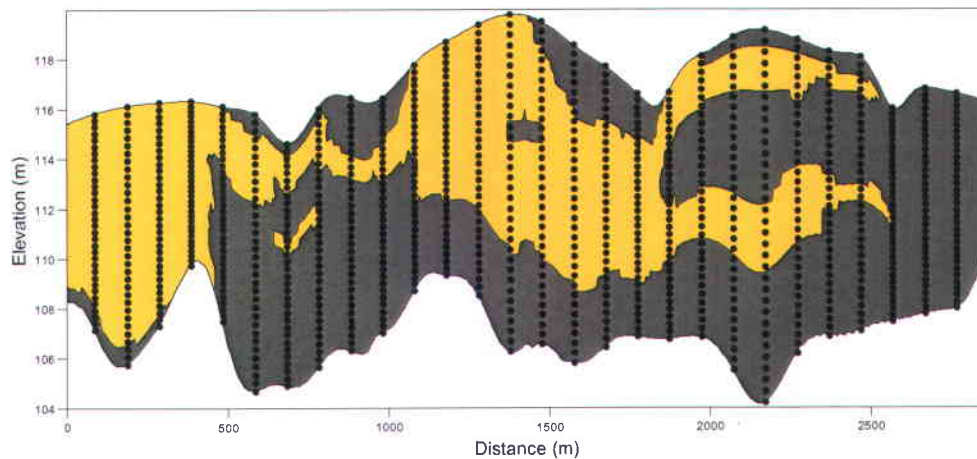


**Figure 3.22** Control-point locations with 100 m spacing in X direction and 0.3 m mean spacing in Z direction.

Furthermore, the pilot point values were not drawn from a continuous uniform distribution, as the main objective is to identify the HF distribution. Thus, the control point K values could only take the two corresponding to each HF; they were extracted from the MP realizations at specified locations (figure 3.22), producing 100 pilot point sets. This was done as an alternative mean to partly ensure control point values respect spatial structure as provided by multiple-point realizations. Hence, the parameter field to optimize (K) related to state-variable calibration (heads) is binary since the K value within each HF is homogeneous. Again, modification of K values implies a local change of HF which might modify the initial structural parameters (multiple point statistics in this case, rather than variogram).

Attempting optimization by modifying control point values simultaneously all at once has proven unsatisfactory, as very slow or no reduction of the objective function occurred. Parameter modification in an area may locally decrease data misfit but increase misfit in its vicinity since it may change the surrounding flow pattern. Thus, the control point values could not be calibrated neither one at a time, nor all values in the entire domain at once; a strategy by optimizing sequentially five regions was applied more successfully. These regions (figure 3.23) have been defined by estimating generally the potential flow paths from topographic highs and lows (recharge and discharge areas where zero flux boundary conditions are found).

The control point values were then updated with the control point sets based upon the following optimization process:

- 1) Subdivision of the cross-section into five flow zones (figure 3.23), as calibration with all control points at once would not converge;
- 2) For a given zone:
  - a. Select control point locations within this zone where head profile data misfit  $\geq$  criterion (MAE);
  - b. Import and propagate the corresponding control point values from a set of realization values;
  - c. Run flow simulation and evaluate head misfit (MAE) for all control point locations;
  - d. Keep interpolated control point values of the current set if  $MAE(i) < MAE(i-1)$ ;

- e. Back to step a. until control point misfit cannot be further lowered;
- 3) Repeat 2) for all 5 zones.

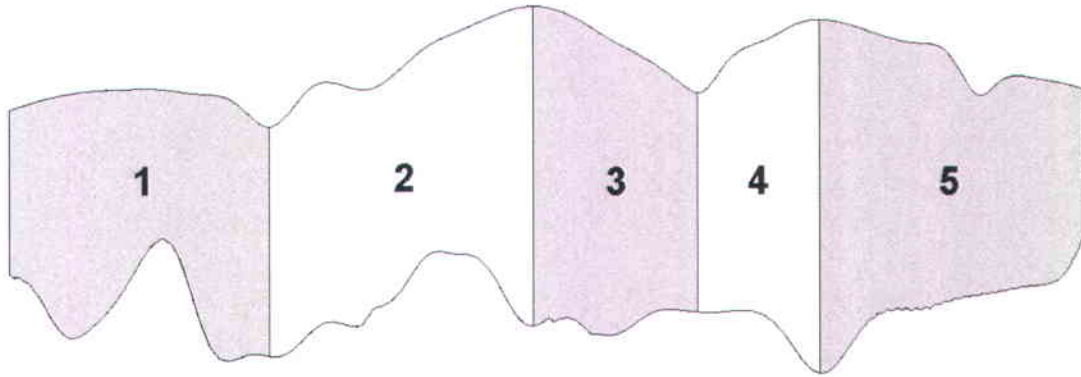


**Figure 3.23** Subdivision of the modeling area in 5 zones for optimization sequence with control points, based upon topographically estimated flow paths and the approximate location of zero-flux limits (distinct flow zones)

### 3.8 RESULTS

This section provides statistics and illustrations to compare the optimal K fields and corresponding hydraulic heads produced with the numerical flow model using geostatistical realizations obtained from different methods to the hydraulic heads of the two reference models (continuous and discontinuous). First, the realizations obtained from multiple-point geostatistics constrained to six synthetic HF (K) logs are presented, followed by the realizations obtained from the selection and calibration approaches (gradual deformation and control points) constrained to hydraulic head profiles relative to the continuous reference model. Practical issues regarding the use of hydraulic head profiles are then explored, in terms of spatial distribution of head errors and of the required spacing between head profiles to have enough constraints to obtain a satisfying definition of the spatial distribution and continuity of hydrofacies. Finally, the effect of discontinuity of HF distribution on head profiles is explored.

### 3.8.1 All multiple points realizations: Continuous reference model

#### 3.8.1.1 Statistics

The 100 HF realizations generated with MPG are all conditioned to the synthetic HF (K) data logs extracted from the continuous reference models as well as to the water levels (inherently), since the top of the model corresponds to the water table. The HF proportions for the continuous reference model, the synthetic wells and the MP realizations are similar, in particular the latter with well data (table 3.6).

**Table 3.6** HF proportions for continuous reference model and all MP realizations.

Statistics	Continuous model	All MP realizations	Extracted well data
<b>HF1 prop</b>	0.4	<b>0.43</b>	0.44
<b>HF2 prop</b>	0.6	<b>0.57</b>	0.56
<b>Global recharge (m3/day)</b>	6.14		

The element-wise standard deviation of all realizations is represented in figure 3.24, which corresponds to the variability of HF representation (or K) per model element for all of the realizations. The standard deviation is minimal near the synthetic well data logs, whereas it is generally at its maximum between wells except for the lower right area. HF representation in this particular area of all realizations is mainly composed of the less permeable HF (HF2), as there is significant continuity between the wells in the lower section of the reference models. Nevertheless, this low variance in the bottom layer of realizations does not impede the main objective of studying the potential application of head profiles, as the flow patterns and resulting heads differ significantly between realizations. The high variance between the wells shows that realizations were generated with MPG in such a way to explore the larger solution space as possible without excluding a priori any possible calibrated models. To ensure proper variability of an ensemble of realizations, the analysis of the ratio of RMSE to Ensemble Spread (ES) can

prove informative, adapted from Xu *et al.* (2013) with the Ensemble Kalman Filter (EnKF) approach:

$$RMSE = \sqrt{\frac{1}{n} \sum_{i=1}^n (s_i^{ref} - \langle s^a \rangle_i)^2} \quad [10]$$

$$ES = \sqrt{\frac{1}{n} \sum_{i=1}^n \sigma_i^2} \quad [11]$$

Where  $n$  is the number of model elements;  $s_i^{ref}$  is the value of the reference model at node  $i$ ;  $\langle s^a \rangle_i$  is the ensemble mean of the realizations at node  $i$  and  $\sigma_i^2$  is the ensemble variance of the realizations at node  $i$ . In this case, the RMSE calculation is an indication of the dissimilarity of the average of the realizations with the reference model. The ES is a measure of the level of variability across the different realizations; a small ES indicates that the realizations have low variability and vice versa. The ratio of RMSE to ES is 0.88 and 1.03 for the continuous and discontinuous cases, respectively (optimal value is 1).

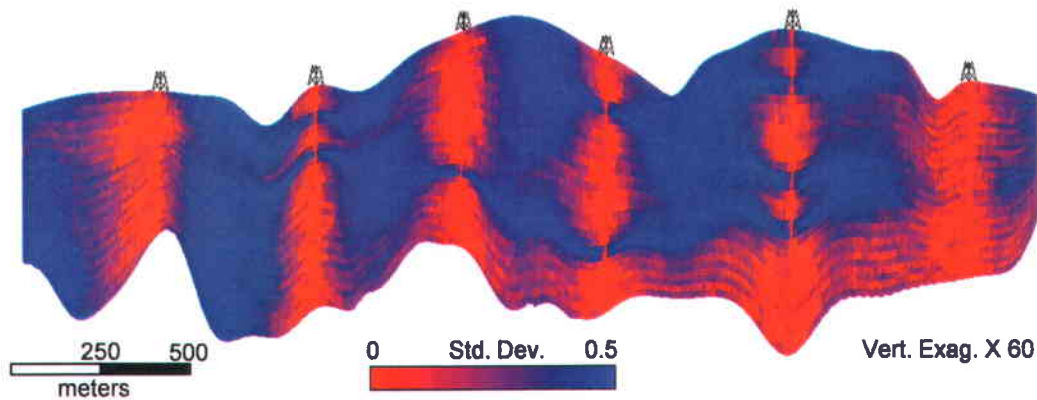


**Figure 3.24** Element-wise standard deviation of HF for all the MPG realizations (100). The standard deviation is minimal near the data logs, whereas it is generally at its maximum between wells.

A few examples of HF (dis)continuity of the realizations are illustrated in figure 3.25. Visual comparison with the reference models can be facilitated by referring to the continuity of HF1

layers: one to the left and two (upper and lower) to the right (figure 3.25a). The MP simulation algorithm produced realizations with significant variability of continuous layers, discontinuous layers and occasionally absence of certain layers. This shows that MPG, without constraints provided by vertical head profiles, cannot define the adequate continuity (connectivity) of the permeable hydrofacies (HF1), at the level of control used to support the MPG realizations. The next subsection will verify if the hydraulic heads obtained from the numerical flow model using these realizations provide plausible flow conditions.

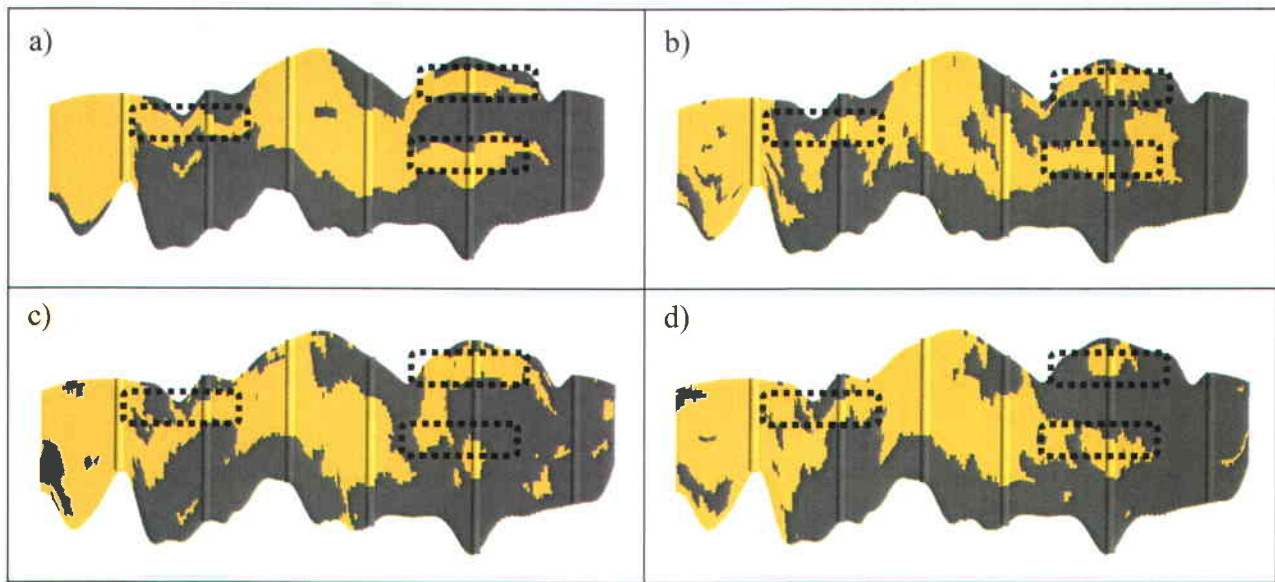


**Figure 3.25** Continuous reference model (a) and examples of variability in HF distribution and continuity in 3 MP realizations (b, c, d).

### 3.8.1.2 Error criteria of all realizations (100 m spacing) relating to the continuous reference model

Running steady-state flow simulations on all of the MP realizations provides hydraulic head fields which enable the comparison of observed and simulated heads. With head profile spacing of 100 m, RMSE and MAE criteria show that there are relatively large mean errors of all the realizations (figure 3.26). The RMSE and MAE histograms (figure 3.26 a and b) are negatively skewed; this illustrates that most of the realizations reproduce relatively poorly the local head distribution. Thus, geostatistical simulations calibrated to typical well data (e.g. K and mean well heads) do not imply hydraulic plausibility for the flow system. Nevertheless, the realizations



with lowest error criteria should provide a better representation of the HF distribution. So the hydraulic head profiles could be first used for geostatistical model selection, i.e. keeping only the realizations with the lowest error criteria.

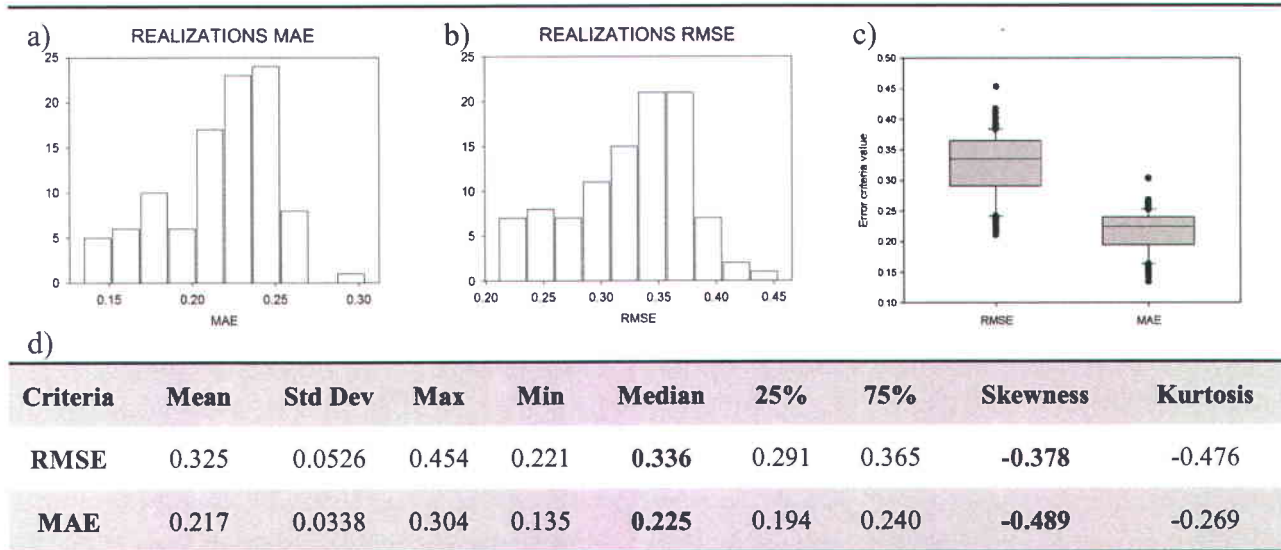


Figure 3.26 Error criteria distribution (a, b and c) and statistics (d) from head profile discrepancies with the continuous reference model (at 100m spacing) for all the MP realizations.

### 3.8.2 Best realizations relative to the continuous reference model

The MP realizations generated from the synthetic HF logs and water table elevation serve as a basis for model selection and model calibration with gradual deformation or control point methods. The results presented here are based upon the error criteria from head discrepancies from profiles with 100 m spacing.

#### 3.8.2.1 Best MP realization

Calculations of MAE and RMSE for flow simulations on all the MP realizations provide minimum criteria values for selecting MP realizations which best fit the observed head profiles. In this case, both minimum criteria coincide with the same MP realization (figure 3.27). The selected realization (figure 3.27a) shares a very similar distribution as the reference continuous model (figure 3.27b), as the three continuous permeable layers are present. Nevertheless, there are some discrepancies in the HF distribution, which produce larger head differences (identified

as points on figure 3.27a), particularly in the layered areas. The scatter plot of simulated and observed profile heads (figure 3.27c) shows a relatively good fit ( $R^2 = 0.975$ ), with the RMSE and MAE error criteria at 0.22 m and 0.135 m, respectively.

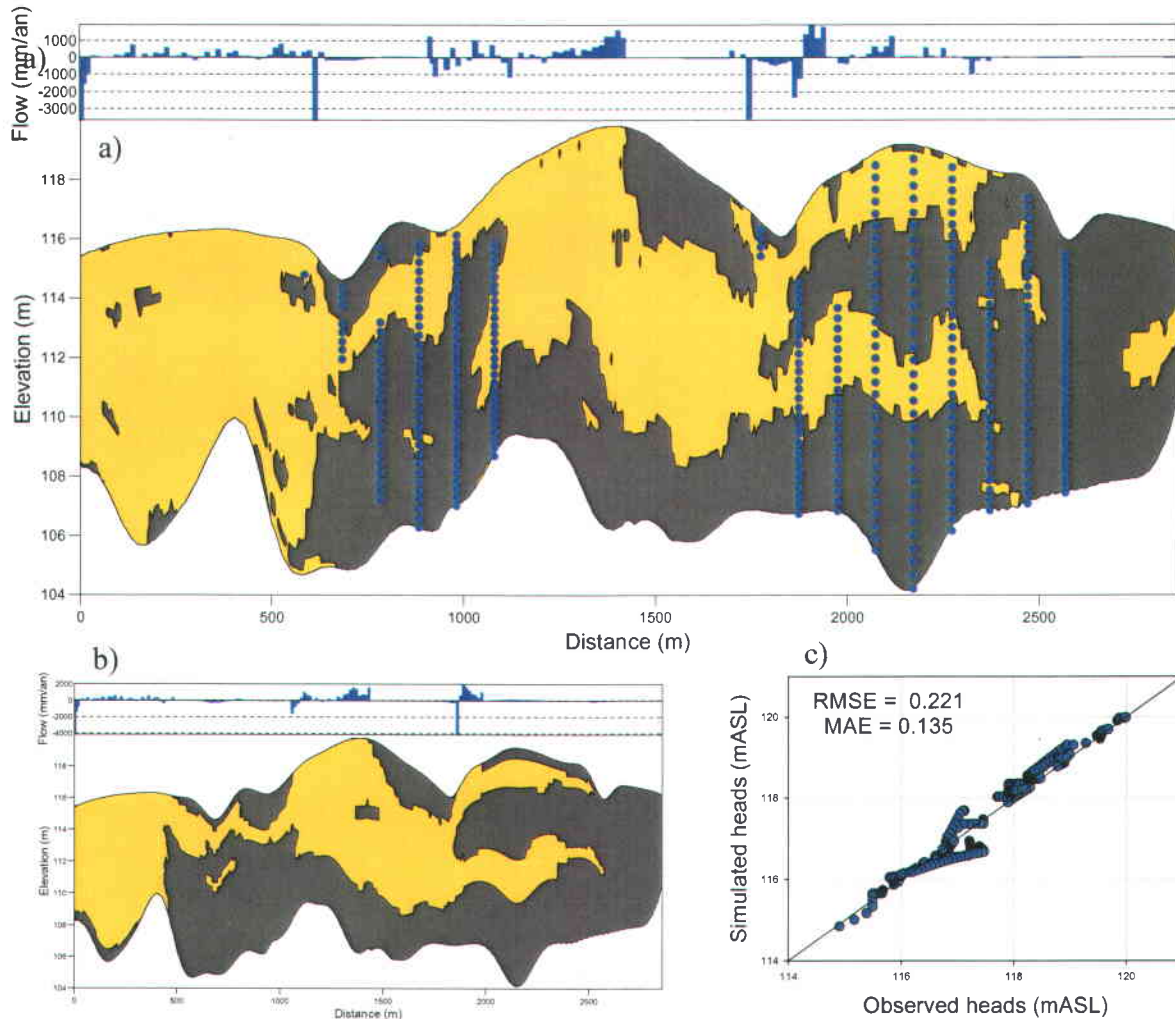


**Figure 3.27** (a) Selection of best MP realization based upon MAE and RMSE criteria with head profile discrepancies over 0.1 m (points) and corresponding recharge distribution on top of profile, (b) Reference continuous model, and (c) Scatter plot of observed and simulated heads with corresponding mean error criteria.

### 3.8.2.2 Optimization with global gradual deformation

The following realization (figure 3.28) is the result of the gradual deformation of an initial MP realization by iteratively combining it with one or more weighted MP realizations. As opposed to

binary HF definition with intra-hydrofacies homogeneous K, the weighted combination of K fields necessarily yields realizations with continuous K values. The optimized realization must nonetheless present the expected K values related to each HF in order to attempt reproduction of the reference field. Thus, a threshold has been applied to continuous K values in order to input binary K values before flow simulations. Then, the continuous K values (by gradual deformation) are reintroduced and the iterative deformation procedure is done on the continuous K values. The resulting optimized HF realization (figure 3.28) has the following characteristics:

- i. Reproduces the 3 layers, although the top right one is discontinuous;
- ii. Adds scattered noise (pixels), as the initial or reference model is very smooth and binary;
- iii. Decreases the number of profile points with head differences larger than 0.1 m;
- iv. Causes a significant decrease of the error criteria (RMSE of 0.136 m and MAE of 0.09 m) and a better fit on the scatter plot of observed and simulated heads.

These results show that optimization with global gradual deformation produces globally a better fit of the head profile data, but this approach might locally fail to reproduce layer continuity in certain areas. The latter might then have locally a lesser impact on heads than in other areas, hence the necessity of local calibration. Unfortunately, combination of conditional realizations is limited to global deformation to preserve the structural parameters (Hu, 2002), unlike gradual deformation of unconditional realizations where local gradual deformation is possible (Hu *et al.*, 2001; Le Ravalec & Mouche, 2012). However, as preservation of spatial covariance of K data is not an objective in this study, the local gradual deformation method could have been adapted.

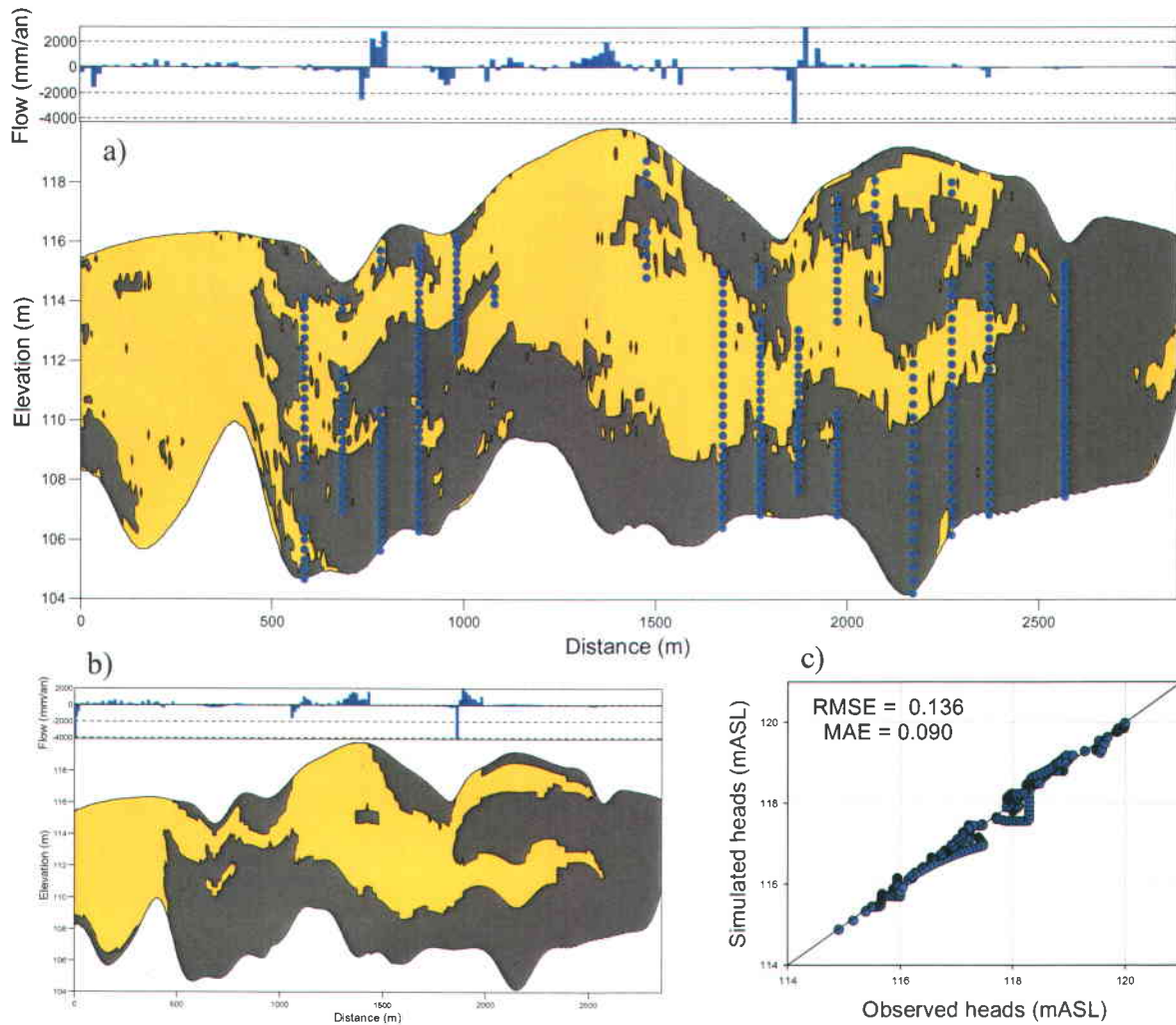


**Figure 3.28** (a) Calibrated realization by gradual deformation based upon MAE and RMSE criteria with head profile discrepancies over 0.1 m (points) and corresponding recharge distribution on top of profile, (b) Reference continuous model, and (c) Scatter plot of observed and simulated heads with corresponding mean error criteria.

### 3.8.2.3 Optimization with control points

This realization (figure 3.29) is the result of optimization with the heuristic method derived from the pilot-point technique. This approach presents the advantage of having the capacity to modify locally the  $K$  (HF) values over short distances (100 m) and evaluating the impact on head profile reproduction. However, as there is no stationary correlation length, the values are simply kriged between the control points.

The resulting control point realization has the following characteristics (figure 3.29):

- i. Reproduces the three layers, but their continuity is better represented;
- ii. Produces greatest decrease of error criteria (RMSE of 0.128 m and MAE of 0.066 m) and the best fit of simulated heads;
- iii. Adds ‘blocky’ noise because the values of the modified control points are kriged;
- iv. Presents few observation points with head differences larger than 0.1 m.

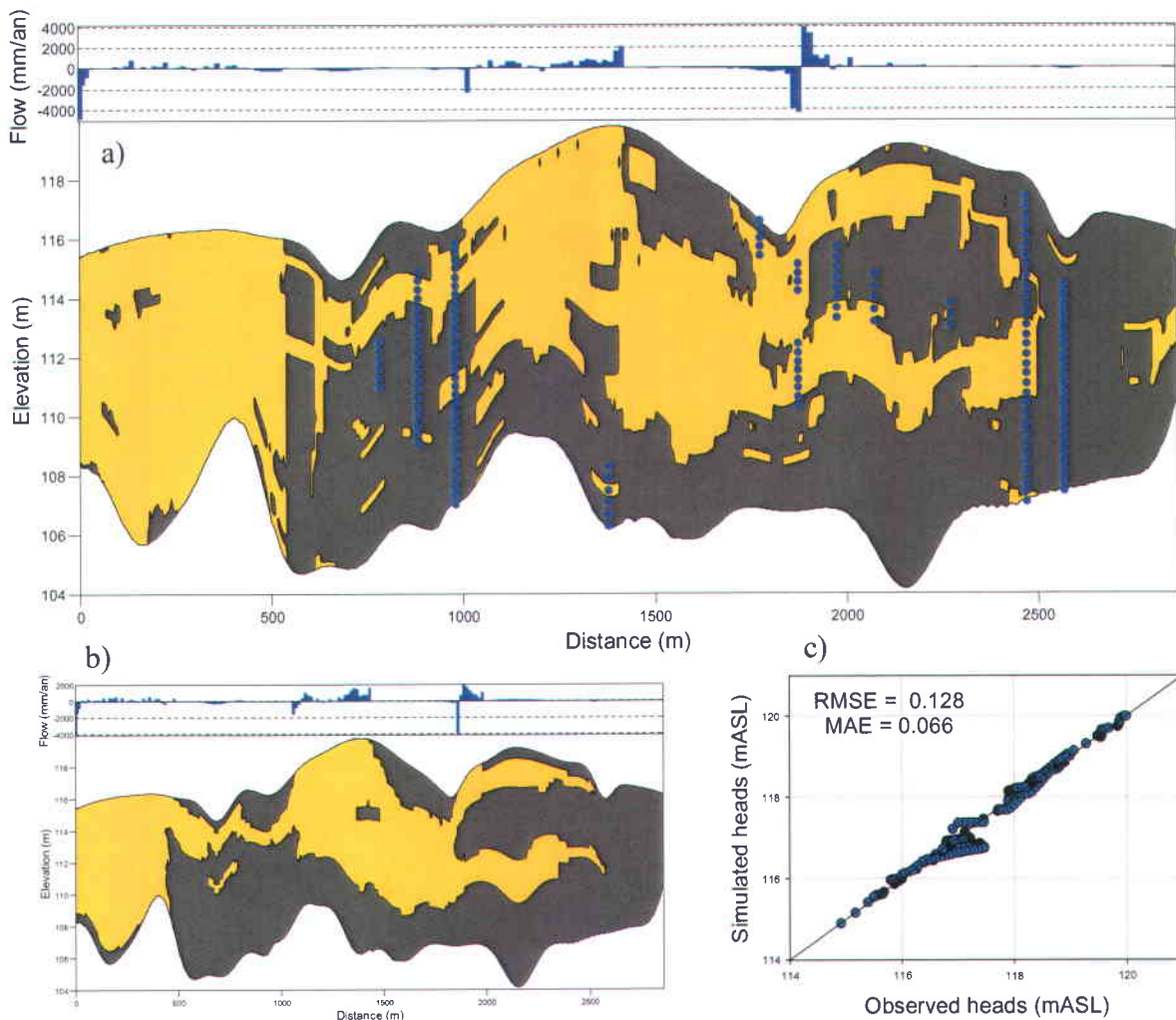


**Figure 3.29** (a) Calibrated realization with control points based upon MAE and RMSE criteria with head profile discrepancies over 0.1 m (points) and corresponding recharge distribution on top of profile, (b) Reference continuous model, and (c) Scatter plot of observed and simulated heads with corresponding mean error criteria.

### 3.8.2.4 Summary of best realizations

At first, selecting multiple point realizations based on head profile discrepancies appears an effective mean of constraining the possible solutions in the distribution and continuity of K. In general, realizations with greater continuity in layering have lower objective functions, thus narrowing the solution space. Moreover, it seems that more can be done with head profile data, as optimization with gradual deformation or control points methods further improves matching the head profile data (table 3.7). However, such minimization of an objective function does not necessarily further improve the representation of heterogeneity. For example, optimization with global gradual deformation produces a realization with mean head profile errors significantly lower than the selected MP realization, although the K (HF) distribution might locally seem somewhat less representative. Thus, local sensitivity of heads to K distribution may be relatively lower in certain areas where appropriate K representation is important. As mentioned earlier, global minimization of an objective function does not ensure proper HF (or K) representation, as the weight of head discrepancies of one or a few wells might impede proper heterogeneity assessment.

**Table 3.7** Summary of the error criteria for the best MP realization, calibration with global gradual deformation and with control points (continuous reference model).

<b>Realization</b>	<b>Mean Absolute Error (MAE)</b>	<b>Root Mean Squared Error (RMSE)</b>
<b>Best MP realization</b>	0.135	0.221
<b>Gradual Deformation</b>	0.090	0.136
<b>Control Points</b>	0.066	0.128

### 3.8.3 Effect of selection and optimization on head differences

Head profile discrepancies are not of equal magnitude throughout the model domain. As illustrated earlier, the greatest discrepancies are generally located near the (dis)continuous layered areas. Overall, the distribution (histogram) of the head differences for a realization

should have a mean error near 0 and with similar error frequency distribution on either side, in the case of unbiased error distribution. Simulated hydraulic head profiles with the best MP realization present some significant differences over 0.4 m with the observed head profiles (figure 3.30a) and a positively biased error distribution near 0.04 m (table 3.8). Nevertheless, this proves that some non-deformed MP realization may fit relatively well head profile data, as the best realization presents over 72% of head data with differences lower than 0.2 m. The realization calibrated with gradual deformation shows an increase of the fit of the head profile data (figure 3.30b), with mean head differences close to 0 and fewer large head differences (table 3.8). This realization presents 87% of head data with differences lesser than 0.2 m. As for the realization calibrated with control points, this local calibration technique proves very efficient as it increases dramatically the fit of the head profiles and further reduces the bias in the error distribution (figure 3.30c). In this case, 91% of head data has discrepancies lesser than 0.2 m.

Thus, the fit of head profile data at observation points increases from selection scheme to global and to local calibration schemes, with a reduction in error distribution bias. This suggests that even more can be done with hydraulic head profile data than realization selection or screening, although the latter can effectively help constraining potential HF distributions. However, reducing head profile discrepancies does not necessarily imply better reproduction of connectivity of permeable HF, as illustrated by gradual deformation results. Hence, local calibration of head profile values is potentially more effective.

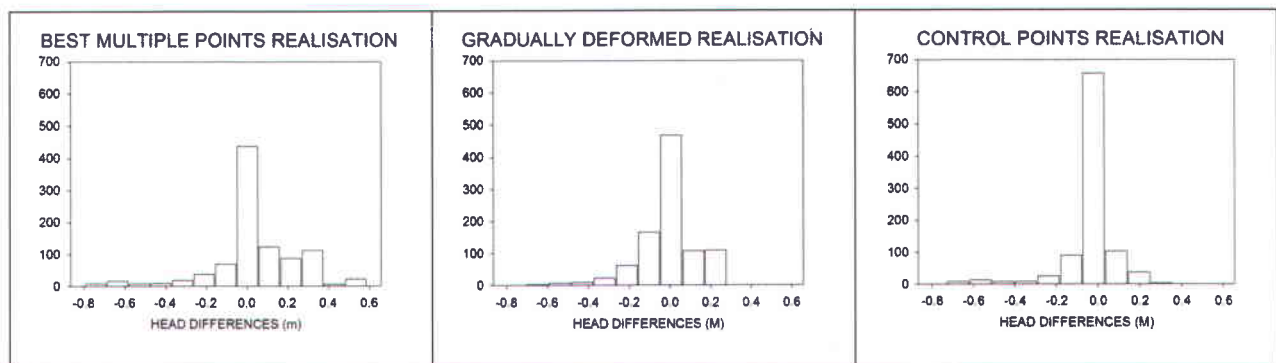


**Figure 3.30** Observed and simulated head differences distribution for the best MP realization and the calibrated realizations with gradual deformation and control points methods.

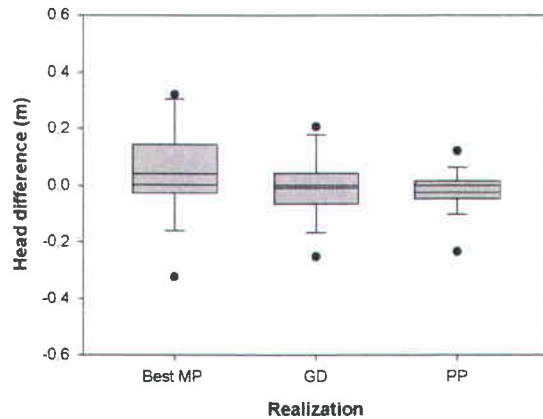


**Figure 3.31** Head difference box plot illustrating the head difference reduction from MP realization selection to global (gradual deformation) and local (control points) calibration methods.

**Table 3.8** Statistics of head differences between observed and simulated heads from selected and calibrated realizations.

Validation method	Observed and simulated head differences		
	Mean	Std Dev	Median
<b>Selection</b>	0.039	0.208	0.0023
<b>Gradual deformation</b>	-0.001	0.136	-0.00026
<b>Control points</b>	-0.024	0.126	-0.00036

### 3.8.4 Effect of horizontal spacing between head profiles

Required level of head profile data to adequately infer aquifer structure and HF distribution depends on the level and scale of heterogeneity which, in turn, is generally unknown without the former. This difficulty cannot be solved without the input of other sources of information, such as continuous data from surface geophysics, direct push soundings or reliable geological interpretation (e.g. outcrops) of the model domain. In order to assess the impact of horizontal spacing of head profiles on the effectiveness of realization selection and optimization, the initial scenario at 100 m spacing was compared with 200 m and 300 m spacing of head profiles.



### 3.8.4.1 Effect on error criteria for all MP realizations

With close spacing of head profiles (100 m), most of the MP realizations poorly fit head data (figure 3.32a) as the distribution of MAE criterion is negatively skewed (-0.49). Thus, few realizations reproduce adequately the model structure. As less detailed information is available for evaluating head profile discrepancies, increasing the profile spacing at 200 m and 300 m produces a more Gaussian-like distribution of error criteria (figure 3.32 b and c) and considerably reduces the skewness (-0.22 and -0.15, respectively). With greater head profile spacing, one may assume the weight of a declining number of head profile data will be reduced proportionally to a stable number of water table data (or mean well heads) in the calculation of error criteria. In the end, a very little number of head profiles could provide error criteria distributions positively skewed, as most of the head data fit the water table level. Thus, such a distribution could falsely indicate that many model realizations are potentially adequate representations of HF distribution, without adequately constraining the solution space.

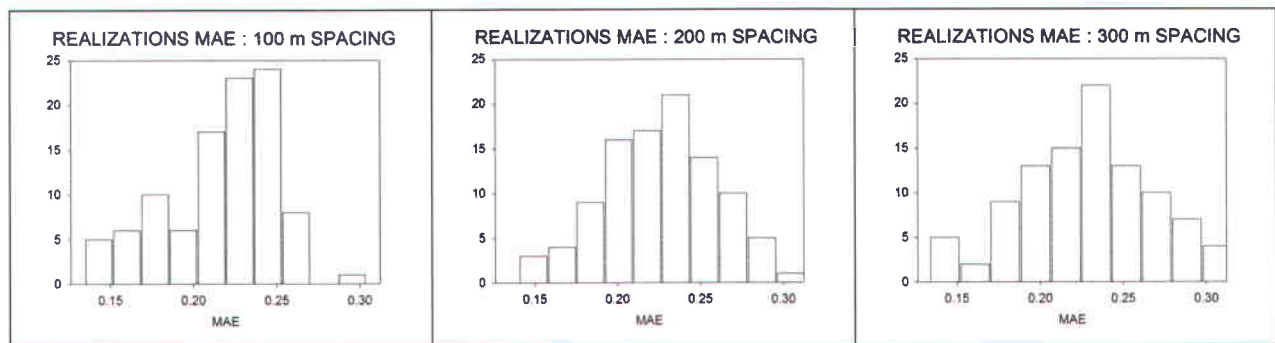


**Figure 3.32** Error criteria distribution from head profile discrepancies for all the MP realizations with a) 100 m spacing, b) 200 m spacing and c) 300 m spacing.

### 3.8.4.2 Effect on optimization outcomes

Using sparse head profile data to constrain the characterization of aquifer HF distribution and continuity is based on the premise that the latter impacts heads over a certain distance. As illustrated in section 2.1, the local distribution of heads do not solely depend on HF distribution and continuity, but also on boundary conditions, HF hydraulic conductivity contrasts and anisotropy (Freeze & Cherry, 1979). Thus, the area of influence of local K values on surrounding

head distribution is case specific. Nevertheless, assessing the impact of head profile spacing on calibration outcomes can provide preliminary information on the potential application of this method to a real field site. Hence, selected and calibrated realizations based upon the use of head profiles with 100 m, 200 m and 300 m spacing are presented in figure 3.33.

Initial **selection** of the best MP realization with MAE criterion from head profiles at 100 m spacing (section 3.8.2.1) provided relatively good results in reproducing the 3 continuous permeable layers (figure 3.33a). Increasing the head profile distance to 200 m still proves relatively satisfactory, as the continuity of the three layers is still distinguishable and there is only a slight increase in the MAE value (+ 0.013m, table 3.9). If the head profile spacing is increased to 300 m, there is significant deterioration of HF continuity, as the two layers to the right are present but discontinuous. The significant rise in the error criteria (+ 0.037m) is indicative of poorer reproduction of head profile data.

Calibration with **gradual deformation** at 100 m spacing of head profiles (section 3.8.2.2) produced a realization with adequate HF continuity, except for the upper right layer, which is discontinuous (figure 3.33b). Increasing the spacing of the profiles to 200 m and 300 m does not affect significantly the resulting realizations, as similar HF distribution and continuity occurs. This is reflected in the MAE error criterion, which increases by less than 0.01m (table 3.9).

Calibration with **control points** at 100 m spacing of head profiles (section 3.8.2.3) produced a realization adequately reproducing HF continuity and distribution (figure 3.33c), with the lowest MAE value. Increasing the spacing of the profiles to 200 m slightly increases the MAE criterion (+ 0.012m) although the three continuous layers are present. The continuity of the upper right layer is apparently disrupted when the spacing of head profiles is increased to 300 m, but the MAE error criterion is almost unchanged. As the head discrepancies are locally below the threshold (0.05 m) near the discontinuity, no further modification has occurred. This might be an effect of the relative thinness of the discontinuity and of lower sensitivity of heads to K near discharge areas. Furthermore, since the low permeability area or layer is only 1 or 2 cells thick, the calculation of Darcy fluxes is not as affected by this low permeability barrier (DHI-WASY, 2013). Thus, the annihilation of the barrier effect may particularly affect subsequent transport and pathline computation.

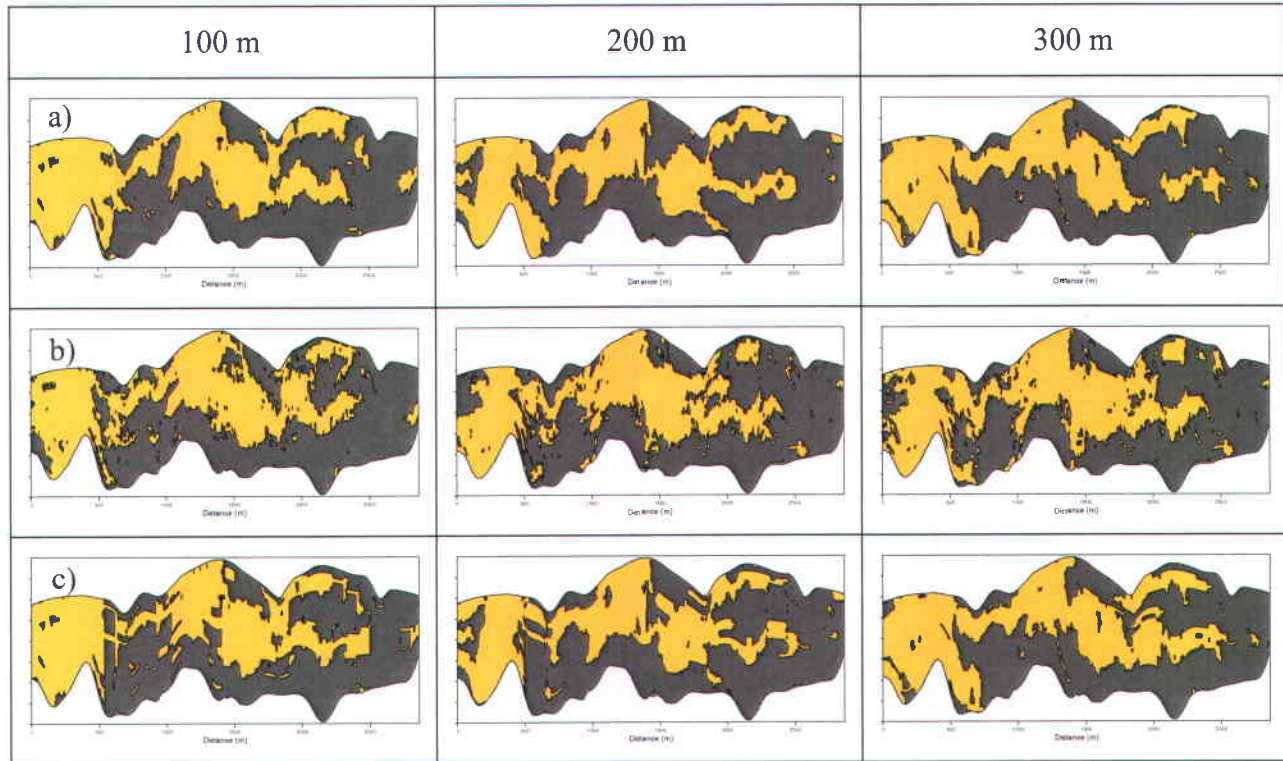


**Figure 3.33** Selected (a) and calibrated (b, gradual deformation; c, control points) realizations based upon using head profiles with 100 m, 200 m and 300 m spacing.

#### 3.8.4.3 Effect on head profile discrepancies

The main error criteria for selected and calibrated realizations with increasing head profile spacing are presented in table 3.9. Generally, the head discrepancies rise with the increase of head profile spacing, more markedly for the selection of MP realizations. Thus, selection of best realizations based on head profiles with large spacing could lead to erroneous interpretation of the HF distribution and continuity. Although the calibration by gradual deformation fails to reproduce the continuity of the upper right layer, it is little impacted by the head profile distance as the HF distribution and the MAE (0.09 m to 0.099 m) are maintained. As for calibration with control points, there is only a slight increase in the head discrepancies with increased profile spacing. Thus, horizontal (and vertical) spacing of measurements must be adapted to local conditions.

**Table 3.9** Error criteria of the selected and optimized realizations with increased spacing between the head profiles.

Realization	100 m spacing		200 m spacing		300 m spacing	
	MAE	RMSE	MAE	RMSE	MAE	RMSE
<b>Best MP realization</b>	<b>0.135</b>	0.221	<b>0.1482</b>	0.2243	<b>0.1856</b>	0.2764
<b>Gradual Deformation</b>	<b>0.090</b>	0.136	<b>0.0983</b>	0.1592	<b>0.0993</b>	0.1518
<b>Control Points</b>	<b>0.066</b>	0.128	<b>0.0786</b>	0.1603	<b>0.08</b>	0.1255

### 3.8.5 Effect of discontinuity of HF distribution (discontinuous model)

Results presented up to here have all been based on calibration and comparison with the continuous reference model. The observed head profile data used for error criteria calculation were extracted from the latter. In light of these results, head profile data appears under certain circumstances to provide sufficient information to select or reproduce continuous HF distributions. In order to assess the potential of head profiles to discriminate discontinuous HF distributions, the head profile data produced from the discontinuous reference model was then used as *observed* head profiles for error criteria calculation. However, the ensemble of MP realizations has been generated with data extracted from the continuous reference model. Fortunately, the 6 synthetic wells showed HF data very similar to those from the discontinuous reference model except for one well (second to the left). Thus, the same ensemble of realizations has been used to apply the selection and calibration approaches than for the continuous reference model; only the observed head profiles were changed for those produced from the discontinuous reference model. In the end, the HF distribution and continuity of selected and calibrated realizations were compared with the discontinuous reference model.

3.8.5.1 All MP realizations

Again, the 100 HF realizations generated with MPG are conditioned to the synthetic K data logs extracted from the continuous reference models and to water table elevation. The HF proportions for the discontinuous reference model are relatively similar than for the ensemble of MP realizations and the synthetic wells (table 3.10).

**Table 3.10 HF proportions for discontinuous reference model and all MP realizations.**

<b>Statistics</b>	<b>Discontinuous model</b>	<b>All MP realizations</b>	<b>Extracted well data</b>
<b>HF1 prop</b>	0.39	<b>0.43</b>	0.44
<b>HF2 prop</b>	0.61	<b>0.57</b>	0.56
<b>Global recharge (m3/day)</b>	7.36		

Hydraulic head fields generated from flow simulations on all MP realizations enabled the evaluation of observed and simulated head differences for the discontinuous reference case. With head profiles at 100 m spacing, RMSE and MAE criteria show a very different distribution than for the continuous reference model. The negative skew of the latter demonstrated a general misfit of most of the MP realizations. In this case, the distribution of both the MAE and RMSE is strongly positively skewed (figure 3.34 a and b), suggesting that most of the MP realizations are more satisfactory in terms of matching heads. Indeed, although the mean criteria values are similar in both cases, the median of the error criteria are lower in the discontinuous case. Again, the realizations with lowest error criteria should provide a better representation of the discontinuous HF distribution.

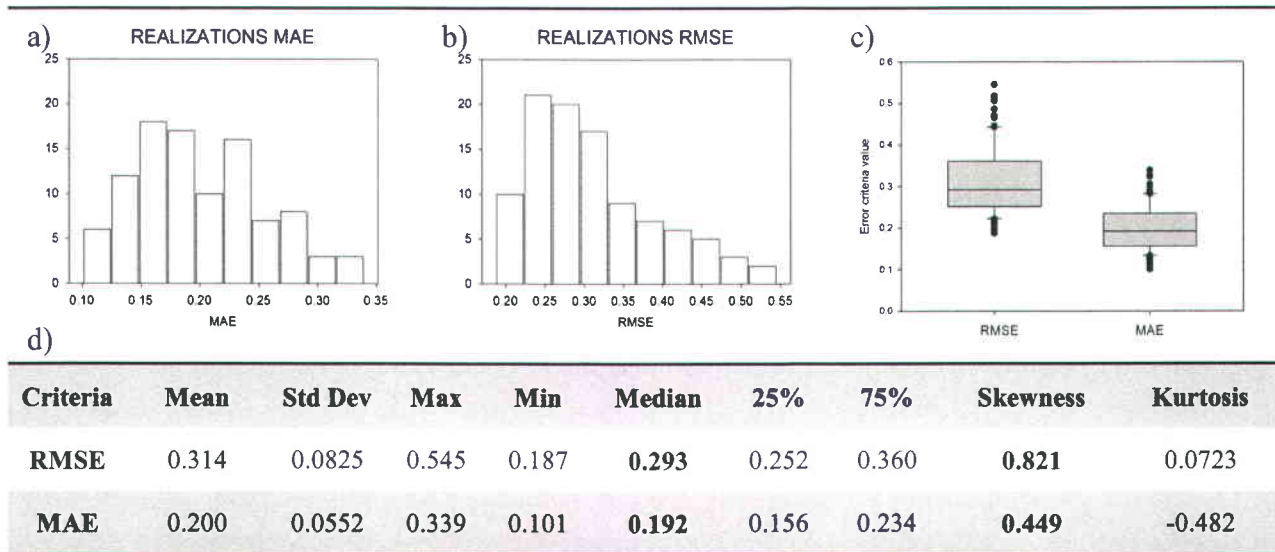


**Figure 3.34** Error criteria distribution (a, b and c) and statistics (d) from head profile discrepancies with discontinuous reference model (100m spacing) for all the MP realizations.

### 3.8.5.2 Best discontinuous MP realization

Calculations of MAE and RMSE for all the MP realizations provide minimum criteria values for selecting MP realizations which best fit the discontinuous head profiles. As for the continuous case, both minimum criteria coincide with the same MP realization (figure 3.35). The selected realization (figure 3.35a) shares a similar HF distribution in the right part of the domain as the reference continuous model, as both discontinuous permeable layers are present. However, the permeable layer on the left side of the domain is not discontinuous as in the reference distribution, as there are no MP realizations showing simultaneously all three discontinuous layers. This underlines a significant limitation in the selection approach, as the solution space of parameter distribution may not cover solutions representative of the studied aquifer. The scatter plot of simulated and observed profile heads (figure 3.35c) shows a relatively good fit ( $R^2 = 0.981$ ), with the RMSE and MAE error criteria at 0.19 m and 0.101 m, respectively.

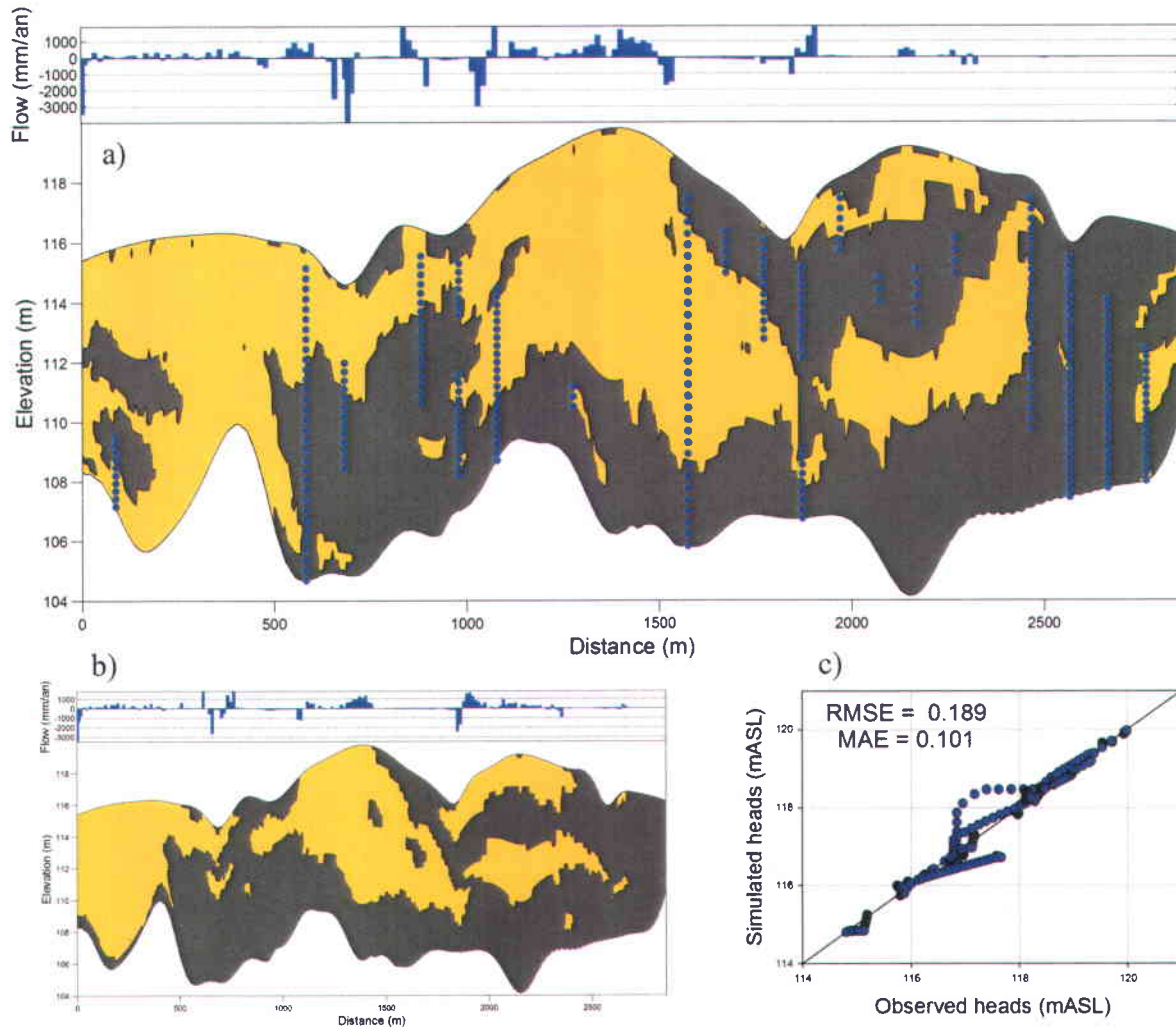


**Figure 3.35** (a) Selection of best MP realization based upon MAE and RMSE criteria with head profile discrepancies over 0.1 m (points) and corresponding recharge distribution on top of profile, (b) Reference discontinuous model, and (c) Scatter plot of observed and simulated heads with corresponding mean error criteria.

### 3.8.5.3 Optimization with global gradual deformation

The resulting calibrated HF realization by combining MP realizations to fit the discontinuous head profiles is presented in figure 3.36. This realization has the following characteristics:

- i. Reproduces the 3 discontinuous layers, although the left one is only partly discontinuous. This may be an effect of the incorrect HF data from second well to the left for generating the MP realizations, as mentioned earlier;

- ii. Still adds scattered noise (pixels) compared to the reference model which is smooth;
- iii. Decreases the number of profile points with head differences larger than 0.1 m;
- iv. Causes the most significant decrease of the error criteria (RMSE of 0.093 m and MAE of 0.057 m) and the best fit on the scatter plot of observed and simulated heads.

In this case, the global gradual deformation causes the best fit of the head profiles overall, while it locally reproduces rather well discontinuities in the HF distribution. Thus, for a same water table and well HF data as the continuous reference case, adding head profile information improves the spatial distribution and continuity of HF.

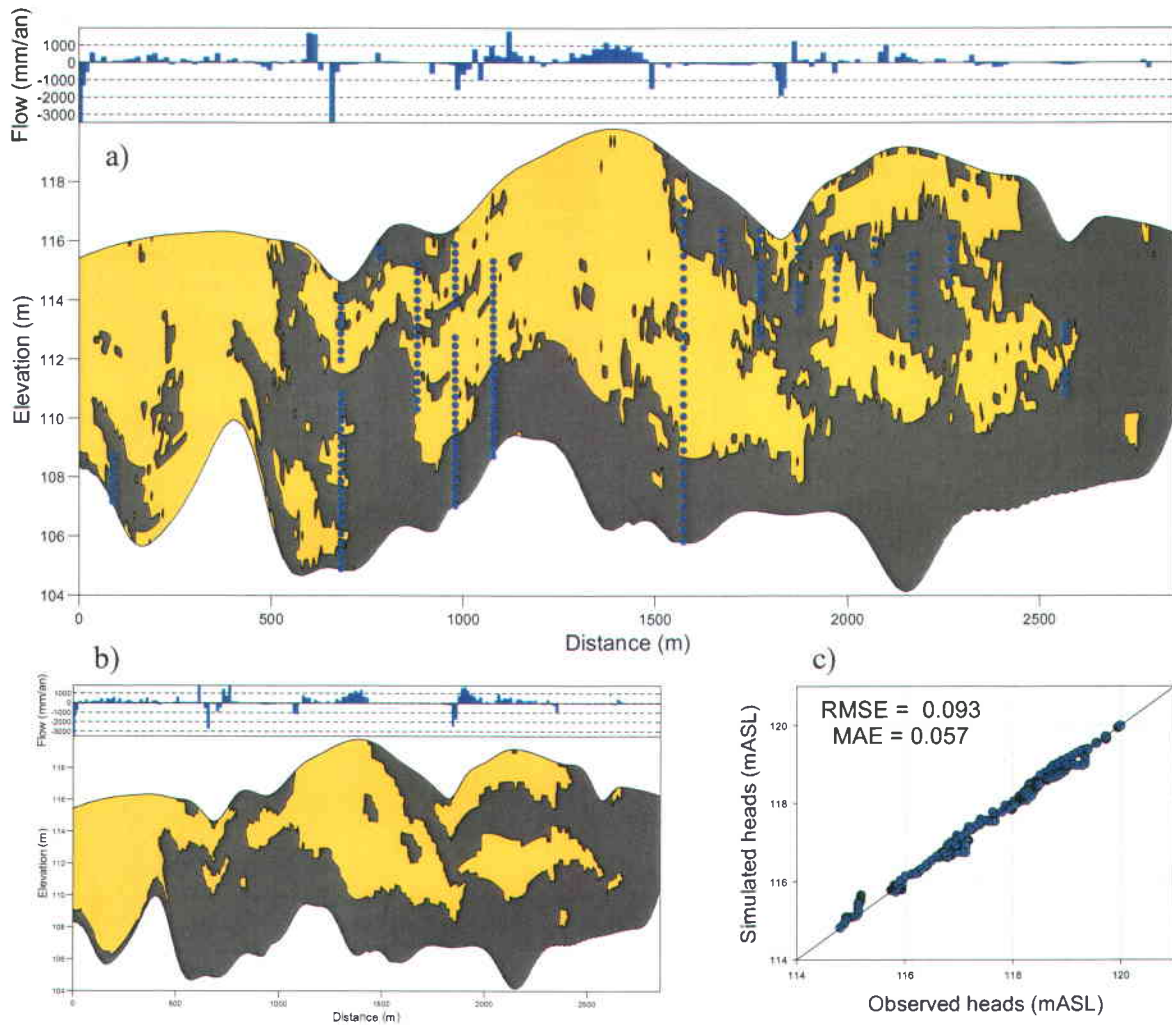


**Figure 3.36** (a) Calibrated realization by gradual deformation based upon MAE and RMSE criteria with head profile discrepancies over 0.1 m (points) and corresponding recharge distribution on top of profile, (b) Reference discontinuous model, and (c) Scatter plot of observed and simulated heads with corresponding mean error criteria.



#### 3.8.5.4 Calibration with control points

Once again, the control points have been arbitrarily located at the head profile data locations and the control point sets of values have been extracted from all the MP realizations to preserve larger scale relations between the K values. The resulting realization has the following characteristics (figure 3.37):

- i. Better reproduces the three discontinuous permeable layers;
- ii. Produces significant decrease of error criteria (RMSE of 0.128 m and MAE of 0.081 m) and the best fit of simulated heads;
- iii. Still adds 'blocky' pattern by kriging of values of the control points;
- iv. Presents few observation points with head differences larger than 0.1 m on the right side of the domain, but there is a significant number of points with head discrepancies over 0.1 m in the left area.

There is a significant number of points with head discrepancies over 0.1 m in the left area (underlined in point iv.), whereas the HF distribution appears reasonably similar to the reference model. This might be caused by differences in the HF representation on the top of the model and consequently to significant differences in the recharge distribution, which affects the whole area. For this particular realization, the correlation coefficient with the reference model recharge is particularly lower in this area (0.63) than for the gradual deformation realization (mean 0.75). Nevertheless, the minimization process of head discrepancies produces relatively adequate HF distribution pattern in the area.

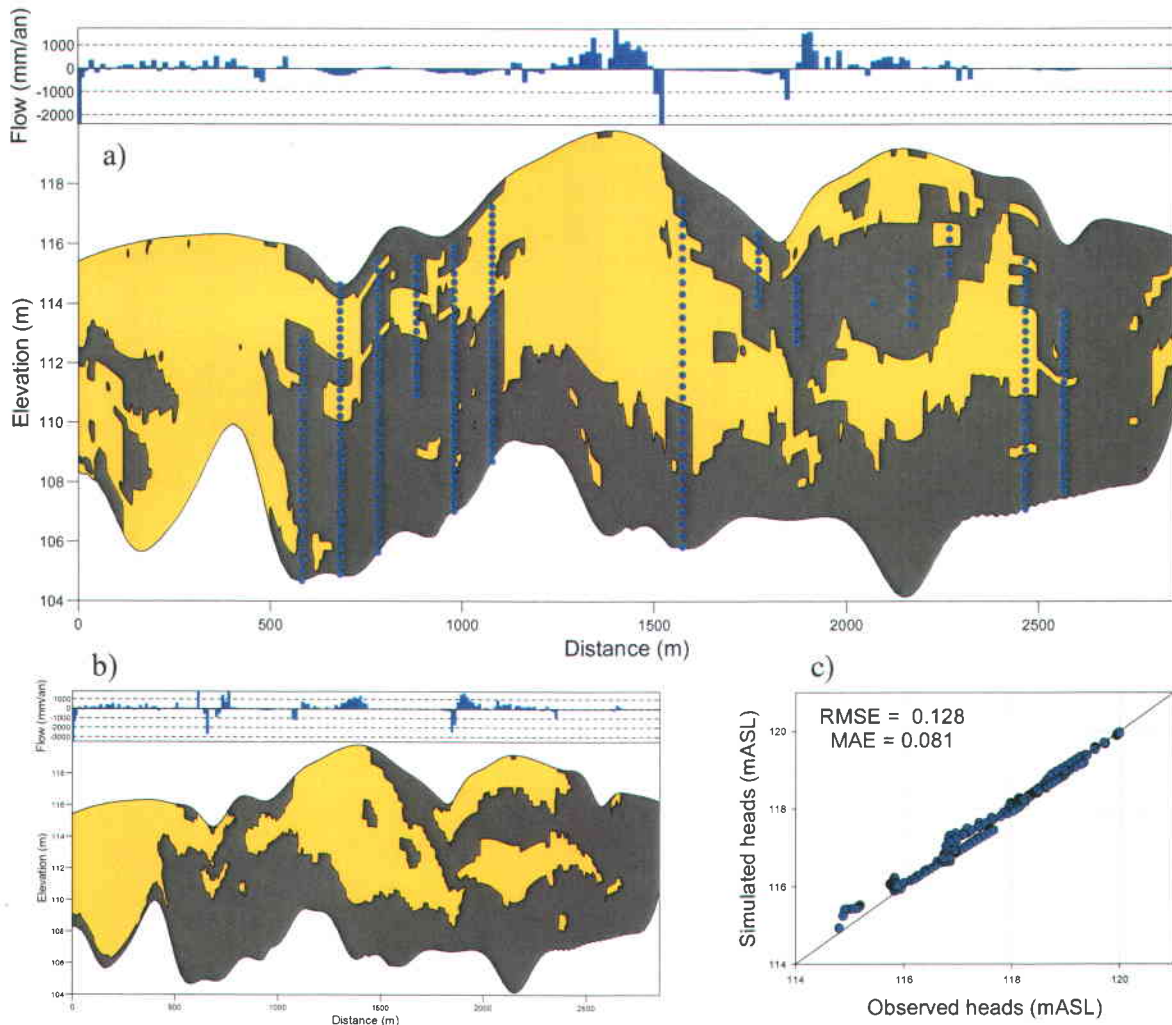


**Figure 3.37** (a) Calibrated realization with control points based upon MAE and RMSE criteria with head profile discrepancies over 0.1 m (points) and corresponding recharge distribution on top of profile, (b) Reference discontinuous model, and (c) Scatter plot of observed and simulated heads with corresponding mean error criteria.

### 3.8.5.5 Summary of best discontinuous realizations

In light of these results (summarized in table 3.11), vertical hydraulic head profiles appear as a measurement sensitive to (dis)continuity in HF layering. First, MP realization selection based on head profile error criteria provides a fairly representative distribution pattern of HF with discontinuities on two of the three target layers, over 76% of correct HF representation, a MAE relatively small (0.1 m) and similar global recharge (110%). There is generally an under-representation in HF1 representation, as consequence of MP methodology which generally under

represents HF with smaller proportions (dell'Arciprete *et al.*, 2012). Global gradual deformation produces a realization with adequate discontinuity representation, apart for the left permeable layer where the discontinuity is farther than for the reference model. There is a slight increase in the correctness of HF representation, a significant decrease of error criteria and similar global recharge representation. Finally, the control points method provides the best HF representation, although the error criteria are slightly higher than with the gradual deformation method. Again, this might be partly explained by the recharge pattern and global recharge value which is almost 20% lower than for the reference model. The under representation of HF1 is partly corrected when using control points (misrepresentation of HF1 as HF2 drops under 10%).

**Table 3.11** Summary of the error criteria for the best MP realization, calibration with global gradual deformation and with control points (discontinuous reference model).

Realization	Mean Absolute Error (MAE)	Root Mean Squared Error (RMSE)
<b>Best MP realization</b>	<b>0.101</b>	<b>0.189</b>
Gradual Deformation	0.057	0.093
<b>Control Points</b>	<b>0.081</b>	<b>0.128</b>

### 3.9 Discussion

Favorable outcomes in selection or calibration of a set of realizations from vertical head profiles suggest this type of detailed hydraulic data can provide valuable information on aquifer structure and HF continuity. As mentioned earlier, local distribution of heads also depends on boundary conditions (e.g. recharge), HF hydraulic conductivity contrasts and anisotropy (Freeze & Cherry, 1979), hydraulic gradients and flow pattern. Fixing the water table while modeling saturated steady-state flow emphasizes the effect of HF distribution on heads, but recharge distribution and magnitude can still play a significant role. The distribution of recharge can locally affect the flow pattern, but overall this distribution is rather comparable for the calibrated realizations (cross-

correlations averaging 0.57). The global recharge or inflow-outflow does generally not depart more than 20% from recharge value of the corresponding reference model.

The assessment of the separate effects of HF hydraulic conductivity contrasts, head profile spacing and HF distribution exposes significant impacts on the effectiveness and applicability of the proposed method. In reality, interactions between these factors with flow orientation and gradients render evaluation of the diagnostic potential of head profiles all the more complex and site-specific.

### **3.9.1 Flow pattern of reference models**

The effects of these interacting factors on resulting flow patterns and head distribution are presented here. Figures 48 and 49 allow partial visualization of the combined effects of recharge, hydraulic conductivity contrasts and HF distribution on flow and heads for the continuous and discontinuous references cases, respectively. Contours of the distribution of head differences with the homogeneous case and velocity vectors illustrated in these figures have been generated with K contrast of 2 orders of magnitude between the 2 HF (see figure 3.16). The main observations are the following:

- i. Recharge distribution is more localized (shorter wavelength) and of smaller magnitude or amplitude in strongly heterogeneous setting (red line) rather than homogeneous setting (dotted line);
- ii. Flow patterns and velocities are significantly modified by varying K contrasts (only two orders of magnitude shown here) and HF distribution (continuous and discontinuous models);
- iii. Changes in K contrasts (one to three orders of magnitude) and continuity in HF distribution does not significantly modify the areas of recharge/discharge and thus the transition zone locations;
- iv. Homogeneous areas (both extremities and central part) are not sensitive to changes in HF hydraulic conductivity contrasts;
- v. Despite significant K contrasts of two or three orders of magnitude, both reference models show very low sensitivity of heads in transition zones and low gradient zones;

- vi. The areas where heads are sensitive to K contrasts are generally the same in continuous and discontinuous setting.

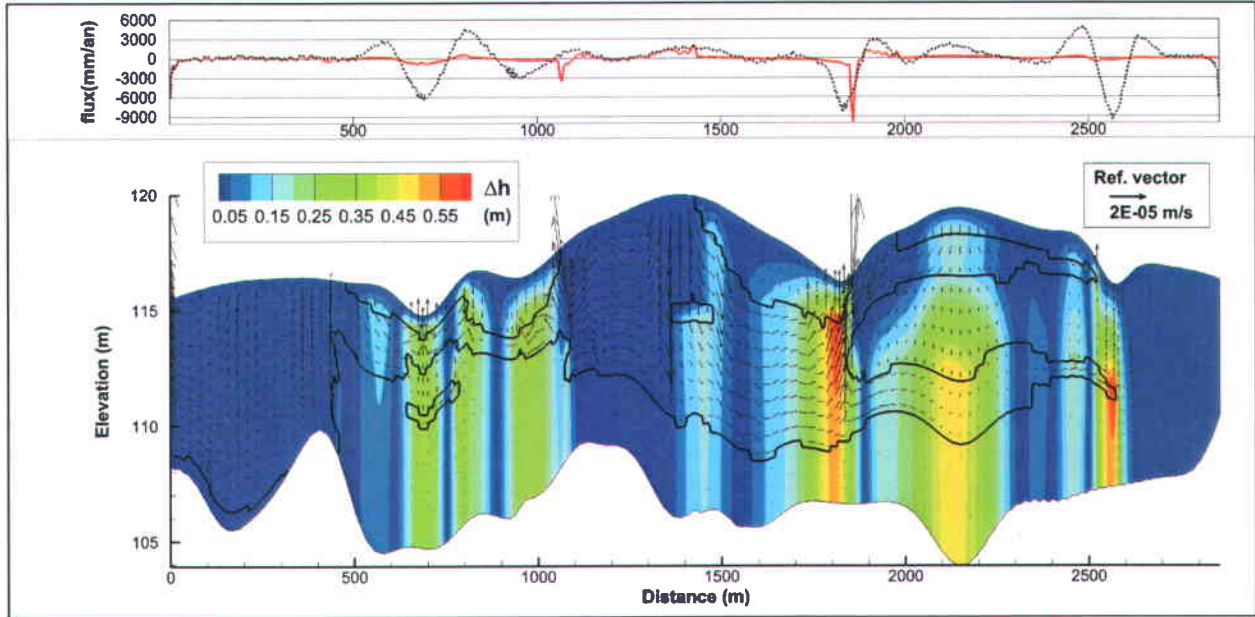


**Figure 3.38** Continuous reference model recharge distribution (top), HF contacts (black thick contours), velocity vectors (arrows) and head differences between homogeneous K model and model with K contrast of 2 orders of magnitude (colored contours, as in figure 3.16).

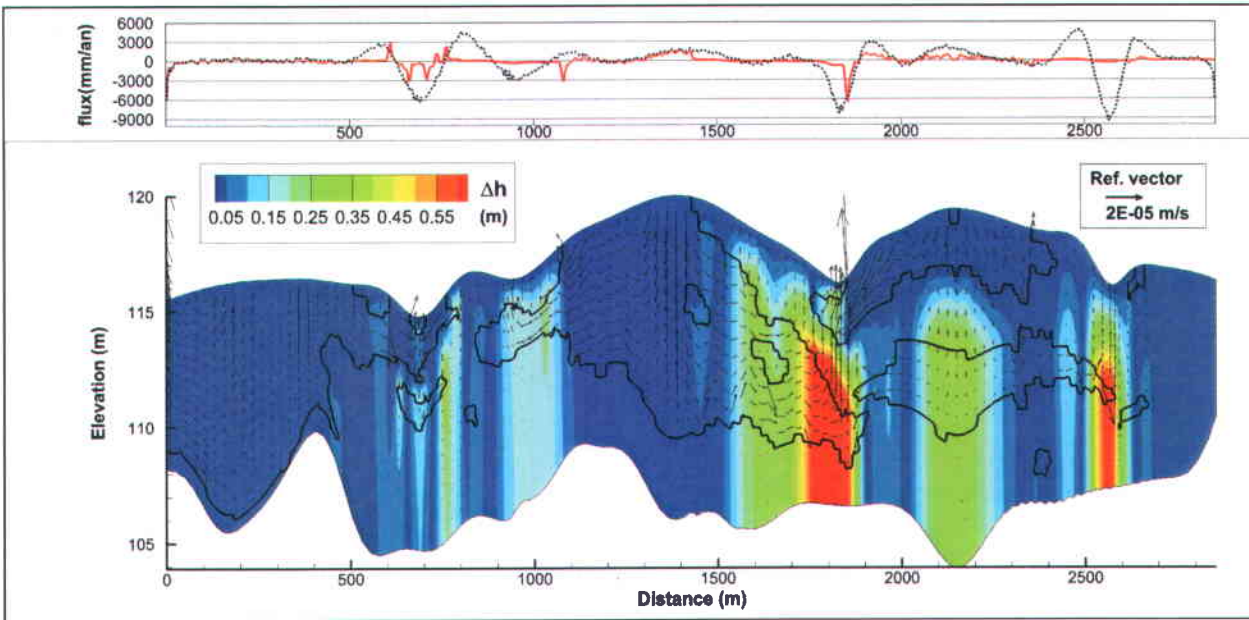


**Figure 3.39** Discontinuous reference model recharge distribution (top), HF contacts (black thick contours), velocity vectors (arrows) and head differences between homogeneous K model and model with K contrast of 2 orders of magnitude (colored contours, as in figure 3.16).

Thus, in settings where flow is superficial and mainly topographically driven as in these reference models, topography could act as a guide to identify hydraulically insensitive zones to HF contrasts and continuity. Alternatively, preliminary flow simulations could help locate target areas for acquisition of potentially informative head profiles.

In practice, it might be better to do realization selection or optimization with vertical differences of heads in profiles or vertical head gradients, as the error on absolute head measurements is much larger than head differences between vertical measurements. Thus, the selection and calibration methodologies applied here are based upon a head discrepancy threshold of 5.0 cm, as Fisher and Twining (2011) have calculated a measurement accuracy for vertical head differences of  $\pm 0.1$  foot (3.0 cm) between adjacent monitoring zones. As the reference continuous and discontinuous models are particular realizations based on real data from the study site (in Saint-Lambert-de-Lauzon, Qc.), the particular settings (model geometry, boundary conditions, level of heterogeneity) of this synthetic exercise are plausible configurations of the site. In these particular settings, such a context would require K contrasts and anisotropy of more than 1.5 orders of magnitude to provide sufficient and measurable head differences. The required K contrasts between HFs and anisotropy ratio could possibly be less if the global gradients at the site were higher, as high hydraulic gradients are favorable for producing larger fluctuations in vertical head differences or vertical gradients (see section 2.1).

Moreover, there is a noticeable loss of sensitivity of hydraulic measurements (heads) in transition zones between recharge and discharge areas where flow is essentially horizontal, thus parallel to layering. For example, the flow lines for the continuous reference model (figure 3.40) are essentially horizontal throughout the entire aquifer thickness between the contoured areas where head differences larger than 0.05 m were calculated. There is also a significant loss of sensitivity where gradients are very low, such as in the area identified by the box in figure 3.40 where a stagnation point is located.

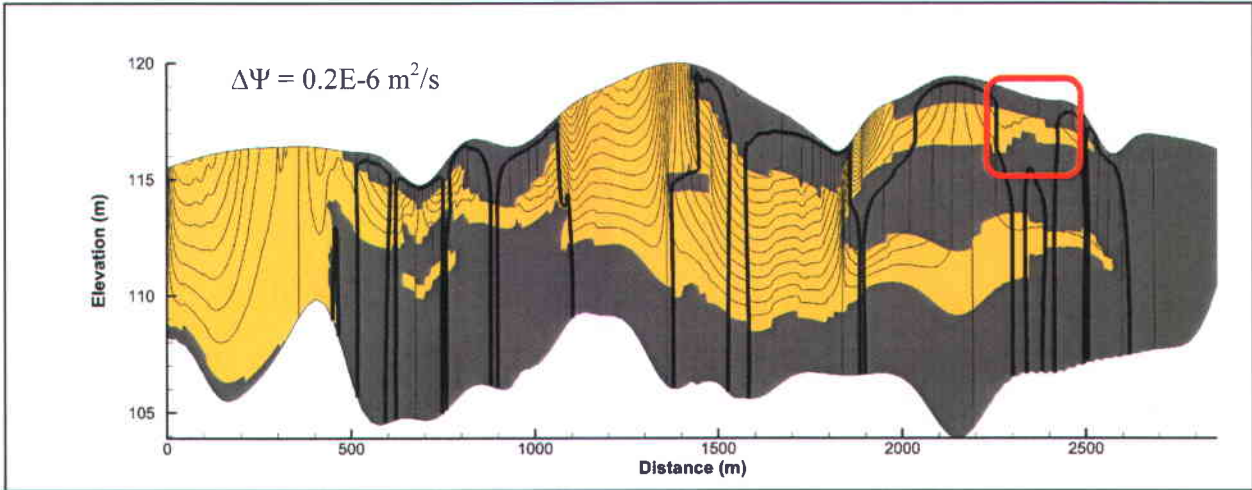


**Figure 3.40** Flow lines for the continuous reference model with  $K$  contrasts between HF of two orders of magnitude. Note the areas between the thick black contoured volumes and the area delimited in the blue box ( $\Delta\Psi$  corresponds to flow within each stream tube).

In summary, sensitivity of hydraulic head distribution depends on the flow system which in turn is a consequence of interaction between model structure and parameters. The hydraulic sensitivity to  $K$  distribution and continuity is not the same as geostatistical sensitivity, in terms of areas with higher variance in HF or  $K$  representation within multiple realizations. Thus, selection of potential areas for collecting informative vertical head profiles should not be solely based on these zones of higher geostatistical variance; the hydraulic sensitivity should also be considered. Adding such hydraulic data to constrain geostatistical realizations provides a valuable and independent input to assure hydraulic plausibility of these realizations.

### 3.9.2 Calibration approaches

Among the large number of available inverse modeling methods, stochastic inverse modeling methods allow generation of multiple equally likely conditional simulations to assess model uncertainties. Thus, subsequent use of global calibration schemes such as gradual deformation of conditional realizations based upon newly acquired data such as vertical head profiles can effectively constrain these uncertainties. However, this study has shown limitations in locally reproducing HF (dis)continuity through decrease of head discrepancies. Le Ravalec and Mouche (2012) underline that GDM succeeds in significantly decreasing the objective function at first

iterations but then a plateau is reached, where it becomes difficult to further reduce it. Understandably, it may become hard to fit heads appropriately everywhere by combining realizations over the entire domain; parts of realizations that fit heads better in certain areas will deteriorate the fit elsewhere. Furthermore, generating realizations with MP geostatistics, though eluding non-stationarity difficulties, does not require definition of any random function model. Thus, local modifications of the K field respecting the prior spatial structure are not as straightforward, as with two-point statistics approaches.

Global GD was applied by systematically evaluating the parameter  $\theta$  (see section 3.7.2) from  $-\pi$  to  $\pi$  for each set of 3 realizations with increments of 0.15, as inverse modeling is performed on simple 2D realizations. Moreover, combination of all the MP realizations (100) required 2009 flow simulations, namely 41 iterations on parameter  $\theta$  on each of the 49 combinations of MP realizations (figure 3.41a). In 3D or more complex cases of data integration, the optimization algorithm could obviously be improved. For instance, Le Ravalec-Dupin and Hu (2007) have proposed using gradient-based techniques such as finite-differences or adjoint-state methods. Capilla and Llopis-Albert (2009) have proposed a gradual refinement method for searching the optimal combination parameter, as «the simplicity of the minimization problem and the smooth variation of the objective function lead to consider a far more straightforward and simpler approach». In an attempt to reduce computational effort, selection of the best MP realizations for combination by gradual deformation has proven unsatisfactory as objective function reduction was tampered. Thus, foreseeing the outcome of realization combinations by selecting best realizations a priori is uncertain. Nevertheless, hundreds of flow simulations are still required for global optimization; much more would be required for local gradual deformation.

As mentioned earlier, a heuristic control points method was applied on a regular grid covering the entire model domain. Calibration at once with many parameters (control points) has led to instabilities in objective function reduction, as reported by Alcolea *et al.* (2006), hence the common approach of starting with one pilot-point and adding new points at each iteration of the optimization process. In this study, such an approach could not be implemented since complex interactions between location of optimized parameter values and flow could impede achieving an overall optimal solution. In order to sequentially find the optimal parameter values at all control points locations, optimization could have been done following the sequence of natural flow coordinates (Rivest *et al.*, 2012). Instead, an intermediate solution was found where groups of



control points were optimized sequentially following five distinct flow areas in terms of recharge/discharge locations (section 3.7.3). For a relatively small 2D model domain, this optimization sequence required almost 500 flow simulations (figure 3.41b). Here again, significant improvements could have been made, as almost all the objective function reduction per zone occurs in the first few iterations. The control point values being calibrated as a whole in each group, decrease of the objective function rapidly reaches a plateau as individual modification of control point values would not be based on underlying spatial statistics.

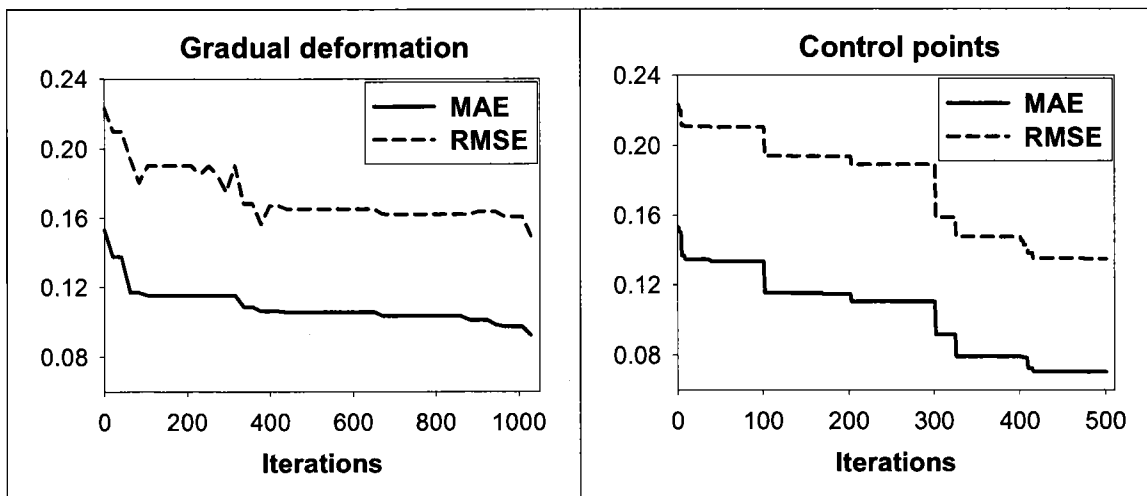


Figure 3.41 Evolution of the objective functions (MAE and RMSE) against the number of iterations (flow simulations).

Such a systematic approach as applied in this simple 2D context could hardly be considered in larger 3D or more complex settings, as computational cost of flow simulations would be prohibitive. Thus, alternative approaches should be considered for calibration to relatively high resolution vertical head profiles. Considering the methodology applied in this study, the two calibration methods were assessed independently. However, as the deformation process of gradual deformation is global, methods that can locally modify a parameter field, such as pilot points, are potentially far more effective. Nevertheless, as these methods come at a higher computational cost, local optimization of parameter fields for 3D aquifers with multiple data sources is an ongoing challenge. In this study, a possible improvement of the calibration method could be sequential application of global and local methods. When optimization reaches a

plateau during global gradual deformation, calibration scheme could switch to pilot-point method (figure 3.41). This combination of these 2 approaches (global, then local) with the aforementioned potential improvements (e.g. gradual refinement of  $\theta_{opt}$  search, limitation of number of iterations if objective function plateau) could potentially render the proposed methodology applicable at relatively larger scales.

### 3.9.3 Application and limitations

This study is essentially a proof of concept for the use of head profiles to constrain geostatistical simulations through a synthetic - but realistic - case. Practical guidelines for field and numerical application of this approach still need to be developed and field tested. Nonetheless, certain practical considerations can be inferred from the results of the present study.

#### 3.9.3.1 Practical considerations

The proposed approach aims at characterizing efficiently aquifer heterogeneity, in order to produce representative models in the context of local contamination issues. The idea is to assess representation of heterogeneity at an intermediate scale, which is generally the scale encompassing mass transport from point sources to potential receptors. For example, the Saint-Lambert-de-Lauzon study site covers approximately 12 km<sup>2</sup>, thus requiring hydrogeophysical-based approach for efficient and detailed aquifer characterization.

In order to implement model calibration to head profile data in a stochastic aquifer modeling context, some essential field requirements must be considered. First, continuous data of relevant field parameters (e.g.  $K_h$ ,  $K_v$ ,  $n$ ) are needed for generating geostatistical realizations. Thus, indirect geophysical data is crucial for efficient detailed characterization of aquifer properties. For example, site-specific relations developed between CPT/SMR data and collocated  $K$  data from slug tests were used in this study to predict  $K$  from widespread CPT/SMR data alone (Paradis et al., 2013). Alternatively, borehole flow meter can possibly be a tool used in such facies-type approach, to identify efficiently the local properties of each facies (Paradis *et al.*, 2011). Then, hydraulic data such as mean well heads (water table elevation) and fluxes are typically acquired for calibration of the geostatistical realizations with these state-variables. As the distribution and continuity of aquifer parameters are not fully sensitive to low resolution

hydraulic data, monitoring wells which allow acquisition of detailed hydraulic head profiles must be installed.

The level of vertical detail in hydraulic head measurements necessary to adequately verify and constrain geostatistical model realizations renders the use of nested wells or well clusters cost-prohibitive. Thus, two options are available in unconsolidated aquifers: 1) fully screened direct-push wells without sand-pack; or 2) multi-level monitoring wells. Only direct-push wells have been installed at the study site in Saint-Lambert-de-Lauzon, as they present numerous advantages documented by Paradis *et al.* (2011), namely: (1) obtaining continuous screens across the whole aquifer; (2) avoiding sand packs and potential flow bypass; and (3) minimizing disturbance to surrounding formations.

Multi-level monitoring wells can be an alternative to direct-push wells in the case of presence of cohesive soils or consolidated sediments. Many multi-level monitoring systems are currently available, such as the SWS Westbay system, the Solinst Waterloo system and the Water FLUTE system (Cherry *et al.*, 2007). The utility of these systems in fractured rock settings has been well established in many studies (e.g. Fisher & Twining, 2011; Meyer *et al.*, 2008; Parker *et al.*, 2006), though the cost-effectiveness of these systems for acquiring solely head profiles in the proposed approach remains uncertain.

### 3.9.3.2 *Application parameters and limitations*

In light of the results from application of synthetic head profile data to the selection and calibration of geostatistical realizations, some potentially favorable settings and parameter conditions can be derived:

- 1) Certain continuity in the distribution of HF relative to the problem scale is required in order to capture the main spatial patterns or (dis)continuities from head profiles. Thus, the number and density of head profiles must be in accordance with expected HF continuity.
- 2) The hydraulic conductivity ratio controls the nature of the hydraulic head or potential field (Freeze & Witherspoon, 1967). Thus, hydraulic conductivity (K) contrasts between

the HF and anisotropy ratio must be significant enough to produce measurable variations in the profiles of hydraulic head. K contrasts and anisotropy ratios reported in this study needed to be approximately 1.5 orders of magnitude or more, with moderate local gradients (generally 0.005 m/m).

- 3) Other than producing head profiles systematically with regular spacing, potentially informative head profile locations could be selectively targeted. Whereas high-variance areas within geostatistical realizations are of particular interest, local sensitivity of head distribution to K should be verified relating to boundary conditions (expected recharge and discharge areas) and local gradients. Thus, geostatistical variance and hydraulic sensibility should be assessed for selection of additional vertical head profiles and K control points, perhaps through preliminary flow numerical modeling.
- 4) The vertical spacing of head measurements is case-specific, as it relates to both HF unit thickness and level of detail required by the modeling objectives. Depending on the type of K distribution (e.g. progressive or sharp hydrofacies transitions), inflections in the profiles should reflect this setting. In addition, « detailed vertical head profiles by themselves can often be extremely useful to identify thin aquitards that constitute strong impediments or barriers to vertical ground water flow» (Parker *et al.*, 2006). They advocate for more detailed monitoring intervals as important information on heads and contaminant concentration would have been missed with few intervals.

#### 3.9.3.3 Study limitations

The initial purpose of this project was to evaluate the use of real head profile data in St-Lambert-de-Lauzon study site for constraining geostatistical realizations. As the level of potential information on K distribution contained in detailed head profiles seemed unclear, preliminary assessment of this with synthetic data was deemed necessary, hence this study. Producing reference models representative of the study site for subsequent synthetic modeling, although providing preliminary insights on the potential of application in this case, carries significant limitations. In summary, sensitivity testing of various model settings and parameters, such as varying the boundary conditions, topography, K contrasts, anisotropy and so forth would have been possible with a simplified synthetic 2-D model. Consequently, the results presented show

the applicability of head profiles in such a workflow, although they are limited in terms of generalization:

- 1) The workflow is applied on a simplified 2D steady-state flow model. Results presented here are based on many assumptions, namely: i) flow is parallel to the cross-section, without considering potential complex deviations in a real 3D setting; ii) there are no temporal variations in the model recharge-discharge and boundary conditions; iii) the only source of uncertainty is related to distribution of model parameters (K), which condition was required for isolating the effects of K distribution.
- 2) The consequences of inadequate representations of HF and K distribution at an intermediate scale (e.g. a few square kilometers) are all the more significant on mass transport than head distributions, as concentrations are considerably affected by dispersion. Therefore, simulating transport data from reference models and geostatistical realizations would have facilitated visualization and evaluation of model performance. For example, plume configuration or concentrations at wells or discharge areas could have supported analysis of optimization results.
- 3) In order to assess first the effect of the distribution of HF on hydraulic head profiles without considering small-scale variability of K, homogeneous K values were attributed to each HF. Thus, inflexions in head profiles are not dampened by K variability within each HF, which could render K transitions less abrupt. As head profile variations are sensible to orders of magnitude K contrasts and anisotropy (e.g. 1.5 and more in this study), this approach could not be applied to define small-scale variability of K within each HF. Nevertheless, K heterogeneity within each HF could have been simulated to assess its potential effect on head profiles. In this case, a simple method such as gaussian sequential simulation could have provided an appropriately correlated distribution of K per HF. For a highly heterogeneous aquifer with significantly different facies, the combination of  $\ln K$  values with a different mean and variance in each facies will produce significantly non-Gaussian profiles (Meerschaert *et al.*, 2013). In the end, intra-HF heterogeneity structure needs to be assessed for mass transport simulation, as dispersion effects must be considered.

- 4) Fixed anisotropy ratio ( $K_v/K_h$ ) has been used throughout this study, based upon a global mean of all collocated  $K_h$  and  $K_v$  data available at the study site. The effects of modifying this ratio should be evaluated similarly as for  $K$  contrasts between HF, as the interaction between anisotropy and flow direction (or flow vectors) should significantly impact the flow field and thus local head values. The anisotropy ratio of the less permeable HF (HF2) required for significant deviations of head profiles was less than anticipated from initial synthetic simulations (section 2.1), which suggests complexity of realistic flow fields may partly lessen the requirements for strong anisotropy.
- 5) Again, the workflow applied in this study assumes the only source of uncertainty comes from the parameter values, i.e. hydraulic conductivity, in order to isolate its effects. Consequently, the simulated head profiles which have been used as field data are the exact values of the reference models. Random errors could have been added to the simulated data based upon literature, e.g. normal distribution with mean error of 0.03 m (Fisher & Twining, 2011).
- 6) Initially, the same recharge distribution calibrated for reference models was applied for flow simulations of each MP realization, with free and moveable water table condition (DHI-WASY, 2012). As the generated MP realizations had varying distributions of low permeability HF on the top layer, fixed recharge applied on these cells generated instabilities and poor convergence (section 3.5.3). Thus, fixing the water table elevation to that of the reference models alleviated this problem, as the fluxes on top of each realization is adjusted during the simulations to fit the water table. A major drawback of this approach is that it reduces the sensitivity of heads at the top of the model to changes in  $K$  values. The flow fields produced are then affected by variations in recharge distribution with very little impact on resulting heads at the top of the model. Nevertheless, as the realizations fit in this way a perfectly known water table configuration, the effect of the latter on variations in vertical head distribution is removed.

The geostatistical realizations were generated with MPS algorithm IMPALA, with non-stationarity of the training image partly addressed with the use of X-coordinates as auxiliary variables (Comunian *et al.*, 2011; Straubhaar *et al.*, 2011). Modeling with no

random function model associated with structural parameters of the reference models has some shortcomings; using inversion procedures while wanting to preserve prior spatial characteristics is somewhat more complex. Although covariance preservation could have been ensured while generating MP realizations, the idea was to avoid imposing a prior covariance structure in order to assess head profile data potential. Thus, no explicit constraint was imposed by prior or regularization term: only the likelihood term was taken in account (for GDM and CP). As the global statistics were generally reproduced in MP realizations, there was no need to constrain the MP simulation process to reproduction of data HF proportions by Bayesian updating or Servo System Correction (Hu & Chugunova, 2008).

### **3.10 Conclusion**

Detailed hydraulic head profiles were identified as potentially useful data to constrain geostatistical realizations of heterogeneous hydrofacies and K fields and improve their representation. Unlike typical water level data, hydraulic head profiles may carry valuable information about the HF and K spatial heterogeneity and might be most beneficial when used in local calibration methods. Integration of such data into the calibration step of numerical flow models enhance the estimation of heterogeneity, but many restrictions as to required parameter values and model settings considerably tampers its applicability. Vertical deviations of hydraulic heads along profiles are largely associated with the strong anisotropy factor of less permeable materials, whereas such conditions allow capturing presence and continuity of preferential flow paths. Whenever favorable conditions for the use of head profile data are satisfied, assimilation of these data cannot capture the short scale variability (intra HF) of the reference models given the smooth variations in hydraulic head and strong K contrasts and anisotropy required. Nevertheless, the main patterns of the reference models could be identified.

In the case of a real study, specific locations for data collection could be targeted according to geostatistical variance in realizations. However, these locations must be validated in terms of local hydraulic sensitivity to variations of K. Moreover, the choice of vertical/lateral resolution

of profiles should be based on a balance between the anticipated degree of aquifer heterogeneity and the resolution limit of the multi-level monitoring system.

Given the relatively low sensitivity of hydraulic head data to K distribution, other data types sensitive to aquifer heterogeneity could be integrated in the calibration process, such as transient heads, geochemical data (e.g. peak concentrations), groundwater age or geophysical data. Thus, recent trends of inverse methods in hydrogeology include integration of multiple sources of information, which subsequently entails handling multi-scale parameterization problems. Furthermore, the complexity of local contamination issues underline the need for new tests that emphasize the role of heterogeneity rather than averaging it, such as tests between packed section of a well rather than in the entire well. In terms of a facies model built for a specific site, such tests could be interpreted within such a model and help define facies parameters.



## 4 SYNTHÈSE ET CONCLUSIONS GÉNÉRALES

### 4.1 Synthèse

Afin d'étudier les effets de la distribution de K sur les profils verticaux de charge hydraulique, les résultats de simulations synthétiques sur un modèle simplifié sont présentés dans la **section 2.1**. Ces résultats mettent en lumière non seulement la nécessité pour les HF de présenter un contraste de K de l'ordre d'un facteur 50 (1.5 ordres de grandeur), mais surtout la sensibilité de la distribution des charges à l'anisotropie de l'HF peu perméable. C'est ce dernier paramètre qui contrôle l'essentiel des variations verticales dans les profils de charge hydraulique et permet ainsi de mettre en lumière la présence et le niveau de continuité de couches perméables. Ces observations restreignent considérablement le potentiel d'application des profils de charge hydraulique, soit pour des milieux présentant d'importants contrastes de K (1.5 ordre de grandeur) et une forte anisotropie des matériaux peu perméables (1.5 ordre de grandeur). Bien que la première condition soit assez couramment rencontrée, la contrainte supplémentaire de conjonction avec la seconde présente des limitations évidentes. De plus, l'orientation de l'écoulement par rapport aux couches perméables et à l'anisotropie affecte également les variations dans les profils de charge; un écoulement essentiellement horizontal (e.g. sans composante de recharge) risque de présenter des variations de profils limitées aux extrémités des couches perméables. Par contre, la magnitude des gradients hydrauliques du système aquifère contribue à accentuer ou restreindre celle des variations dans les profils de charge. Ainsi, pour les conditions aux limites et valeurs de paramètres susmentionnées (K et anisotropie), le système aquifère doit présenter des gradients hydrauliques de l'ordre de 0.005 ou plus; plus les gradients locaux sont importants, plus les variations dans les profils seront accentuées.

Le site d'étude, les données et le développement des modèles de référence sont présentés sommairement aux **sections 2.2-2.3** et avec un peu plus de détail aux **sections 3.4-3.5**. L'aquifère granulaire de surface étudié a une épaisseur moyenne de 10 m et présente une hétérogénéité des propriétés hydrauliques (K). Des données colocalisées de K et de sondage au piézocône (CPT/SMR) ont permis d'obtenir des données quasi-continues de K réparties sur l'ensemble du site d'étude (53 sondages). Ces données de K ont été groupées en deux hydrofaciès de conductivité hydraulique distincte. Les profils d'HF et les niveaux d'eau des puits localisés sur

ou près d'une ligne d'écoulement ont été projetés en coupe sur cette ligne, afin de servir de support pour des simulations stochastiques des HF par points multiples (PM). Ces simulations par PM ont produit des réalisations assez variées en termes de distribution/continuité des HF malgré qu'elles aient été bien contraintes (par CPT/SMR). De ces simulations, deux réalisations dont l'hétérogénéité est distincte par rapport au niveau de continuité de l'HF perméable ont été sélectionnées et développées, afin de vérifier l'effet de la continuité sur les profils de charge et la capacité à retrouver la connectivité du modèle de référence lors de la calibration. Pour les simulations synthétiques subséquentes, les données de K et les profils de charge hydraulique extraits de ces modèles de référence ont été considérées comme étant des données de terrain (observations).

Les 100 réalisations MP ont été générées à partir des profils de K des modèles de référence (six profils) et contraintes à l'élévation de la nappe des modèles de référence, de telle sorte qu'il y ait une grande variance entre les données (**section 3.6**). Les profils de charge hydraulique extraits des simulations d'écoulement sur les réalisations géostatistiques permettent de sélectionner ou d'optimiser des réalisations plus représentatives des modèles de référence, et d'en calculer les écarts entre ces profils simulés et ceux de référence (**section 3.7**). La sélection de réalisations sur la base des profils de charge peut être relativement satisfaisante, dans la mesure où l'ensemble des réalisations est suffisamment large pour couvrir des représentations de K près du modèle de référence. Cet aspect est d'autant plus contraignant que des inconnues quant aux paramètres structurels de l'aquifère feront que l'ajout des données de profils de charge ne puisse améliorer l'estimation. L'approche par points de contrôle est plus souple en ce qu'elle permet de modifier localement les paramètres et de sortir d'un ensemble de réalisations. L'approche par déformation graduelle représente une forme intermédiaire puisqu'elle permet de déformer une réalisation par une succession de combinaisons linéaires.

Les résultats présentés à la **section 3.8**, bien qu'ils soient spécifiques à la configuration du site et aux paramètres appliqués, confirment le potentiel des profils de charge à améliorer l'estimation de l'hétérogénéité dans ce contexte. Les réalisations produites à partir des processus de sélection et de calibration reproduisent assez bien la distribution et continuité des HF, pour des espacements entre les profils de 100 et 200 m. Par contre, la sélection de réalisations ne reproduit pas la continuité adéquatement lorsque l'espacement des profils passe à 300 m, alors que les approches d'optimisation font un peu mieux. Ainsi, les profils de charge doivent être localisés

judicieusement en fonction des secteurs où des précisions quant à l'hétérogénéité doivent être apportées. Dans le cas discontinu, les résultats de sélection et d'optimisation à partir des profils de charge sont relativement similaires à ceux du cas continu, en termes de capacité à reproduire le champ de référence. Par contre, on voit bien dans ce cas la limitation de l'approche de sélection, alors qu'aucune réalisation produite par points multiples ne présente les trois discontinuités simultanément.

## 4.2 Discussion

### 4.2.1 Sensibilité hydraulique et géostatistique

Les résultats des simulations synthétiques initiales (section 2.1) illustrent bien la sensibilité relative faible des charges par rapport à la distribution de  $K$ . La relation entre les charges hydrauliques et  $K$  est plus complexe puisque non linéaire, alors que celle de  $K$  avec les flux est linéaire (loi de Darcy). Ainsi, le réseau d'écoulement et les vitesses sont modifiés de façon significative par des variations dans la distribution ou les contrastes de  $K$ , alors que les charges hydrauliques ne sont modifiées que légèrement. Ces variations dans les profils de charge hydraulique doivent être suffisantes afin d'être mesurables sur le terrain avec des erreurs de mesure relatives de l'ordre de 3 cm (Fisher & Twining, 2011). Malgré des contrastes de  $K$  de près de deux ordres de magnitude, les modèles de référence ne montrent que très peu de sensibilité des charges dans les zones de transition (écoulement parallèle aux couches) et les zones de faible gradients hydrauliques. Malgré cela, l'utilisation des profils de charge à partir des modèles de référence pour la sélection et l'optimisation semblent montrer de meilleurs résultats que dans le cas des simulations synthétiques initiales (section 2.1). Ceci peut s'expliquer par le fait que des modèles hétérogènes plus réalistes ont des patrons d'écoulement forcément plus complexes que pour un cas synthétique simplifié à deux ou trois couches. Par ailleurs, le système d'écoulement du site d'étude est superficiel ; tout l'écoulement est confiné dans la couche de sédiments d'une dizaine de mètres d'épaisseur. Ainsi, les gradients locaux sont généralement plus élevés qu'en observant le gradient global ou régional de la nappe. Ces gradients hydrauliques locaux plus importants contribuent également à l'augmentation de la magnitude des variations dans les profils de charge hydraulique.

Afin de contraindre les réalisations géostatistiques de l'hétérogénéité d'un aquifère, l'utilisation de ce type de données est d'intérêt dans des secteurs ciblés où la variance des réalisations est importante par rapport aux réponses de la modélisation qui sont attendues en ces endroits. Par contre, les localisations où la variance géostatistique est plus grande ne correspondent pas forcément à celles où la sensibilité hydraulique aux variations de  $K$  est suffisante. Il serait donc important de valider a priori la sensibilité hydraulique potentielle des localisations ciblées par la géostatistique avec des simulations numériques préliminaires ou des cartes piézométriques. Par exemple, les endroits avec de faibles gradients hydrauliques ou les zones de transition peuvent représenter un faible potentiel pour l'utilisation de profils de charge.

Par ailleurs, les profils de charge présentent des variations verticales essentiellement dans les 100-150 m de part et d'autre des discontinuités, dans le cas d'étude présent. La sensibilité relativement locale des charges hydrauliques par rapport aux variations de  $K$  est en partie tributaire de la proportion de recharge relativement faible qui transite dans l'HF peu perméable. Ce dernier doit présenter une valeur de  $K$  de 1.5 ordres de grandeur inférieur à celui de l'HF perméable ainsi qu'un facteur d'anisotropie de près de 1.5 ordres de grandeur afin que des variations verticales des charges hydrauliques soient mesurables.

#### **4.2.2 Approche d'optimisation et perspectives**

Compte tenu que les variations de charge hydraulique sont de faible magnitude et relativement localisées, la représentation adéquate de la distribution et continuité de  $K$  à l'échelle des sites contaminés requiert des approches permettant une calibration localisée. L'utilisation de méthodes de calibration localisées, telles les points-pilotes ou l'auto-calibration séquentielle, s'avère essentielle afin de pouvoir modifier localement la connectivité de certaines structures. Par contre, ces types de méthodes de paramétrisation lors de l'inversion viennent généralement avec un coût computationnel important. L'utilisation d'une séquence de méthodes d'inversion globale suivie d'une approche locale (e.g. déformation graduelle puis points-pilotes) pourrait permettre l'intégration de données de profils de charge hydraulique par un processus d'inversion d'un modèle en 3D plus lourd.

### **4.2.3 Applicabilité des profils de charge hydraulique pour contraindre l'hétérogénéité des champs de K**

La séquence des étapes appliquées dans cette étude afin de vérifier le potentiel d'exploitation des profils de charge est sensiblement la même que celle qui pourrait être requise à partir d'un cas réel. D'abord, des données continues ou détaillées de K sont nécessaires afin de pouvoir générer des réalisations géostatistiques, ainsi que des données de niveau d'eau pour contraindre l'élévation de la nappe. Ensuite, les localisations d'intérêt présentant une variance géostatistique jugée trop importante doivent être étudiées sur la base de leur sensibilité hydraulique potentielle. L'installation de puits multi-niveaux, de puits par enfoncement (direct-push) ou l'utilisation d'une sonde de profilage hydraulique par enfoncement représentent des approches possibles afin de pouvoir recueillir des profils de charge (dont les coûts vont décroissants).

L'approche proposée quant à l'utilisation de sondages au piézocône et de profils de charge hydraulique suppose la caractérisation d'aquifères granulaires de proche surface. L'utilisation de profils de charge hydraulique pourrait toujours être examinée dans le cas d'aquifères rocheux, mais le coût d'installation de puits multi-niveaux pourrait être prohibitif suivant le projet considéré. Le contexte géologique et la structure des dépôts sédimentaires doivent être soigneusement étudiés, puisque l'utilisation des profils de charge requiert une certaine continuité des couches par rapport à l'échelle du problème étudié. De plus, les conditions pour lesquelles les charges hydrauliques détaillées verticalement pourraient être informatives sont passablement restrictives, soient : 1) des gradients hydrauliques suffisants ( $\geq 0.005$ ) ; 2) des contrastes de K de près de 1.5 ordres de grandeur ou plus entre les HF ; 3) un facteur d'anisotropie du (des) HF peu perméable (s) de près de 1.5 ordres de grandeur ou plus ; et 4) une certaine variabilité des directions d'écoulement quant à l'orientation des couches. Cette dernière condition est certainement plus difficile à évaluer et pourrait rendre l'approche des profils de charge un peu risquée en termes du niveau d'information qui pourrait en être tirée. Cependant, pour les conditions d'écoulement généralement rencontrées en climat humide avec une recharge distribuée spatialement, la contribution de cette composante verticale produit des systèmes d'écoulement plus favorables à l'utilisation de profils de charge hydraulique. Par ailleurs, l'espacement requis entre les profils ou les localisations ciblées doivent être évalué spécifiquement en relation avec l'hétérogénéité attendue au niveau du site.

À la lumière de ce qui précède, tant les résultats des simulations préliminaires que celles à partir des modèles de référence illustrent le potentiel théorique de l'utilisation de profils de charge pour contraindre les réalisations géostatistiques, mais seulement sous des conditions particulières plutôt que pour une application généralisée aux aquifères granulaires de surface. Les conditions hydrogéologiques présentes au site d'étude à Saint-Lambert-de-Lauzon sont partiellement défavorables à l'utilisation de profils de charge hydraulique. Bien que le système aquifère présente une distribution hétérogène de  $K$  avec une certaine continuité latérale, les gradients hydrauliques du site sont généralement faibles à modérés et limitent ainsi la plage possible de variations verticales des charges hydrauliques mesurables sur le terrain. Dans ce cas, les contrastes de  $K$  entre les HF et l'anisotropie de l'HF peu perméable se doivent être d'autant plus grands. Au site d'étude, ceux-ci sont en deçà des valeurs qui sont estimées nécessaires (en termes d'ordre de grandeur) en fonction des gradients hydrauliques que l'on y retrouve. Par exemple, le contraste de  $K$  entre les HF utilisé pour les modèles de référence a dû être augmenté à deux ordres de grandeur (plutôt que de 1 en moyenne) afin de s'assurer de produire des variations verticales de charge hydrauliques significatives.

#### **4.2.4 Limitations de cette étude**

Plusieurs limitations quant à l'approche et la méthodologie appliquée dans le cadre de ces travaux réduisent en partie la généralisation de certaines conclusions présentées. D'une part, les simulations réalisées en 2D suivant une ligne d'écoulement sous-tend que l'écoulement se fait dans ce plan sur toute l'épaisseur de la coupe. Pourtant, dans les milieux hétérogènes tels que ceux considérés dans cette approche, il est fort possible pour l'écoulement de dévier localement de ce plan afin de contourner une lentille peu perméable par exemple. De plus, plusieurs simplifications dans la modélisation des propriétés hydrauliques ont été volontairement imposées afin d'isoler l'effet de la distribution seule des HF sur les profils de charge hydraulique. L'imposition d'une valeur de  $K$  et d'un facteur d'anisotropie homogènes pour chacun des HF ne représente pas la variabilité attendue dans de vrais dépôts sédimentaires. Dans une perspective de travaux de modélisation futurs, la représentation de l'hétérogénéité et de l'anisotropie de  $K$  pourrait aisément être implantée par simulations séquentielles gaussiennes (SSG) par exemple. Par ailleurs, les erreurs de mesure sur les profils de charge n'ont pas été considérées puisque l'idée était plutôt de démontrer le concept de l'utilisation de profils de charge ; des erreurs

aléatoires auraient pu être ajoutées aux données extraites des modèles de référence afin de rendre la modélisation plus réaliste. En appliquant la méthode des points de contrôle, l'effet de cette omission était moindre puisque la calibration des réalisations a été faite à partir des points dont l'écart entre les charges observées et simulées était de plus de 5 cm.

Par ailleurs, l'application d'une contrainte de charge fixe au sommet du modèle correspondant à l'élévation de la nappe, bien qu'elle ait permis d'isoler l'effet de la distribution de  $K$  sur les profils de charge, sur-contraint la modélisation et rend la calibration moins sensible à la surface du modèle. Dans un cas réel, les données d'élévation de nappe et de profils seraient sans doute intégrées simultanément à la calibration. Encore une fois, comme l'objectif de ces travaux était de vérifier le potentiel des profils de charge, aucune structure spatiale n'a été explicitement intégrée dans le processus de calibration. Cependant, dans le cas où une telle structure serait connue ou soupçonnée, l'application d'un terme de régularisation (un a priori géologique) dans la calibration par points pilotes pourrait être aisément intégrée. Finalement, la meilleure méthode afin de valider l'efficacité des approches proposées aurait certainement été de simuler le transport de masse, puisque les concentrations et courbes d'arrivée sont beaucoup plus sensibles à la structure et connectivité du champ de  $K$  résultant que la distribution des charges.

### 4.3 Conclusion

Les profils verticaux détaillés de charge hydraulique sont des données pouvant potentiellement contraindre les réalisations géostatistiques de champs de  $K$  et aider à l'estimation des paramètres hydrauliques. Les résultats présentés illustrent, contrairement aux niveaux d'eau dans les puits communément utilisés pour la calibration des modèles numériques d'écoulement, que les profils détaillés de charge peuvent contenir de l'information significative au sujet de l'hétérogénéité du champ de  $K$ . L'étude du potentiel de telles données est novatrice et pourrait mener à des changements quant aux méthodes de caractérisation des aquifères. Il pourrait être intéressant d'inclure de telles données dans la calibration des modèles numériques d'écoulement, en particulier lorsqu'associées avec des méthodes de calibration locale des paramètres. Par contre, le potentiel d'utilisation de ces données se limite à des conditions d'application spécifiques. La variabilité verticale des charges est en grande partie tributaire d'une anisotropie importante des matériaux peu perméables, mais celle-ci permet alors de capter de l'information quant à la

présence et continuité de voies d'écoulement préférentiel. Dans la mesure où les conditions favorables à l'utilisation des profils de charge sont réunies, l'intégration des charges ne peut aider à définir la variabilité à petite échelle intra-HF, compte tenu des variations lisses des charges hydrauliques et des conditions de contraste et d'anisotropie requises. Ce constat est similaire à celui de Xu *et al.* (2013) qui observent, avec l'utilisation de charges transitoires cette fois, que les charges hydrauliques ne parviennent pas à saisir la variabilité à petite échelle du champ de référence mais que les patrons principaux peuvent être identifiés.

Les conditions hydrogéologiques retrouvées au site d'étude sont plutôt défavorables à l'utilisation de profils verticaux de charge hydraulique. Dans le cas où les conditions favorables à l'utilisation des profils de charge hydraulique seraient réunies, les localisations ciblées pour la collecte des profils de charge doivent être validées en termes de sensibilité hydraulique aux variations de K. D'autre part, le choix de résolution verticale et d'espacement latéral entre les profils devrait être basé essentiellement sur le degré d'hétérogénéité anticipé de l'aquifère. Compte tenu de la sensibilité relativement faible des charges hydrauliques à la distribution de K, d'autres types de données doivent être intégrés dans la calibration, soient les charges hydrauliques transitoires, des données géochimiques (pics de concentrations), d'âge des eaux souterraines ou des données géophysiques. Ainsi, les tendances récentes dans les méthodes inverses en hydrogéologie comprennent l'intégration de sources multiples d'observations à diverses échelles (Zhou *et al.*, 2014).



## 5 REFERENCES

- Alabert F (1987) The practice of fast conditional simulations through the LU decomposition of the covariance matrix. *Mathematical Geology* 19(5):369-386.
- Alcolea A, Carrera J & Medina A (2006) Pilot points method incorporating prior information for solving the groundwater flow inverse problem. *Advances in Water Resources* 29(11):1678-1689.
- Anderson MP & Woessner WW (1992) Applied Groundwater Modeling: Simulation of Flow and Advective Transport. *Academic Press*, 381 p.
- Bélanger C, Giroux B, Gloaguen E & Lefebvre R (2010) GPR, ERT and CPT data integration for high resolution aquifer modeling. *Ground Penetrating Radar (GPR), 2010 13th International Conference on.21-25 June 2010*, p 1-6.
- Blouin M, Martel R & Gloaguen E (2013) Accounting for Aquifer Heterogeneity from Geological Data to Management Tools. *Groundwater* 51(3):421-431.
- Bolduc A (2003) Géologie des formations superficielles, Charny, Québec [Geology of surficial formations of the Charny area, Canada]. Dossier public 1976, échelle 1/50000, Commission Géologique du Canada, Québec.
- Bredehoeft J (2005) The conceptualization model problem—surprise. *Hydrogeology Journal* 13(1):37-46.
- Capilla JE, Gómez-Hernández JJ & Sahuquillo A (1997) Stochastic simulation of transmissivity fields conditional to both transmissivity and piezometric data 2. Demonstration on a synthetic aquifer. *Journal of Hydrology* 203(1-4):175-188.
- Capilla JE, Gómez-Hernández JJ & Sahuquillo A (1998) Stochastic simulation of transmissivity fields conditional to both transmissivity and piezometric head data - 3. Application to the Culebra Formation at the Waste Isolation Pilot Plan (WIPP), New Mexico, USA. *Journal of Hydrology* 207(3-4):254-269.
- Capilla JE & Llopis-Albert C (2009) Gradual conditioning of non-Gaussian transmissivity fields to flow and mass transport data: 1. Theory. *Journal of Hydrology* 371(1-4):66-74.
- Carle S (1999) T-PROGS: Transition Probability Geostatistical Software. University of California, Davis, 1999, 76 pp.
- Carle S & Fogg G (1996) Transition probability-based indicator geostatistics. *Mathematical Geology* 28(4):453-476.
- Carrera J, Alcolea A, Medina A, Hidalgo J & Slooten L (2005) Inverse problem in hydrogeology. *Hydrogeology Journal* 13(1):206-222.
- Carrera J & Neuman SP (1986) Estimation of Aquifer Parameters Under Transient and Steady State Conditions: 1. Maximum Likelihood Method Incorporating Prior Information. *Water Resources Research* 22(2):199-210.

- Cherry JA, Parker BL & Keller C (2007) A New Depth-Discrete Multilevel Monitoring Approach for Fractured Rock. *Ground Water Monitoring & Remediation* 27(2):57-70.
- Clifton PM & Neuman SP (1982) Effects of kriging and inverse modeling on conditional simulation of the Avra Valley Aquifer in southern Arizona. *Water Resources Research* 18(4):1215-1234.
- Comunian A, Renard P, Straubhaar J & Bayer P (2011) Three-dimensional high resolution fluvio-glacial aquifer analog – Part 2: Geostatistical modeling. *Journal of Hydrology* 405(1–2):10-23.
- Davis M (1987) Production of conditional simulations via the LU triangular decomposition of the covariance matrix. *Mathematical Geology* 19(2):91-98.
- De Marsily G, Delay F, Gonçalves J, Renard P, Teles V & Violette S (2005) Dealing with spatial heterogeneity. *Hydrogeology Journal* 13(1):161-183.
- De Marsily G, Delhomme J-P, Delay F & Buoro A (1999) Regards sur 40 ans de problèmes inverses en hydrogéologie. *Comptes Rendus de l'Académie des Sciences - Series IIA - Earth and Planetary Science* 329(2):73-87.
- De Marsily G, Lavedan G, Boucher M & Fasanino G (1984) Interpretation of interference tests in a well field using geostatistical techniques to fit the permeability distribution in a reservoir model. *Geostatistics for natural resources characterization, Part 2*:831-849.
- de Vries JJ & Simmers I (2002) Groundwater recharge: An overview of process and challenges. *Hydrogeology Journal* 10(1):5-17.
- dell'Arciprete D, Bersezio R, Felletti F, Giudici M, Comunian A & Renard P (2012) Comparison of three geostatistical methods for hydrofacies simulation: A test on alluvial sediments. *Hydrogeology Journal* 20(2):299-311.
- Deutsch C & Cockerham P (1994) Practical considerations in the application of simulated annealing to stochastic simulation. *Mathematical Geology* 26(1):67-82.
- Deutsch CV & Journel AG (1992) GSLIB: Geostatistical Software Library and User's Guide, *Oxford University Press*, New York, NY, 1992, 340 p.
- DHI-WASY Software (2012) FEFLOW 6.1 Finite element subsurface flow and transport simulation system: user's manual. DHI-WASY GmbH, Berlin, 116 p.
- DHI-WASY (2013) Modeling Subsurface Flow and Transport using FEFLOW 6.1. Software training presentation slides, Quebec November 2013.
- Doherty J (2003) Ground Water Model Calibration Using Pilot Points and Regularization. *Ground water* 41(2):170-177.
- Doherty JE, Fienen MN & Hunt RJ (2011) Approaches to highly parameterized inversion: Pilot-point theory, guidelines, and research directions. in *Scientific Investigations Report* (U.S. Geological Survey, Reston, VA), p iv, 36 p.
- Emery X (2004) Properties and limitations of sequential indicator simulation. *Stochastic Environmental Research and Risk Assessment* 18(6):414-424.
- Eslami A & Fellenius BH (1997) Pile capacity by direct CPT and CPTu methods applied to 102 case histories. *Canadian Geotechnical Journal* 34(6):886-904.

- Fisher JC & Twining BV (2011) Multilevel Groundwater Monitoring of Hydraulic Head and Temperature in the Eastern Snake River Plain Aquifer, Idaho National Laboratory, Idaho, 2007-08. (U. S. Geological Survey).
- Fleckenstein JH, Niswonger RG & Fogg GE (2006) River-Aquifer Interactions, Geologic Heterogeneity, and Low-Flow Management. *Ground water* 44(6):837-852.
- Freeze RA & Cherry JA (1979) Groundwater. *Prentice-Hall*, Englewood Cliffs, NJ, 604 p.
- Freeze RA & Witherspoon PA (1967) Theoretical analysis of regional groundwater flow: 2. Effect of water-table configuration and subsurface permeability variation. *Water Resources Research* 3(2):623-634.
- Frei S, Fleckenstein JH, Kollet SJ & Maxwell RM (2009) Patterns and dynamics of river-aquifer exchange with variably-saturated flow using a fully-coupled model. *Journal of Hydrology* 375(3-4):383-393.
- Galli A, Beucher, H, Le Loc'h G, & Doligez B (1994) The pros and the cons of the truncated Gaussian method, in Armstrong, M., and Dowd, P. A., eds., *Geostatistical simulations*: Kluwer Academic Publishers, Dordrecht, The Netherlands, 217-233.
- Geovariances (2012) ISATIS Software: Beginner's guide. *Geovariances*, Avon Cedex, France, 188 p.
- Gloaguen E, Lefebvre R, Ballard J-M, Paradis D, Tremblay L & Michaud Y (2012) Inference of the two dimensional GPR velocity field using collocated cokriging of Direct Push permittivity and conductivity logs and GPR profiles. *Journal of Applied Geophysics* 78(0):94-101.
- Gómez-Hernández JJ, Sahuquillo A & Capilla JE (1997) Stochastic simulation of transmissivity fields conditional to both transmissivity and piezometric data - I. Theory. *Journal of Hydrology* 203(1-4):162-174.
- Goode DJ (1996) Direct Simulation of Groundwater Age. *Water Resources Research* 32(2):289-296.
- Hines WW, Reny-Nolin E, Carmichael JP & Adjengue L (2011) *Probabilités et Statistique Pour Ingénieurs*. Les Editions de la Cheneliere, Montréal, 597 p.
- Hu LY (2000) Gradual deformation and iterative calibration of Gaussian-related stochastic models. *Mathematical Geology* 32(1):87-108.
- Hu LY (2002) Combination of dependent realizations within the gradual deformation method. *Mathematical Geology* 34(8):953-963.
- Hu LY, Blanc G & Noetinger B (2001) Gradual Deformation and Iterative Calibration of Sequential Stochastic Simulations. *Mathematical Geology* 33(4):475-489.
- Hu LY & Chugunova T (2008) Multiple-point geostatistics for modeling subsurface heterogeneity: A comprehensive review. *Water Resources Research* 44(11):W11413.
- Journel AB & Alabert FG (1989) *Focusing on spatial connectivity of extreme-valued attributes: stochastic indicator models of reservoir heterogeneities*. Medium: X; Size: Pages: 370 p

- Koltermann CE & Gorelick SM (1996) Heterogeneity in Sedimentary Deposits: A Review of Structure-Imitating, Process-Imitating, and Descriptive Approaches. *Water Resources Research* 32(9):2617-2658.
- LaVenue AM, RamaRao BS, de Marsily G & Marietta MG (1995) Pilot Point Methodology for Automated Calibration of an Ensemble of Conditionally Simulated Transmissivity Fields: 2. Application. *Water Resources Research* 31(3):495-516.
- Lavenue M & de Marsily G (2001) Three-dimensional interference test interpretation in a fractured aquifer using the Pilot Point Inverse Method. *Water Resources Research* 37(11):2659-2675.
- Le Ravalec-Dupin M & Hu LY (2007) Combining the pilot point and gradual deformation methods for calibrating permeability models to dynamic data. *Oil and Gas Science and Technology* 62(2 SPECIAL ISSUE):169-180.
- Le Ravalec-Dupin M & Noetinger B (2002) Optimization with the gradual deformation method. *Mathematical Geology* 34(2):125-142.
- Le Ravalec M (2005) *Inverse stochastic modeling of flow in porous media: applications to reservoir characterization*. Editions Technip, Paris, 197 p.
- Le Ravalec M & Hu L.Y. (2007) Combining the Pilot Point and Gradual Deformation Methods for Calibrating Permeability Models to Dynamic Data. *Oil & Gas Science and Technology – Rev. IFP*, Vol. 62 (2007), No. 2, pp. 169-180.
- Le Ravalec M & Mouche E (2012) Calibrating transmissivities from piezometric heads with the gradual deformation method: An application to the culebra dolomite unit at the waste isolation pilot plant (WIPP), New Mexico, USA. *Journal of Hydrology* 472-473:1-13.
- Lee SY, Carle SF & Fogg GE (2007) Geologic heterogeneity and a comparison of two geostatistical models: Sequential Gaussian and transition probability-based geostatistical simulation. *Advances in Water Resources* 30(9):1914-1932.
- Liu Y (2006) Using the Snesim program for multiple-point statistical simulation. *Computers & Geosciences* 32(10):1544-1563.
- Llopis-Albert C & Capilla JE (2009a) Gradual conditioning of non-Gaussian transmissivity fields to flow and mass transport data: 2. Demonstration on a synthetic aquifer. *Journal of Hydrology* 371(1-4):53-65.
- Llopis-Albert C & Capilla JE (2009b) Gradual conditioning of non-Gaussian transmissivity fields to flow and mass transport data: 3. Application to the Macrodispersion Experiment (MADE-2) site, on Columbus Air Force Base in Mississippi (USA). *Journal of Hydrology* 371(1-4):75-84.
- Mariethoz G, Renard P, Cornaton F & Jaquet O (2009) Truncated Plurigaussian Simulations to Characterize Aquifer Heterogeneity. *Ground water* 47(1):13-24.
- Matheron G (1963) Principles of geostatistics. *Economic geology* 58(8):1246-1266.
- McLaughlin D & Townley LR (1996) A Reassessment of the Groundwater Inverse Problem. *Water Resources Research* 32(5):1131-1161.

- Meerschaert MM, Dogan M, Van Dam RL, Hyndman DW & Benson DA (2013) Hydraulic conductivity fields: Gaussian or not? *Water Resources Research* 49(8):4730-4737.
- Meyer JR, Parker BL & Cherry JA (2008) Detailed hydraulic head profiles as essential data for defining hydrogeologic units in layered fractured sedimentary rock. *Environmental Geology* 56(1):27-44.
- Millet E (2013) Modélisation de l'hétérogénéité de l'aquifère deltaïque de Valcartier et son impact sur la dispersivité et l'âge de l'eau souterraine. Mémoire de maîtrise en Sciences de la terre, (Université du Québec, Institut national de la recherche scientifique, Québec), 81 p.
- Molson JW & Frind EO (2013). FLONET/TR2 Two-Dimensional Simulator for Groundwater Flonets, Contaminant Transport and Residence Time. User Guide Version 3.0 June 2013
- Murphy S, Ouellon T, Ballard J-M, Lefebvre R & Clark I (2011) Tritium-helium groundwater age used to constrain a groundwater flow model of a valley-fill aquifer contaminated with trichloroethylene (Quebec, Canada). *Hydrogeology Journal* 19(1):195-207.
- Ouellon T, Lefebvre R, Marcotte D, Boutin A, Blais V & Parent M (2008) Hydraulic conductivity heterogeneity of a local deltaic aquifer system from the kriged 3D distribution of hydrofacies from borehole logs, Valcartier, Canada. *Journal of Hydrology* 351(1-2):71-86.
- Paradis D, Gloaguen E, Lefebvre R & Giroux B (in correction) Sensitivity and resolution analysis of the information content of tomographic slug tests. 2013WR014785, *Water Resources Research*. *Water Resources Research* 2013WR014785.
- Paradis D, Gloaguen E, Lefebvre R & Rivera A (2011) Tying geophysics to hydrogeology: a learning machine approach to characterise heterogeneous granular aquifers. GeoHydro2011 : 1st Joint Canadian Quaternary Association (CANQUA) and Canadian Chapter of the International Association of Hydrogeologists (IAH-CNC) Conference : Conference Proceedings, August 28-31, 2011, Quebec, Canada.
- Paradis D & Lefebvre R (2013) Single-well interference slug tests to assess the vertical hydraulic conductivity of unconsolidated aquifers. *Journal of Hydrology* 478(0):102-118.
- Paradis D, Lefebvre R, DeLouis C, Martin D & Ballard J-M (2010) Vertical Interference slug tests for the measurement of vertical hydraulic conductivity : GeoAlberta'10 : 63rd Canadian Geotechnical Conference & 6th Canadian Permafrost Conference : Conference proceedings, September 12-16, 2010, Calgary, Canada.
- Paradis D, Lefebvre R, Gloaguen E & Rivera A (submitted) Predicting hydrofacies and hydraulic conductivity from direct-push data using a data-driven relevance vector machine approach: motivations, algorithms and application. *Water Resources Research* 2014WR015452( submitted February 14, 2014).
- Paradis D, Lefebvre R, Morin RH & Gloaguen E (2011) Permeability Profiles in Granular Aquifers Using Flowmeters in Direct-Push Wells. *Ground water* 49(4):534-547.
- Paradis D, Tremblay L, Lefebvre R, Gloaguen E, Rivera A, Parent M, Ballard J-M, Michaud Y & Brunet P (2014) Field characterization and data integration to define the hydraulic

- heterogeneity of a shallow granular aquifer at a sub-watershed scale. *Environmental Earth Sciences*, 72 (5), 1325-1348.
- Parent M & Occhietti S (1999) Late wisconsinan deglaciation and glacial lake development in the appalachians of southeastern Quebec. *Géographie physique et Quaternaire*, 53(1):117-135.
- Parker BL, Cherry JA & Swanson BJ (2006) A multilevel system for high-resolution monitoring in rotasonic boreholes. *Ground Water Monitoring and Remediation* 26(4):57-73.
- Poeter EP & Hill MC (1997) Inverse Models: A Necessary Next Step in Ground-Water Modeling. *Ground water* 35(2):250-260.
- RamaRao BS, LaVenue AM, de Marsily G & Marietta MG (1995) Pilot Point Methodology for Automated Calibration of an Ensemble of conditionally Simulated Transmissivity Fields: 1. Theory and Computational Experiments. *Water Resources Research* 31(3):475-493.
- Refsgaard JC, Christensen S, Sonnenborg TO, Seifert D, Højberg AL & Troldborg L (2012) Review of strategies for handling geological uncertainty in groundwater flow and transport modeling. *Advances in Water Resources* 36:36-50.
- Refsgaard JC, van der Sluijs JP, Brown J & van der Keur P (2006) A framework for dealing with uncertainty due to model structure error. *Advances in Water Resources* 29(11):1586-1597.
- Rivest M, Marcotte D & Pasquier P (2012) Sparse data integration for the interpolation of concentration measurements using kriging in natural coordinates. *Journal of Hydrology* 416-417:72-82.
- Rojas R, Feyen L & Dassargues A (2008) Conceptual model uncertainty in groundwater modeling: Combining generalized likelihood uncertainty estimation and Bayesian model averaging. *Water Resources Research* 44(12):W12418.
- Ronayne MJ, Gorelick SM & Caers J (2008) Identifying discrete geologic structures that produce anomalous hydraulic response: An inverse modeling approach. *Water Resources Research* 44(8).
- Ruggeri P, Gloaguen E, Lefebvre R, Irving J & Holliger K (accepted) Integration of hydrological and geophysical data beyond the local scale: Application of Bayesian sequential simulation to field data from the Saint-Lambert-de-Lauzon site. Quebec, Canada. HYDROL 15482, to *J. of Hydrology*.
- Sanford W (2002) Recharge and groundwater models: An overview. *Hydrogeology Journal* 10(1):110-120.
- Sanford W (2011) Calibration of models using groundwater age. *Hydrogeology Journal* 19(1):13-16.
- Sanford W, Plummer LN, McAda D, Bexfield L & Anderholm S (2004) Hydrochemical tracers in the middle Rio Grande Basin, USA: 2. Calibration of a groundwater-flow model. *Hydrogeology Journal* 12(4):389-407.
- Scanlon BR, Healy RW & Cook PG (2002) Choosing appropriate techniques for quantifying groundwater recharge. *Hydrogeology Journal* 10(1):18-39.

- Seifert D, Sonnenborg TO, Refsgaard JC, Højberg AL & Troldborg L (2012) Assessment of hydrological model predictive ability given multiple conceptual geological models. *Water Resources Research* 48(6).
- Straface S, Chidichimo F, Rizzo E, Riva M, Barrash W, Revil A, Cardiff M & Guadagnini A (2011) Joint inversion of steady-state hydrologic and self-potential data for 3D hydraulic conductivity distribution at the Boise Hydrogeophysical Research Site. *Journal of Hydrology* 407(1-4):115-128.
- Straubhaar J, Renard P, Mariethoz G, Froidevaux R & Besson O (2011) An improved parallel multiple-point algorithm using a list approach. *Mathematical Geosciences* 43(3):305-328.
- Strebelle S (2002) Conditional simulation of complex geological structures using multiple-point statistics. *Mathematical Geology* 34(1):1-21.
- Sudicky EA, Illman WA, Goltz IK, Adams JJ & McLaren RG (2010) Heterogeneity in hydraulic conductivity and its role on the macroscale transport of a solute plume: From measurements to a practical application of stochastic flow and transport theory. *Water Resources Research* 46(1):W01508.
- Sun N-Z (1995) *Inverse Problems in Groundwater Modeling*. Kluwer Academic Publishers, Dordrecht, The Netherlands, 337p.
- Sun N-Z & Yeh WWG (1992) A stochastic inverse solution for transient groundwater flow: Parameter identification and reliability analysis. *Water Resources Research* 28(12):3269-3280.
- Tarantola A (2005) *Inverse problem theory: methods for data fitting and model parameter estimation*. SIAM, Philadelphia, 342 p.
- Tremblay L (2013) Caractérisation intégrée d'un aquifère granulaire pour l'évaluation des processus géochimiques influençant l'atténuation naturelle d'un panache de lixiviat. Thèse de doctorat en Sciences de la terre, (Université du Québec, Institut national de la recherche scientifique, Québec), 301 p.
- Tremblay L, Lefebvre R, Brunet P & Cloutier V (submitted) Direct and indirect indicators of the spatial distribution of recharge and discharge in a shallow granular aquifer affected by a leachate plume. *J. of Hydrology* Submitted February 21, 2014.
- Tremblay L, Lefebvre R, Paradis D & Gloaguen E (2013) Conceptual model of leachate migration in a granular aquifer derived from the integration of multi-source characterization data (St-Lambert, Canada). *Hydrogeology Journal*:1-22.
- Varni M & Carrera J (1998) Simulation of groundwater age distributions. *Water Resources Research* 34(12):3271-3281.
- Wellmann JF, Finsterle S & Croucher A (2014) Integrating structural geological data into the inverse modelling framework of iTOUGH2. *Computers & Geosciences* 65(0):95-109.
- Wen XH, Deutsch CV & Cullick AS (2002) Construction of geostatistical aquifer models integrating dynamic flow and tracer data using inverse technique. *Journal of Hydrology* 255(1-4):151-168.

- Wiese B & Nützmann G (2011) Calibration of spatial aquitard distribution using hydraulic head changes and regularisation. *Journal of Hydrology* 408(1–2):54-66.
- Willmott CJ & Matsuura K (2005) Advantages of the mean absolute error (MAE) over the root mean square error (RMSE) in assessing average model performance. *Climate Research* 30(1):79.
- Xu T, Jaime Gómez-Hernández J, Zhou H & Li L (2013) The power of transient piezometric head data in inverse modeling: An application of the localized normal-score EnKF with covariance inflation in a heterogenous bimodal hydraulic conductivity field. *Advances in Water Resources* 54:100-118.
- Zhou H, Gómez-Hernández JJ, Hendricks Franssen H-J & Li L (2011) An approach to handling non-Gaussianity of parameters and state variables in ensemble Kalman filtering. *Advances in Water Resources* 34(7):844-864.
- Zhou H, Gómez-Hernández JJ & Li L (2014) Inverse methods in hydrogeology: Evolution and recent trends. *Advances in Water Resources* 63(0):22-37.